THE INTERSECTION BETWEEN AEROBIC GLYCOLYSIS, CEREBELLAR NEUROGENESIS, AND MEDULLOBLASTOMA

Katherine Rose Tech

A dissertation submitted to the faculty at the University of North Carolina at Chapel Hill in partial fulfillment of the requirements for the degree of Doctor of Philosophy in the Department of Biomedical Engineering.

Chapel Hill
2016

Approved by:

Jeffrey M. Macdonald

Timothy R. Gershon

Mohanish Deshmukh

Mark Tommerdahl

Robert G. Dennis

ABSTRACT

Katherine Rose Tech: The Intersection between Aerobic Glycolysis, Cerebellar Neurogenesis, and Medulloblastoma
(Under the direction of Jeffrey M. Macdonald and Timothy R. Gershon)

Aerobic glycolysis supports proliferation in development and cancer through unresolved mechanisms. Aerobic glycolysis, which supports the generation of biomass, is integral to cerebellar granule neuron progenitors (CGNPs) for normal growth and is hijacked in medulloblastoma. Medulloblastoma, the most common malignant pediatric brain tumor, is approached as a disorder of normal brain development. Arising as a disruption of normal cerebellar growth, medulloblastoma exploits the cellular processes used for cerebellar development to promote tumor formation. Thus, genes that are involved in developmentally-regulated progenitor growth may contribute to tumorigenesis when aberrantly expressed. A better understanding of cerebellar development and thus the pathogenesis of medulloblastoma, may lead to more targeted cancer treatments.

In response to the developmental mitogen Sonic Hedgehog (SHH), CGNPs increase aerobic glycolysis and up-regulate key glycolytic enzymes *Hexokinase-2* (*Hk2*) and *Pyruvate Kinase M2* (*Pkm2*). HK2, which catalyzes the first step in glycolysis, is required for aerobic glycolysis in brain progenitors and medulloblastomas. *Hk2* deletion blocks aerobic glycolysis, disrupts proliferation, and restricts medulloblastoma growth to prolong survival. Moreover, *Hk2* was found by others to be up-regulated in medulloblastomas resistant to SHH pathway inhibition by vismodegib treatment. These findings raise the question if *Hk2* deletion sensitizes medulloblastoma to vismodegib. Downstream of *Hk2*, the effect of deleting PKM2 and disrupting the last step in glycolysis in cerebellar neurogenesis and medulloblastoma is unknown. This dissertation examines the importance of aerobic glycolysis to development and cancer. Specifically, I determined the effect of *Pkm2* deletion on the cerebellar neurogenesis and medulloblastoma tumorigenesis and the effect of vismodegib treatment on *Hk2*-deleted

medulloblastomas. I demonstrate that CGNPs and medulloblastomas specifically express *Pkm* as the less active PKM2 isoform. *Pkm2* deletion in CGNPs reduces aerobic glycolysis, alters metabolism to increase progenitor proliferation, and accelerates medulloblastoma growth to shorten survival. Thus PKM2 is not required for neural progenitor proliferation or tumorigenesis. Rather, the loss of pyruvate kinase releases cells from growth inhibition. I also found that vismodegib treatment of *Hk2*-deleted tumors further restricts tumor growth but does not extend survival. Together, these studies demonstrate the potential of targeting aerobic glycolysis as an anti-cancer strategy.

To my family and friends, I could not have done this without you.

Thank you for all of your support.

ACKNOWLEDGEMENTS

The work I describe here was made possible by the support and generosity of many people. First, I would like to thank my two advisors, Jeffrey M. Macdonald and Timothy R. Gershon. Thank you, Jeff and Tim, for your guidance, for encouraging me to think critically, for supporting my professional development side quests, for helping me to write analytically, and for creating an environment that enabled me to achieve greater.

I would also like to thank my thesis committee members for their advice and support. Mohanish Deshmukh, Mark Tommerdahl, and Robert G. Dennis, each of you brought a different perspective to this project and provided much appreciated support.

Thank you to the funding sources that made this work possible, which include the National Institute of Neurological Disorders and Stroke (NINDS; R01NS088219), the National Institutes of Health (NIH; 1K08NS077978-01), the St. Baldrick's Foundation, and the American Institute for Cancer Research. Thank you to the UNC CGBID Histology Core supported by P30 DK 034987, the UNC Tissue Pathology Laboratory Core supported by NCI CA016086 and UNC UCRF, UNC Neuroscience Center Confocal and Multiphoton Imaging Core, and the LCCC Animal Studies Core supported by the NCI Center Core Support Grant CA16086 to the UNC LCCC. These facilities provided expertise and technical assistance in immunohistochemistry, confocal imaging, and in drug studies. With the kindness and support of the core facility staff this work has been greatly accelerated.

This research would not have been possible without collaborators. Thank you to Matthew Vander Heiden at MIT, Michael D. Taylor at The Hospital for Sick Children, and their respective labs for sharing the *Pkm2*$^{fl/fl}$ mice and human medulloblastoma data. Thank you both for also critically reviewing the manuscript for publication. The animal models used for this research were graciously provided by James Olson (*ND2:SmoA1*; Fred Hutchinson Cancer Research Center), David Rowitch (*Math1-Cre*; UCSF), Robert Wechsler-Reya (*Math1-Cre*; Sanford-Burnham Medical Research Institute), and Eva Anton (*hGFAP-Cre*; UNC-CH).

To all of my nuclear and sister lab mates, both past and present, I am truly honored to have the opportunity to work with each and every one of you. I have learned so much from each of you in regards to both science and life. Thank you for being there to talk, providing advice and encouragement, and being there to shoot rapid-fire ideas around. With laughter and fun, you made the long lab meetings, long experiments, and setbacks seem like dust in the wind, or rather, meninges in HBSS.

Thank you to my wonderful friends, whom I cannot thank enough for their support, lending their ears, insightful advice, and knowing how to make a jokester laugh. You have been the light to my late nights and so much more. You gave me the strength when I had none, and for that, I cannot thank you enough.

I would like to thank my family for encouraging me to be my very best. Your endless support for me was all that I could ask for. I could not be person I am today without you and words cannot express my gratitude for everything that you have given me.

Finally, to everyone who served as a teacher, scientific Yoda, career counselor, mentor, and mentee – thank you so much for your guidance, dedication, and effort.

PREFACE

Chapter Four of this dissertation was previously published. Permission to include the following article was provided by Elsevier:

Tech K, Deshmukh M, Gershon TR. 2014. Adaptations of energy metabolism during cerebellar neurogenesis are co-opted in medulloblastoma. *Cancer Lett* 356: 268–272. doi:10.1016/j.canlet.2014.02.017.

TABLE OF CONTENTS

LIST OF TABLES

LIST OF FIGURES

LIST OF ABBREVIATIONS

Acc1	Acetyl-CoA carboxylase 1
Acox1	Acyl-CoA oxidase
ADP	Adenosine diphosphate
AMP	Adenosine monophosphate
AMPK	Adenosine monophosphate-activated kinase
ATP	Adenosine triphosphate
cC3	Cleaved caspase-3
CCND2	Cyclin D2
CDK	Cyclin-dependent kinases
CGNs	Cerebellar granule neurons
CGNPs	Cerebellar granule neuron progenitors
CNS	Central nervous system
CoA	Coenzyme A
DNA	Deoxyribonucleic acid
E	Embryonic day
E2F1	E2F Transcription Factor 1
E4P	Erythrose 4-phosphate
EdU	5'-ethynyl-2'-deoxyuridine
EGL	External granule layer
F6P	Fructose 6-phosphate
FASN	Fatty acid synthase
FBP	Fructose-1,6-bisphosphate
FDG	Fluorodeoxyglucose
FE	Fractional enrichment
FPKM	Fragments per kilobase of transcript per million mapped reads
GAP	Glyceraldehyde 3-phosphate
H&E	Hematoxylin and eosin

HCC	Hepatocellular carcinoma
hGFAP	Human glial fibrillary acidic protein
HK2	Hexokinase-2
^{1}H NMR	Proton nuclear magnetic resonance
iEGL	Inner external granule layer
IGFR	Insulin growth factor receptor
IGL	Internal granule layer
IHC	Immunohistochemistry
IP	Intraperitoneal injection
LC-MS	Liquid chromatography-mass spectrometry
LDH	Lactate dehydrogenase
MCAD	Medium chain acyl-CoA dehydrogenase
MCT	0.5% Methylcellulose in 0.2% Tween-80
MEF	Mouse embryonic fibroblast
MRI	Magnetic resonance imaging
mRNA	Messenger ribonucleic acid
ND2	Neuronal differentiation 2
NeuroD2	Neuronal differentiation 2
NMP	N-methyl-2-pyrrolidone
Non-OxPPP	Non-oxidative phase of pentose phosphate pathway
oEGL	Outer external granule layer
OxPPP	Oxidative phase of pentose phosphate pathway
P	Postnatal day
PC	Pyruvate carboxylation
PCL	Purkinje cell layer
PCNA	Proliferating cell nuclear antigen
PCR	Polymerase chain reaction
PDH	Pyruvate dehydrogenase

PEG	Polyethylene glycol
PEP	Phosphoenolpyruvate
PET	Positron emission tomography
PGAM1	Phosphoglycerate mutase 1
PI3K	Phosphoinositide 3-kinase
Pklr	Pyruvate kinase, liver and red blood cell
Pkm	Pyruvate kinase, muscle
PKM1	Pyruvate kinase isoform M1
PKM2	Pyruvate kinase isoform M2
$Pkm2^{cKO}$	Pyruvate kinase isoform M2 conditional deletion
PPARγ	Peroxisome proliferator-activated receptor-γ
PPP	Pentose phosphate pathway
Ptc	Patched 1
R5P	Ribose 5-phosphate
Rb	Retinoblastoma
RBC	Red blood cell
RMS	Rostral migratory stream
RNA	Ribonucleic acid
RNA-seq	Ribonucleic acid sequencing
Ru5P	Ribulose 5-phosphate
S7P	Sedoheptulose 7-phosphate
SB	Sleeping beauty
SHH	Sonic hedgehog
shRNA	Short hairpin ribonucleic acid
Smo	Smoothened
SVZ	Subventricular zone
Vismo	Vismodegib
Wnt	Wingless

X5P	Xylulose 5-phosphate

CHAPTER I: INTRODUCTION

1.1 Aerobic glycolysis

1.1.1 Overview

Glucose is a major source of cellular energy and carbons for biosynthetic reactions. Cells may metabolize glucose through glycolysis to produce pyruvate. Under high cellular energy demands, pyruvate is oxidized into CO_2 in the Krebs cycle to produce 38 ATP per glucose molecule through coupled oxidative phosphorylation. Pyruvate can have other metabolic fates such as its conversion into ethanol, acetate, alanine, and lactate. Aerobic glycolysis is the conversion of glucose to lactate and 2 ATP even in the presence of sufficient oxygen needed for oxidative phosphorylation. Likewise, cells with large ATP requirements are less likely to use aerobic glycolysis over energy-efficient oxidative phosphorylation for ATP production. In addition to low energy production, glucose catabolism through aerobic glycolysis generates metabolic intermediates that can be used for lipid, amino acid, and nuclei acid biosynthesis. Thus, proliferating cells exhibiting increased aerobic glycolysis must use this metabolic phenotype to meet competing cellular demands for energy production and biosynthesis. Increased aerobic glycolysis is a metabolic phenotype found in both unicellular and multicellular organisms used to support normal and aberrant proliferation[1].

1.1.2 Supporting biosynthesis

Glycolysis is inefficient at ATP production compared to oxidative phosphorylation. Aerobic glycolysis, however, can produce more ATP than oxidative phosphorylation by generating ATP at a faster rate[2]. However, it is unlikely that rapidly dividing cells are opting for the faster but less efficient route for primary ATP production when glycolysis-derived ATP only makes up on average 17% of the total ATP pool[3]. Moreover, a low ATP:AMP ratio is needed to prevent inhibition of key, rate-limiting steps in

glycolysis[4]. Specifically, phosphofructokinase is sensitive to the ATP:AMP ratio, controlling the downstream flow of glycolytic intermediates[5]. To maintain low ATP:AMP ratio, proliferating cells can also increase ATP consumption to promote the catabolism of glucose to lactate, increasing glycolytic flux[6]. In all, aerobic glycolysis serves a more important function beyond energy metabolism in proliferating cells.

The major function of increased aerobic glycolysis is to support biosynthesis. Rapidly dividing cells use anabolic reactions to generate nucleotides, amino acids, and lipids required for cell division. Glucose catabolism can generate the precursors needed for these synthesis reactions, and increased aerobic glycolysis is likely used to maintain the glycolytic intermediate pool needed for biosynthesis[1,7]. For example, in *de novo* nucleotide synthesis carbon atoms are needed from the extracellular environment. Once phosphorylated, glucose can supply carbons to nucleotide synthesis as the ribose ring in two ways. The direct way is through the oxidative phase of the pentose phosphate pathway where glucose 6-phosphate (G6P) becomes ribose 5-phosphate (R5P)[8]. The indirect route is through glycolytic intermediates fructose 6-phosphate (F6P) and glyceraldehyde-3-phosphate (GAP) feeding into the non-oxidative pentose phosphate pathway to generate the ribose ring[9,10]. R5P is then converted to 5-phosphoribosyl-α-pyrophosphate (PRPP), the last common intermediate in the *de novo* synthesis pathways for pyrimidine and purine nucleotides[11]. The generation of PRPP is catalyzed by PRPP synthetase, which exhibits increased activity in response to mitogen stimulation[12]. Moreover, PRPP is specifically important for purine nucleotides as its synthesis is the rate-limiting step in the production of purine precursors[11]. Thus, PRPP production is important for nucleotide synthesis during cell growth. In addition to the ribose ring, glucose metabolism through glycolysis can source up to an additional 3 and 4 carbons to the synthesis of the pyrimidine and purine bases[1]. The purine base, adenine, furthers the reach of glucose-derived carbons as adenine is an essential component of cofactor biosynthesis[1,5].

In addition to nucleotide synthesis, glucose catabolism through glycolysis also supplies carbons to amino acids. As proliferating cells must generate a large amount of protein for cell division[1], there is a large amino acid requirement. Cells may increase aerobic glycolysis to meet these amino acid demands as glycolytic intermediates are direct precursors for nonessential amino acids cysteine, glycine, serine, and alanine[1,5]. Offshoot serine metabolism is a component in phosphatidylserine biosynthesis and a

precursor for other major phospholipid head groups ethanolamine and choline, further emphasizing the importance of glucose-derived carbons[5]. Downstream of glycolysis, glucose-derived pyruvate can enter the Krebs cycle to generate oxaloacetate and α-ketoglutarate. These intermediates are, in turn, used to make asparagine, aspartate, glutamate, glutamine, proline and arginine[1,5]. Thus, aerobic glycolysis can supply the carbons required for amino acid synthesis during proliferation.

As for lipid synthesis, the glycolytic intermediate dihydroxyacetone phosphate is the precursor to glycerol 3-phosphate and lipids such as cardiolipin. Glycerol 3-phosphate is critical for the generation of phospholipids and triglycerides, which are major structural lipids in cell membranes, while cardiolipin is a component of mitochondrial membranes[5]. Another glycolytic intermediate, 3-phosphoglycerate, is the precursor to sphingolipids, which are important membrane components and mediate cell signaling[13]. Glucose metabolism through glycolysis also indirectly supplies carbons for acetyl-CoA, an important component of lipid synthesis. After the conversion of glucose to pyruvate, pyruvate is decarboxylated and becomes acetyl-CoA in the mitochondria. As acetyl-CoA cannot cross the mitochondrial membrane, acetyl-CoA must enter the Krebs cycle and be exported as citrate. ATP-citrate lyase then converts citrate to acetyl-CoA in the cytosol. The recovered cytosolic acetyl-CoA provides the carbons for fatty acid chains and for mevalonate, a precursor to cholesterol. In all, the ability to produce cytosolic acetyl-CoA[14] and synthesize fatty acids from extracellular nutrients[15,16] is critical to proliferation.

Nucleotide, amino acid, and lipid synthesis all rely on glycolysis to source glucose carbons for their respective reactions. The increased aerobic glycolysis of proliferating cells is used to maintain pools of precursors needed for biosynthesis. Thus, the function of aerobic glycolysis extends beyond energy metabolism as a metabolic phenotype that supports rapid growth.

1.1.3 Lactate

Excess lactate is not a driver but a by-product of increased aerobic glycolysis. As described previously, high glycolytic flux maintains precursor pools for biosynthetic reactions. Biosynthesis, a low-flux pathway, is paired to aerobic glycolysis, a high-flux pathway, such that the former would stop if there

was a slight decrease in the latter[17]. High glycolytic flux produces pyruvate, and as a way to remove excess from the cell, pyruvate is converted to alanine and lactate[18] given that its entry into the Krebs cycle is rate limited by slower pyruvate dehydrogenase activity[1,19]. Lactate generation efficiently produces NAD+[20], balancing the NAD+/NADH ratio and supplying the NAD+ used in upstream glycolytic reactions[1,5]. NAD+ is also used during nucleotide and amino acid synthesis, suggesting that lactate generation facilitates high glycolytic flux and faster utilization of glucose-derived carbons by anabolic reactions. Nonetheless, the production of excess lactate is a wasteful and inefficient use of glucose-derived carbons. However, proliferating cells are willing to accept the cost of lactate production over efficient carbon utilization because of the biosynthetic growth advantage provided by aerobic glycolysis.

1.1.4 In cancer

In 1924, Otto Warburg first reported in that cancer cells consume more glucose and produce more lactate than their normal counterparts in oxygen-rich environments[21]. This metabolic phenotype of increased aerobic glycolysis in cancer cells became to be known as the “Warburg effect”. Initially, Warburg thought that a defect in mitochondrial respiration caused cancer cells to increase glycolytic flux. However, most cancer cells do not have impaired mitochondrial respiration[3,22] and enhanced aerobic glycolysis actually supports rapid, aberrant growth. After Warburg’s discovery, a major focus in cancer research now is the study of metabolic reprogramming and its unanswered questions. What is the impact of altered metabolism and increased aerobic glycolysis? What are the exact reactions that mediate this phenotype? What are the cellular mechanisms upstream of this phenotype? Can we target metabolism as an anticancer therapy? Briefly described below are few of the ways that cancer reprograms its cellular metabolism to increase aerobic glycolysis and support growth.

To support aberrant growth, cancer cells hijack and reprogram signaling pathways, increasing aerobic glycolysis and altering metabolism. For example, cancer cells are known to activate the phosphoinositide 3-kinase (PI3K) signaling pathway, which increases glucose uptake and glycolysis[23,24]. Moreover, cancer cells are able to alter other pathways including Src, Myc, Ras, and p53, to promote proliferation through changes in metabolism[1,23,25,26].

In addition to appropriating signaling pathways, altering metabolic enzymes is another mechanism used during tumorigenesis to tailor metabolism for growth. One prominent example is Pyruvate kinase M (*Pkm*), which catalyzes the conversion of phosphoenolpyruvate (PEP) to pyruvate in glycolysis. *Pkm* is preferentially expressed in cancer cells and normal proliferating cells as the PKM2 isoform. The alternative to PKM2 is the PKM1 isoform, which is typically found in differentiated tissues requiring constitutively high pyruvate kinase activity[27]. PKM2, with its intrinsically low pyruvate kinase activity, is expressed ubiquitously in cancer, suggesting that this isoform may mediate a growth advantage. At the level of PEP, cancer cells can redirect glycolytic intermediates upstream of PEP by expressing PKM2. Thus, during increased aerobic glycolysis, glucose is metabolized quickly and not immediately turned into lactate as PKM2 expression lowers pyruvate production and replenishes glycolytic intermediate pools for biosynthesis. A seminal study by Israelsen *et al* demonstrated that low pyruvate kinase activity provides a growth advantage as their *Pkm2*-deleted breast cancers exhibited accelerated tumorigenesis[28]. In the case of nutrient stress during rapid growth, cancer cells can activate PKM2 through intracellular signaling pathways[29] or allosterically[30]. Increasing pyruvate kinase activity would shift the metabolic program from anabolic reactions and growth to efficient ATP production[31,32]. Thus, PKM2 is a tool cancers can use to direct glycolytic intermediates in response to changes in precursor pools and nutrient availability.

In contrast to the well-known PKM2 isoform paradigm, is the lesser-known phosphofructokinase/fructose-2,6-bisphosphatase B3 gene (*PFKFB3*). While PFKFB3 is not a canonical glycolytic enzyme, its catalytic activity increases the rate of glycolysis resulting in its high expression in human tumors[33]. PFKFB3 has six splice variants that are preferentially expressed in specific cancerous and normal tissues to support growth[23]. Besides expressing specific isoforms, cancer cells can also mutate metabolic enzymes such as succinate dehydrogenase[34], fumarate hydratase[35], and isocitrate dehydrogenase[36,37]. Mutations in these enzymes facilitate a metabolic phenotype that is conducive towards growth in diverse cancers[23,38]. In all, metabolic reprogramming is a signature of cancer cells used to support aberrant proliferation and is a potential target of anticancer strategies[23–25].

Since Warburg's first report of increased aerobic glycolysis in cancer cells, cancer diagnoses and treatment strategies have been developed around the Warburg effect. The most commonly known diagnostic method is fluorodeoxyglucose-position emission tomography (FDG-PET) imaging. FDG is a glucose analogue that cannot be metabolized and competes with glucose for transport across the cell membrane. FDG-PET is based on the assumption that malignant tissues have a higher rate of glucose uptake than normal tissues, such that tumors are identified by FDG accumulation when visualized by PET imaging. However, FDG uptake is influenced by confounding factors such as endogenous glucose pools, tissue heterogeneity, tissue volume, and non-glycolytic catabolism of glucose, which limit the usefulness of the FDG-PET technique[3,39].

As for cancer treatments, inhibition of glycolysis alone is not potent enough to induce significant anti-cancer effects[40,41]. The lack of potency in targeting glycolysis alone most likely arises from tumor heterogeneity and metabolic plasticity such that malignant cells can use alternative metabolic pathways to sustain rapid growth. Targeted therapies against glycolysis are being tested to determine if they potentiate the cytotoxic effects of other therapies[40,41] or should be multiplexed with additional metabolically-based therapies. For example, 2-deoxyglucose (2DG), the unlabeled form of FDG, may be used in combination with radiation therapy in the treatment of glioblastoma multiforme (GBM)[42]. However, further clinical studies are required to determine efficacy of this combination therapy. Another strategy in the treatment of GBM could be 2DG and metformin combination therapy. Metformin, an inhibitor of oxidative phosphorylation, in combination with 2DG decreased the invasiveness of tumorspheres and significantly prolonged survival in a GBM xenograft model[43]. Furthermore, direct and selective therapies against aerobic glycolysis can be limited by the lack of small molecule inhibitors. Hexokinase-2 (HK2) catalyzes the first irreversible step in glycolysis and is considered to be a potent target for cancer treatment. However, for the past 50 years, the intrinsic properties of the HK2 enzyme have delayed the development of selective HK2 small molecule inhibitors and their application in the clinic. Only recently has a potential HK2 inhibitor been made[44]. In all, further research into the intersection of metabolism, aerobic glycolysis, and cancer biology will provide the insight required for the development of novel metabolism-based cancer therapies.

1.2 Medulloblastoma and cerebellar development

1.2.1 Overview

Medulloblastoma is the most common malignant pediatric brain tumor. Current therapies for medulloblastoma rely on the sensitivity of the tumor to DNA damage. Craniospinal radiation therapy, which was first implemented in the 1950s, transformed medulloblastoma from a 100% fatal disease into a treatable cancer with 60% long-term survival[45–47]. Since then, the coupling of optimized radiation regimens with chemotherapeutics has improved patient outcomes to 80% long-term survival[48–51]. The success of these therapies, however, is dampened by their debilitating side effects. Survivors must live with significant long-term injuries, such as growth impairment, early strokes, cognitive deficits, and endocrine failure, while acutely aware of the risk of recurrence[46,52,53]. Importantly, 20-30% of medulloblastoma patients ultimately die from the disease. Thus, the identification of new therapeutic targets in addition to DNA damage-based chemotherapies is necessary. By improving our understanding of medulloblastoma tumorigenesis, we may discover novel pathways to target in the clinic, which may also bring reduced toxicity and improved patient outcomes.

Defined by molecular analyses, there are four distinct subgroups of medulloblastoma: wingless (WNT), sonic hedgehog (SHH), Group 3, and Group 4[54–56]. Approximately 35% of all medulloblastomas are Group 4 tumors, followed by SHH (30%), Group 3 (25%), and (10%) WNT tumors[56]. Among infants and adults, however, the SHH subgroup is the most common medulloblastoma, representing more than 50% of patient cases, with significant decreased frequency in children[54]. In contrast, the WNT (1%) and Group 4 (11%) subgroups rarely arise in infants while Group 3 (6%) is less common in adults[54]. Each medulloblastoma subgroup presents as a distinct disease with different patient demographics, transcriptomics, and genomics[54–58]. Of the four subgroups, SHH-driven medulloblastoma is the best characterized as animals models that recapitulate the disease[59] have enabled and progressed basic, preclinical, and clinical research.

In research, medulloblastoma has been increasingly approached as a disorder of brain development. During the first year of life in humans, or the first 15 days of life in mice, neural progenitors rapidly divide. Cerebellar granule neuron progenitors (CGNPs) proliferate in the external granule cell layer (EGL), located along the outside of the cerebellum. In mice, peak CGNP proliferation and expansion occurs between postnatal day (P) 5 and 8[60]. Then, CGNPs switch to the postmitotic, premigratory state in the inner EGL (iEGL)[61] before differentiating and migrating to the internal granule cell layer (IGL) where they reside as cerebellar granule neurons (CGNs)[60,62,63]. By P20, CGNP migration and differentiation is complete. CGNPs represent the largest population of neurons in the brain and the cell of origin for SHH-driven medulloblastoma. SHH-medulloblastoma specifically arises in the cerebellum from CGNPs that aberrantly proliferate, lacking normal growth control[62,64,65]. Thus, developmentally-regulated genes involved in normal cerebellar growth may contribute to tumorigenesis when they fail to turn off during differentiation.

1.2.2 SHH-driven medulloblastoma

SHH-driven medulloblastoma is characterized by activation of the SHH signaling pathway. This developmental pathway regulates postnatal CGNP proliferation at physiological levels but mutations that activate the SHH pathway can prolong proliferation and lead to SHH-driven medulloblastoma[61,63,66]. During normal cerebellar development, Purkinje cells secrete the SHH mitogen which diffuses to the EGL where CGNPs proliferate[61] (Fig. 1.1A). In CGNPs, SHH binds to the transmembrane protein Patched 1 (PTC), inducing a conformational change that releases the transmembrane protein Smoothened (SMO) from inhibition (Fig. 1.1B). Activated SMO then initiates an intracellular signal transduction pathway that activates the GLI transcription factor family and other target genes such as *cyclinD1* and *D2*[67,68] (Fig. 1.1B). SHH signaling drives CGNP expansion and wanes as progenitors differentiate and migrate to the IGL in response to negative growth regulation[63]. However, mutations in *Ptc*[69,70], Suppressor of fuse homolog (*Sufu*)[71], and *Smo*[72] aberrantly activate the SHH signaling pathway in patients to drive medulloblastoma tumorigenesis.

These activating mutations in patients have led to the development of animal models that recapitulate the disease. These models are critical for elucidating medulloblastoma tumorigenesis and have allowed for unprecedented, preclinical *in vivo* studies that test for targeted therapies against SHH-driven medulloblastoma. Multiple models of SHH-driven medulloblastoma have been made; activating the developmental pathway through manipulation of different pathway effectors. One of the first models was the *Ptc1*-knockout mouse in which viable heterozygotes (*Ptc*$^{+/-}$) developed tumors at a 15% incidence[73]. This model has been significantly improved as a research tool after crossing with *Tp53*$^{-/-}$ mice, as tumor incidence increased to 100% with loss of p53[74].

Of the tumor models that alter the SHH pathway downstream of *Ptc*, the *ND2:SmoA1* model is the most widely used[75]. In these tumor-prone transgenic mice, the SHH subgroup is recapitulated in pathology and transcriptionally by the constitutive expression of the activated Smoothened transgene, *SmoA1*. The activating point mutation in *SmoA1* is the single amino acid substitution W539L, derived from a sporadic basal cell carcinoma patient exhibiting SHH pathway activation[59,76,77]. The mutation, a conversion of Trp to Leu at residue 539, alters the binding pocket where PTC adheres to permit *SmoA1*-mediated activation. Thus, the SHH pathway is activated and primarily in CGNPs as controlled by the NeuroD2 promoter, *ND2*[59,78]. In mice hemizygous for *ND2:SmoA1*, tumor incidence is about 50% over 6 months[59] while the homozygous *Smo/Smo* model has >90% incidence over 2 months[78]. Similar to these models is the Cre-driven *SmoM2* model, which expresses the constitutively active SMO-W539L mutant when activated by Cre recombinase[79]. In *Math1-Cre;SmoM2* mice, mutant SMO activates the SHH pathway in *Math1* lineage CGNPs to induce medulloblastoma with 100% incidence and with an average survival of 41 days[64]. As for *hGFAP-Cre* driven *SmoM2* tumors, the developmental pathway is activated in the stem cells that give rise to the neurons and glia of the cerebrum and cerebellum, excluding Purkinje cells[80]. These animals have 100% medulloblastoma formation with an average survival of 33 days[64]. Together, these models provide a way to study how SHH-regulated genes impact both cerebellar development and medulloblastoma tumorigenesis, resulting in new targets for clinical treatments and insight into the overall link between disordered development and cancer.

Using animal models, previous work has shown that the SHH pathway induces aerobic glycolysis during CGNP proliferation and medulloblastoma formation[81,82]. To increase aerobic glycolysis, SHH up-regulates the expression of key glycolytic enzymes, HK2 and PKM2, which catalyze virtually irreversible reactions at opposing ends of glycolysis[81,82]. Required for proper CGNP proliferation and tumor growth, as previously shown in SHH-driven medulloblastoma and glioblastoma multiforme, HK2 is a potential target to inhibit in metabolism-based clinical interventions[82–84]. The role of PKM2 in neural progenitors and tumorigenesis, however, needs to be elucidated in order to assess its potential as a therapeutic target. Identifying PKM2 as a target is particularly important as the dual targeting of direct SHH pathway effectors and an interacting non-SHH pathway (such as aerobic glycolysis) is a clinical strategy in the treatment of SHH-driven medulloblastoma. In all, studies with these models have led to the development of targeted therapies for the SHH subgroup[56] and continued work will provide the insight needed to treat the primary and recurrent tumor in new ways.

1.3 Metabolomics

1.3.1 Overview

Metabolites are low molecular weight compounds (<2 kDa), not encoded by the genome, and are produced and altered by cells under a specific state[85–87]. The *metabolome* refers to all metabolites present in and produced by an organism[86,88]. Analytical techniques that can detect changes in metabolites are critical to the study of metabolism and its role in cancer. While routinely used in other disciplines such as analytical chemistry and biochemistry, methods based on mass spectrometry (MS) and nuclear magnetic resonance (NMR) are just starting to be used by the cancer research community to study metabolism[89]. The resurgent interest in metabolomics and cancer stems from its inherent measurement of cell function and phenotype[23,86,87,89]. In contrast to the transcriptome and proteome, changes in the metabolome reflect upstream, amplified changes in genes, transcripts, and proteins such that minute differences can be quantified[90,91]. Thus, metabolomic analysis is a tool that is driven by and generates hypotheses, as knowledge of expected metabolic differences can vary. In sum, metabolic profiling by MS or NMR detects a broad range of metabolites to provide a quick snapshot of metabolism.

1.3.2 Nuclear magnetic resonance spectroscopy

NMR is a nondestructive, unbiased method to analyzing metabolites. Independently developed by Felix Bloch[92] and Edward Mills Purcell[93] in the 1940s, NMR is a technique use to determine physical, chemical, and electronic properties of molecules. NMR, the foundation for magnetic resonance imaging (MRI), uses the magnetic properties of atomic nuclei, such that any nucleus possessing a magnetic moment can be studied. After applying a strong, external magnetic field, nuclei are observed by the absorption and emission of electromagnetic radiation at a wavelength that corresponds to radiofrequencies, or megahertz (MHz) (Fig. 1.2). Zeeman levels, the induced energy differences between nuclear spin states, is relatively small in NMR compared to other techniques and reduces sensitivity[94]. Since the 1940s, NMR sensitivity has improved greatly by the use of higher magnetic fields and with the advent of Fourier transform NMR[95] and noise decoupling[96]. Together, these innovations have made ^{1}H and ^{13}C NMR robust analytical techniques.

^{1}H NMR is a analytical technique used to study biologically important metabolites in normal and malignant cells and tissues, including alanine in ovarian cancer[97] and lactate in CGNPs and medulloblastoma[82]. The proton nucleus (^{1}H) is the most sensitive nucleus for NMR besides the hydrogen isotope tritium, which has a low natural abundance and is radioactive. ^{1}H has a high natural abundance (>99%) and intrinsically high sensitivity for NMR as indicated by its high gyromagnetic ratio. The gyromagnetic ratio is the ratio of the magnetic moment to the angular moment of a particle, a constant for a given nuclei[94]. However, the application of ^{1}H NMR can be challenging, as the precise resonance frequency range (i.e., the chemical shift range) is only 8 ppm for nonexchangeable protons. The short chemical shift range limits the separation and quantification of many overlapping metabolites[94]. Thus, spectral processing methods such as line broadening correction, phase/frequency adjustment, baseline correction, and water signal removal, are required to distinguish and measure metabolites in ^{1}H NMR spectra.

^{13}C NMR analysis complements ^{1}H NMR analysis as almost all metabolites contain carbon. In contrast to the small chemical shift range of ^{1}H NMR, ^{13}C NMR has a large range (>200 ppm). ^{13}C also

has a 1.1% natural abundance and low gyromagnetic ratio, resulting in relatively low sensitivity for detection by NMR. To overcome low sensitivity, dynamic nuclear polarization (DNP) is used to increase ^{13}C NMR sensitivity by 5-fold. The concept behind DNP is to increase the polarization of nuclear spins in order to overcome the low gyromagnetic ratio. DNP is achieved in an amorphous solid state at ~1 K by coupling the nuclear spins with unpaired electrons through an organic-free radical[94]. As another way to achieve spectral sensitivity, metabolites of interest can be fractionally enriched using ^{13}C precursors. If there is enough signal, ^{13}C NMR can provide positional information with better resolution compared to ^{1}H NMR, as a simpler system with inherently fewer coupling partners[85]. Moreover, ^{13}C-labeled metabolites are detectable by ^{1}H NMR as ^{1}H-^{13}C coupling gives rise to distinct satellite peaks around the main ^{1}H peak on the spectra. Notably, ^{13}C is a naturally abundant tracer that can be studied and does not interfere with the intact metabolism of a system. Thus, ^{13}C-labeled precursors can be used in ^{1}H and ^{13}C NMR analyses to study metabolic flux, i.e. the mass balance of a system[85].

1.3.3 Metabolic footprint and fingerprint

The metabolic footprint and fingerprint of a given system are the profiles of metabolites outside and inside of the analyzed system[86]. In metabolic footprinting, the less technically-demanding process begins with tissue or cell culture in complete medium. After reaching equilibrium with cells, media are sampled and analyzed, a design that permits high-throughput studies. Media analysis is used to determine the change in metabolites consumed from and secreted into the media. The consequent metabolite profile of the media represents the effect of a specific, cellular metabolic program on the extracellular environment. For example, lactate and alanine secretion into the media are indicators of increased, intracellular glutamine metabolism in transformed cells[18]. For metabolic fingerprinting, the transformed cell extracts would be analyzed to detect changes in a wide range of metabolites at a given time. Metabolic fingerprinting detects changes from the norm to provide functional insight into a mutant cell or disease state. Interpretation of metabolic fingerprints, however, should be performed carefully and account for experimental design and limitations. For example, changes in metabolites in response to drug treatment could have several interpretations. If drug treatment increases intracellular citrate

concentration, it could mean that elevated glycolysis is replenishing intermediate pools of the Krebs cycle. Another interpretation is that decreased activity in the later reactions of the Krebs cycle is causing a backflux of intermediates such as citrate. Moreover, the increased citrate could be sourced from increased glutamine consumption in response to drug treatment. To improve clarity in metabolic fingerprinting studies, ^{13}C tracers should be used. ^{13}C precursor studies provide the added benefit of studying metabolic flux while determining metabolite concentration. Thus, in this described example, labeled glutamine or glucose would elucidate the carbon source for the increased citrate and show which metabolic pathway(s) are altered.

1.4 Figures and Legends

Figure 1.1 SHH signaling pathway

During postnatal cerebellar development, (A) CGNPs located in the EGL proliferate in response to SHH secreted by Purkinje cells. Postmitotic, premigratory CGNPs reside in the inner EGL before migrating to the IGL. In active SHH signaling, (B) the mitogen SHH binds with PTC, releasing SMO from inhibition. Active SMO initiates intracellular signal transduction to activate the GLI family of transcription factors to express target genes and support growth. SUFU is degraded and GLI can initiate transcription. EGL, external granule layer; PCL, purkinje cell layer, IGL, internal granule layer; ECM, extracellular matrix; SHH, sonic hedgehog; PTC, Patch 1; SMO, Smoothened; SUFU, suppressor of fused homolog.

Figure 1.1

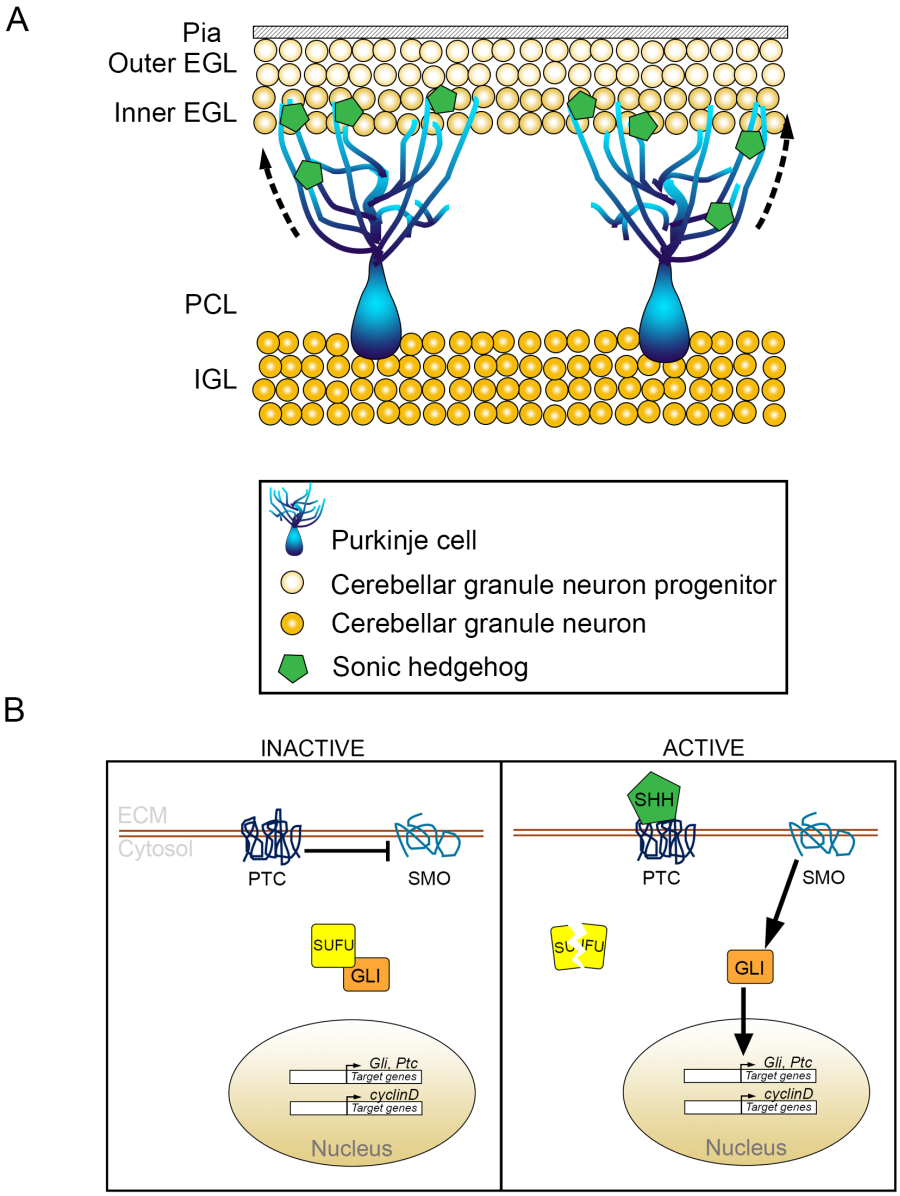
A
Pia
Outer EGL
Inner EGL
PCL
IGL
Purkinje cell
Cerebellar granule neuron progenitor
Cerebellar granule neuron
Sonic hedgehog
B
INACTIVE
ACTIVE
ECM
Cytosol
PTC
SMO
SUFU
GLI
SHH
Gli, Ptc
Target genes
cyclinD
Target genes
Nucleus

Figure 1.2 The basis of NMR

Spin-1/2 nuclei include ^{1}H and ^{13}C nuclei. As in (A), nuclei are electrically charged and have an intrinsic spin that causes them to act like a magnet. Once an external magnetic field (B_o) is applied, nuclei spin at two energy states, β and α. In the (B) higher energy state β, the nucleus spins to generate a magnetic field in the opposite direction to the applied field. In the (C) lower energy state α, the nucleus spins to generate a magnetic field that aligns with the applied field. NMR spectroscopy is the measurement of the energy difference that reads as radiofrequencies.

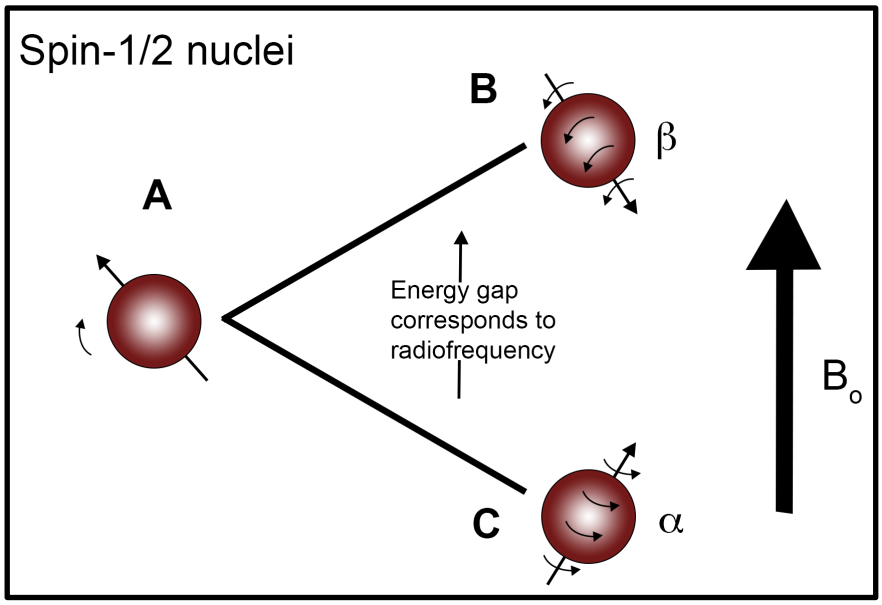

1.5 REFERENCES

1 Lunt SY, Vander Heiden MG. Aerobic Glycolysis: Meeting the Metabolic Requirements of Cell Proliferation. *Annu Rev Cell Dev Biol* 2011; **27**: 441–464.

2 Pfeiffer T, Schuster S, Bonhoeffer S. Cooperation and competition in the evolution of ATP-producing pathways. *Science* 2001; **292**: 504–507.

3 Zu XL, Guppy M. Cancer metabolism: Facts, fantasy, and fiction. *Biochem Biophys Res Commun* 2004; **313**: 459–465.

4 Racker E. Why do tumor cells have a high aerobic glycolysis? *J Cell Physiol* 1976; **89**: 697–700.

5 Lehninger AL. *Lehninger Principles of Biochemistry*. 4th ed. W.H. Freeman: New York, USA, 2005.

6 Fang M, Shen Z, Huang S, Zhao L, Chen S, Mak TW *et al.* The ER UDPase ENTPD5 promotes protein N-glycosylation, the Warburg effect, and proliferation in the PTEN pathway. *Cell* 2010; **143**: 711–724.

7 Hume A, Weidemann MJ. Role and regulation of glucose metabolism in proliferating cells. *Natl Cancer Inst* 1956; **62**: 3–8.

8 Katz J, Rognstad R. Labeling of Pentose Phosphate from Glucose-14C and Estimation of Rates of Transaldolase Transketolase Contribution of Pentose Cycle and Ribose Phosphate Synthesis. *Biochemistry* 1967; **6**: 2227–2246.

9 Lee W-NP, Boros LG, Puigjaner J, Bassilian S, Lim S, Cascante M. Mass isotopomer study of the nonoxidative pathways of the pentose cycle with [1,2-13C2]glucose. *Am J Physiol* 1998; **274**: 843–851.

10 Boros LG, Lee PWN, Brandes JL, Cascante M, Muscarella P, Schirmer WJ *et al.* Nonoxidative pentose phosphate pathways and their direct role in ribose synthesis in tumors: Is cancer a disease of cellular glucose metabolism? *Med Hypotheses* 1998; **50**: 55–59.

11 Green CD, Martin DW. A direct, stimulating effect of cyclic GMP on purified phosphoribosyl pyrophosphate synthetase and its antagonism by cyclic AMP. *Cell* 1974; **2**: 241–245.

12 Chambers DA, Martin DW, Weinstein Y. The effect of cyclic nucleotides on purine biosynthesis and the induction of PRPP synthetase during lymphocyte activation. *Cell* 1974; **3**: 375–380.

13 Hannun YA, Obeid LM. Principles of bioactive lipid signalling: lessons from sphingolipids. *Nat Rev Mol Cell Biol* 2008; **9**: 139–150.

14 Hatzivassiliou G, Zhao F, Bauer DE, Andreadis C, Shaw AN, Dhanak D *et al.* ATP citrate lyase inhibition can suppress tumor cell growth. *Cancer Cell* 2005; **8**: 311–321.

15 Menendez JA, Lupu R. Fatty acid synthase and the lipogenic phenotype in cancer pathogenesis. *Nat Rev Cancer* 2007; **7**: 763–777.

16 Abramson HN. The lipogenesis pathway as a cancer target. *J Med Chem* 2011; **54**: 5615–5638.

17 Newsholme EA, Crabtree B, Ardawi MSM. The role of high rates of glycolysis and glutamine utilization in rapidly dividing cells. *Biosci Rep* 1985; **5**: 393–400.

18 DeBerardinis RJ, Mancuso A, Daikhin E, Nissim I, Yudkoff M, Wehrli S *et al.* Beyond aerobic glycolysis: transformed cells can engage in glutamine metabolism that exceeds the requirement for protein and nucleotide synthesis. *Pnas* 2007; **104**: 19345–19350.

19 Curi R, Newsholme P, Newsholme EA. Metabolism of pyruvate by isolated rat mesenteric lymphocytes, lymphocyte mitochondria and isolated mouse macrophages. *Biochem J* 1988; **250**: 383–388.

20 Wuntch T, Chen RF, Vesell ES. Lactate Dehydrogenase Isozymes : Kinetic Properties at High Enzyme Concentrations. *Science* 2013; **167**: 63–65.

21 Warburg O. On the Origin of Cancer Cells. *Science* 1956; **123**: 309–314.

22 Moreno-Sánchez R, Rodríguez-Enríquez S, Marín-Hernández A, Saavedra E. Energy metabolism in tumor cells. *FEBS J* 2007; **274**: 1393–1418.

23 Ward PS, Thompson CB. Metabolic Reprogramming: A Cancer Hallmark Even Warburg Did Not Anticipate. *Cancer Cell* 2012; **21**: 297–308.

24 DeBerardinis RJ, Lum JJ, Hatzivassiliou G, Thompson CB. The Biology of Cancer: Metabolic Reprogramming Fuels Cell Growth and Proliferation. *Cell Metab* 2008; **7**: 11–20.

25 Zhang G, Yang P, Guo P, Miele L, Sarkar FH, Wang Z *et al.* Unraveling the mystery of cancer metabolism in the genesis of tumor-initiating cells and development of cancer. *Biochim Biophys Acta* 2013; **1836**: 49–59.

26 Hanahan D, Weinberg RA. Hallmarks of cancer: The next generation. *Cell* 2011; **144**: 646–674.

27 Mazurek S. Pyruvate kinase type M2 : A key regulator of the metabolic budget system in tumor cells. *Int J Biochem Cell Biol* 2011; **43**: 969–980.

28 Israelsen WJ, Dayton TL, Davidson SM, Fiske BP, Hosios AM, Bellinger G *et al.* PKM2 isoform-specific deletion reveals a differential requirement for pyruvate kinase in tumor cells. *Cell* 2013; **155**: 397–409.

29 Iqbal MA, Siddiqui FA, Gupta V, Chattopadhyay S, Gopinath P, Kumar B *et al.* Insulin enhances metabolic capacities of cancer cells by dual regulation of glycolytic enzyme pyruvate kinase M2. *Mol Cancer* 2013; **12**: 72–83.

30 Ikeda Y, Noguchi T. Allosteric regulation of pyruvate kinase M2 isozyme involves a cysteine residue in the intersubunit contact. *J Biol Chem* 1998; **273**: 12227–12233.

31 Israelsen WJ, Vander Heiden MG. Pyruvate kinase: Function, regulation and role in cancer. *Semin Cell Dev Biol* 2015; **43**: 43–51.

32 Anastasiou D, Yu Y, Israelsen WJ, Jiang J-K, Boxer MB, Hong BS *et al.* Pyruvate kinase M2 activators promote tetramer formation and suppress tumorigenesis. *Nat Chem Biol* 2012; **8**: 839–847.

33 Atsumi T, Chesney J, Metz C, Leng L, Donnelly S, Makita Z *et al.* High expression of inducible 6-phosphofructo-2-kinase / fructose-2,6-bisphosphatase (iPFK-2; PFKFB3) in human cancers. *Cancer Res* 2002; **62**: 5881–5887.

34 Baysal BE, Ferrell RE, Willett-brozick JE, Lawrence EC, Myssiorek D, Bosch A *et al.* Mutations in SDHD, a mitochondrial complex II gene, in hereditary paraganglioma. *Science* 2000; **287**: 848–851.

35 Tomlinson IPM, Alam NA, Rowan AJ, Barclay E, Jaeger EEM, Kelsell D *et al.* Germline mutations in FH predispose to dominantly inherited uterine fibroids, skin leiomyomata and papillary renal cell cancer. *Nat Genet* 2002; **30**: 406–410.

36 Parsons DW, Jones S, Zhang X, Lin JC, Leary RJ, Angenendt P *et al.* An Integrated Genomic Analysis of HUman Glioblastoma Multiforme. *Science* 2008; **321**: 1807–1812.

37 Sjoblom T, Jones S an, Wood LD, Parsons DW, Lin J, Barber TD *et al.* The consensus coding sequences of human breast and colorectal cancers. *Science* 2006; **314**: 268–274.

38 Yen KE, Bittinger M a, Su SM, Fantin VR. Cancer-associated IDH mutations: biomarker and therapeutic opportunities. *Oncogene* 2010; **29**: 6409–6417.

39 Pauwels EKJ, Sturm EJC, Bombardieri E, Cleton FJ, Stokkel MPM. Positron-emission tomography with [18F]fluorodeoxyglucose. *J Cancer Res Clin Oncol* 2000; **126**: 549–559.

40 Gatenby RA, Gillies RJ. Glycolysis in cancer: A potential target for therapy. *Int J Biochem Cell Biol* 2007; **39**: 1358–1366.

41 Tennant D a, Durán R V, Gottlieb E. Targeting metabolic transformation for cancer therapy. *Nat Rev Cancer* 2010; **10**: 267–277.

42 Singh D, Banerji AK, Dwarakanath BS, Tripathi RP, Gupta JP, Mathew TL *et al.* Optimizing Cancer Radiotherapy with 2-Deoxy-D-Glucose. *Strahlentherapie und Onkol* 2005; **181**: 507–514.

43 Kim EH, Lee J-H, Oh Y, Koh I, Shim J-K, Park J *et al.* Inhibition of glioblastoma tumorspheres by combined treatment with 2-deoxyglucose and metformin. *Neuro Oncol* 2016; : now174.

44 Lin H, Zeng J, Xie R, Schulz MJ, Tedesco R, Qu J *et al.* Discovery of a Novel 2,6-Disubstituted Glucosamine Series of Potent and Selective Hexokinase 2 Inhibitors. *ACS Med Chem Lett* 2016; **7**: 217–222.

45 Paterson E, Farr RF. Cerebellar Medulloblastoma: Treatment by Irradiation of the whole central nervous system. *Acta radiol* 1952; **39**: 323–336.

46 Hirsch JF, Renier D, Czernichow P, Benveniste L, Pierre-Kahn A. Medulloblastoma in Childhood. Survival and Functional Results. *Acta Neurochir (Wien)* 1979; **48**: 1–15.

47 Park TS, Hoffman HJ, Hendrick EB, Humphreys RP, Becker LE. Medulloblastoma: clinical presentation and management. *J Neurosurg* 1983; **58**: 543–552.

48 Packer RJ, Sutton LN, Elterman R, Lange B, Goldwein J, Nicholson HS *et al.* Outcome for children with medulloblastoma treated with radiation and cisplatin, CCNU, and vincristine chemotherapy. *J Neurosurg* 1994; **81**: 690–698.

49 Packer RJ, Goldwein J, Nicholson HS, Vezina LG, Allen JC, Ris MD *et al.* Treatment of Children With Medulloblastomas With Reduced-Dose Craniospinal Radiation Therapy and Adjuvant Chemotherapy : A Children ' s Cancer Group Study. *J Clin Oncol* 1999; **17**: 2127–2136.

50 Packer RJ, Gajjar A, Vezina G, Rorke-Adams L, Burger PC, Robertson PL *et al.* Phase III study of craniospinal radiation therapy followed by adjuvant chemotherapy for newly diagnosed average-risk medulloblastoma. *J Clin Oncol* 2006; **24**: 4202–8.

51 Gajjar A, Chintagumpala M, Ashley D, Kellie S, Kun LE, Merchant TE *et al.* Risk-adapted craniospinal radiotherapy followed by high-dose chemotherapy and stem-cell rescue in children with newly diagnosed medulloblastoma (St Jude Medulloblastoma-96): long-term results from a prospective, multicentre trial. *Lancet Oncol* 2006; **7**: 813–20.

52 Johnson DL, McCabe MA, Nicholson HS, Joseph AL, Getson PR, Byrne J *et al.* Quality of long-term survival in young children with medulloblastoma. *J Neurosurg* 1994; **80**: 1004–1010.

53 Duffner PK. Long-term effects of radiation therapy on cognitive and endocrine function in children with leukemia and brain tumors. *Neurologist* 2004; **10**: 293–310.

54 Kool M, Korshunov A, Remke M, Jones DTW, Schlanstein M, Northcott PA *et al.* Molecular subgroups of medulloblastoma: an international meta-analysis of transcriptome, genetic aberrations, and clinical data of WNT, SHH, Group 3, and Group 4 medulloblastomas. *Acta Neuropathol* 2012; **123**: 473–484.

55 Northcott PA, Korshunov A, Witt H, Hielscher T, Eberhart CG, Mack S *et al.* Medulloblastoma comprises four distinct molecular variants. *J Clin Oncol* 2011; **29**: 1408–1414.

56 Northcott PA, Korshunov A, Pfister SM, Taylor MD. The clinical implications of medulloblastoma subgroups. *Nat Rev Neurol* 2012; **8**: 340–351.

57 Northcott P a., Shih DJH, Peacock J, Garzia L, Sorana Morrissy a., Zichner T *et al.* Subgroup-specific structural variation across 1,000 medulloblastoma genomes. *Nature* 2012; **488**: 49–56.

58 Northcott P a, Dubuc AM, Pfister S, Taylor MD. Molecular subgroups of medulloblastoma. *Expert Rev Neurother* 2012; **12**: 871–884.

59 Hallahan AR, Pritchard JI, Hansen S, Benson M, Stoeck J, Hatton BA *et al.* The SmoA1 Mouse Model Reveals That Notch Signaling Is Critical for the Growth and Survival of Sonic Hedgehog-Induced Medulloblastomas. *Cancer Res* 2004; **21**: 7794–7800.

60 Hatten ME, Alder J, Zimmerman K, Heintz N. Genes involved in cerebellar cell specification and differentiation. *Curr Opin Neurobiol* 1997; **7**: 40–47.

61 Dahmane N, Ruiz i Altaba A. Sonic hedgehog regulates the growth and patterning of the cerebellum. *Development* 1999; **126**: 3089–3100.

62 Vaillant C, Monard D. SHH pathway and cerebellar development. *Cerebellum* 2009; **8**: 291–301.

63 Hatten ME, Roussel MF. Development and cancer of the cerebellum. *Trends Neurosci* 2011; **34**: 134–42.

64 Schüller U, Heine VM, Mao J, Kho AT, Dillon AK, Han Y-G *et al.* Acquisition of granule neuron precursor identity is a critical determinant of progenitor cell competence to form Shh-induced medulloblastoma. *Cancer Cell* 2008; **14**: 123–134.

65 Yang Z-J, Ellis T, Markant SL, Read T-A, Kessler JD, Bourboulas M *et al.* Medulloblastoma can be initiated by deletion of Patched in lineage-restricted progenitors or stem cells. *Cancer Cell* 2008; **14**: 135–145.

66 Wechsler-Reya RJ, Scott MP. Control of Neuronal Precursor Proliferation in the Cerebellum by Sonic Hedgehog. *Neuron* 1999; **22**: 103–114.

67 Kenney AM, Rowitch DH. Sonic hedgehog Promotes G1 Cyclin Expression and Sustained Cell Cycle Progression in Mammalian Neuronal Precursors. *Mol Cell Biol* 2000; **20**: 9055–9067.

68 Ciemerych M a, Kenney AM, Sicinska E, Kalaszczynska I, Bronson RT, Rowitch DH *et al.* Development of mice expressing a single D-type cyclin. *Genes Dev* 2002; **16**: 3277–3289.

69 Zurawel RH, Allen C, Wechsler-Reya R, Scott MP, Raffel C. Evidence that haploinsufficiency of Ptch leads to medulloblastoma in mice. *Genes Chromosomes Cancer* 2000; **28**: 77–81.

70 Zurawel RH, Allen C, Chiappa S, Cato W, Biegel J, Cogen P *et al.* Analysis of PTCH/SMO/SHH pathway genes in medulloblastoma. *Genes Chromosomes Cancer* 2000; **27**: 44–51.

71 Taylor MD, Liu L, Raffel C, Hui C, Mainprize TG, Zhang X *et al.* Mutations in SUFU predispose to medulloblastoma. *Nat Genet* 2002; **31**: 306–310.

72 Reifenberger J, Wolter M, Weber RG, Megahed M, Ruzicka T, Lichter P *et al.* Missense mutations in SMOH in sporadic basal cell carcinomas of the skin and primitive neuroectodermal tumors of the central nervous system. *Cancer Res* 1998; **58**: 1798–1803.

73 Goorich L V, Milenkovic L, Higgins KM, Scott M. Altered neural cell fates and medulloblastoma in mouse patched mutants. *Science* 1997; **277**: 1109–1113.

74 Wetmore C, Eberhart DE, Curran T. Loss of p53 but not ARF accelerates medulloblastoma in mice heterozygous for patched. *Cancer Res* 2001; **61**: 513–516.

75 Markant SL, Wechsler-Reya RJ. Personalized mice: Modelling the molecular heterogeneity of medulloblastoma. *Neuropathol Appl Neurobiol* 2012; **38**: 228–240.

76 Xie J, Murone M, Luoh S-M, Ryan A, Gu Q, Zhang C *et al.* Activating Smoothened mutations in sporadic basal-cell carcinoma. *Nature* 1998; **391**: 90–92.

77 Taipale J, Chen JK, Cooper MK, Wang B, Mann RK, Milenkovic L *et al.* Effects of oncogenic mutations in Smoothened and Patched can be reversed by cyclopamine. *Nature* 2000; **406**: 1005–1009.

78 Hatton BA, Villavicencio EH, Tsuchiya KD, Pritchard JI, Ditzler S, Pullar B *et al.* The Smo/Smo model: Hedgehog-induced medulloblastoma with 90% incidence and leptomeningeal spread. *Cancer Res* 2008; **68**: 1768–1776.

79 Mao J, Ligon KL, Rakhlin EY, Thayer SP, Bronson RT, Rowitch D *et al.* A Novel Somatic Mouse Model to Survey Tumorigenic Potential Applied to the Hedgehog Pathway. *Cancer Res* 2006; **66**: 10171–10178.

80 Zhuo L, Theis M, Alvarez-Maya I, Brenner M, Willecke K, Messing A. hGFAP-cre transgenic mice for manipulation of glial and neuronal function in vivo. *Genesis* 2001; **31**: 85–94.

81 Bhatia B, Potts CR, Guldal C, Choi S, Korshunov A, Pfister S *et al.* Hedgehog-mediated regulation of PPARγ controls metabolic patterns in neural precursors and shh-driven medulloblastoma. *Acta Neuropathol* 2012; **123**: 587–600.

82 Gershon TR, Crowther AJ, Tikunov A, Garcia I, Annis R, Yuan H *et al.* Hexokinase-2-mediated aerobic glycolysis is integral to cerebellar neurogenesis and pathogenesis of medulloblastoma. *Cancer Metab* 2013; **1**: 1–17.

83 Gershon TR, Crowther AJ, Liu H, Miller CR, Deshmukh M. Cerebellar granule neuron progenitors are the source of Hk2 in the postnatal cerebellum. *Cancer Metab* 2013; **1**: 15–16.

84 Wolf A, Agnihotri S, Munoz D, Guha A. Developmental profile and regulation of the glycolytic enzyme hexokinase 2 in normal brain and glioblastoma multiforme. *Neurobiol Dis* 2011; **44**: 84–91.

85 Tikunov AP, Winnike JH, Tech K, Jeffries RE, Semelka C, Martin J *et al.* Fluxomics by NMR spectroscopy from cells to organisms focusing on liver. *Curr Metabolomics* 2013; **1**: 1–32.

86 Goodacre R, Vaidyanathan S, Dunn WB, Harrigan GG, Kell DB. Metabolomics by numbers: Acquiring and understanding global metabolite data. *Trends Biotechnol* 2004; **22**: 245–252.

87 Rochfort S. Biology and Implications for Natural Products Research. *J Nat Prod* 2005; **68**: 1813–1820.

88 Oliver S. Systematic functional analysis of the yeast genome. *Trends Biotechnol* 1998; **16**: 373–378.

89 Patel S, Ahmed S. Emerging field of metabolomics: Big promise for cancer biomarker identification and drug discovery. *J Pharm Biomed Anal* 2015; **107**: 63–74.

90 Raamsdonk LM, Teusink B, Broadhurst D, Zhang N, Hayes A, Walsh MC *et al.* A functional genomics strategy that uses metabolome data to reveal the phenotype of silent mutations. *Nat Biotechnol* 2001; **19**: 45–50.

91 Urbanczyk-Wochniak E, Luedemann A, Kopka J, Selbig J, Roessner-Tunali U, Willmitzer L *et al.* Parallel analysis of transcript and metabolic profiles: a new approach in systems biology. *EMBO Rep* 2003; **4**: 989–993.

92 Freeman R. A short history of NMR. *Chem Heterocycl Compd* 1995; **31**: 1004–1005.

93 Purcell E, Torrey H, Pound R. Resonance Absorption by Nuclear Magnetic Moments in a Solid. *Phys Rev* 1946; **69**: 37–38.

94 Fan TW-M, Lane AN, Higashi RM (eds.). *The Handbook of Metabolomics*. Springer: New York, NY, 2012 doi:10.1007/978-1-61779-618-0.

95 Ernst RR, Anderson WA. Application of fourier transform spectroscopy to magnetic resonance. *Rev Sci Instrum* 1966; **37**: 93–102.

96 Ernst RR. Nuclear magnetic double resonance with an incoherent radio-frequency field. *J Chem Phys* 1966; **45**: 3845–3861.

97 Odunsi K, Wollman RM, Ambrosone CB, Hutson A, McCann SE, Tammela J *et al.* Detection of epithelial ovarian cancer using 1H-NMR-based metabonomics. *Int J Cancer* 2005; **113**: 782–788.

CHAPTER II: PYRUVATE KINASE INHIBITS PROLIFERATION DURING POSTNATAL CEREBELLAR NEUROGENESIS AND SUPPRESSES MEDULLOBLASTOMA FORMATION

2.1 Overview

Aerobic glycolysis supports proliferation in development and cancer through unresolved mechanisms. Aerobic glycolysis is integral to cerebellar neurogenesis and medulloblastoma, a malignant cerebellar tumor. Blocking glycolysis in cerebellar granule neuron progenitors (CGNPs) by deleting *Hexokinase-2* (*Hk2*) disrupts proliferation and restricts medulloblastoma growth. In contrast, we now show that inhibiting the later stages of glycolysis by disrupting *Pyruvate kinase-M* (*Pkm*) increases CGNP proliferation and medulloblastoma growth. Differentiated neurons splice *Pkm* to the more active PKM1 isoform while neural progenitors and medulloblastomas exclusively express the less active PKM2. Isoform-specific *Pkm2* deletion in CGNPs ablated PKM2 without inducing compensatory PKM1, resulting in reduced glycolysis and increased progenitor proliferation. Moreover, *Pkm2* deletion accelerated tumor formation in medulloblastoma-prone *ND2:SmoA1* mice. Thus PKM2 is not required for neural progenitor proliferation or tumorigenesis. Rather, the loss of pyruvate kinase releases cells from growth inhibition. We show that aerobic glycolysis supports growth through steps upstream of pyruvate kinase.

2.2 Introduction

Increased aerobic glycolysis is a common feature of proliferating cells during developmental and malignant growth[1–3]. CGNPs are transit amplifying cells that proliferate in the postnatal brain[4,5] and utilize aerobic glycolysis during normal brain development[6]. CGNP proliferation is strictly regulated; excessive CGNP growth and delayed maturation promote the formation of medulloblastoma, the most common malignant pediatric brain tumor[7–9]. Medulloblastomas co-opt developmentally-regulated programs of CGNPs[10,11], including the metabolic phenotype of increased aerobic glycolysis[6,12]. Determining how

aerobic glycolysis supports CGNP proliferation and medulloblastoma tumorigenesis may provide new insight into both neurodevelopmental disorders and cancer biology.

During postnatal brain development, CGNPs proliferate in the cerebellum in response to locally secreted Sonic Hedgehog (SHH), generating the largest neuron population in the mammalian brain[13–16]. In synchrony with increased proliferation, SHH signaling in CGNPs induces Hexokinase-2 (HK2) expression and aerobic glycolysis[6,12]. 30% of medulloblastoma patients show SHH-pathway activation[17–19] and mice with activating SHH-pathway mutations develop spontaneous medulloblastomas that recapitulate the human disease[20–22]. These tumors, like CGNPs, up-regulate HK2 and aerobic glycolysis. Examining CGNP proliferation and SHH-driven tumorigenesis in mice provides an *in vivo* model for determining how aerobic glycolysis supports developmental and malignant growth.

We have previously shown that conditional deletion of *Hk2* in the developing brain blocks SHH-induced aerobic glycolysis, disrupts the typical pattern of CGNP differentiation, and reduces medulloblastoma growth, extending the survival of medulloblastoma-prone mice[6]. These findings suggest that blocking glycolysis through HK2 inhibition may produce a clinically significant anti-tumor effect. Development of HK2 inhibitors for anti-cancer therapy however, has been problematic[23]. Furthermore, while the effects of HK2 inhibition demonstrate the importance of aerobic glycolysis in development and cancer, the specific glycolytic reactions or products that support proliferation have not been identified. To better characterize how glycolysis supports physiologic and malignant proliferation, we investigated the role of pyruvate kinase in cerebellar growth and medulloblastoma.

While HK2 catalyzes the first step in glycolysis[24], pyruvate kinase catalyzes the final step in the pathway, converting phosphoenolpyruvate (PEP) and ADP into pyruvate and ATP[25]. *Pkm* is the pyruvate kinase gene expressed in most tissues including the central nervous system[26]. Alternative splicing of a single exon from *Pkm* gives rise to either *Pkm1*, which includes exon 9, or *Pkm2*, which replaces exon 9 with exon 10[27]. PKM1 is expressed in differentiated tissues and is a constitutively active enzyme, while PKM2 is commonly expressed in cancer and has activity that is subject to regulation[28–34]. Fructose-1,6-bisphosphate (FBP), an upstream intermediate in glycolysis, regulates PKM2 by stabilizing the enzyme as a tetramer. This tetrameric conformation is comparable to the constitutively active PKM1

tetramer[26,33,34]. PKM2 activation can be suppressed by interaction with tyrosine-phosphorylated proteins in response to growth factor receptor signaling[31,33,35]. The ability to regulate PKM2 through both endogenous allosteric effectors and intracellular signaling pathways may allow proliferating cells to adjust their metabolism to meet dynamic cellular requirements[29].

Because PKM2 is the pyruvate kinase isoform expressed in most cancers, it has been suggested as a potential target for anti-cancer therapy. Xenograft tumors engineered to overexpress either PKM1 or PKM2 showed that PKM2 isoform expression confers a growth advantage[36]. Other studies have reported nonmetabolic, growth-promoting functions such as transcriptional regulation[37,38] and histone phosphorylation[30,39–41], however, whether PKM2 can act as a protein kinase is controversial[42]. Moreover, the oncogenic potential of *Pkm2* was challenged by the finding that the isoform-specific deletion of PKM2 accelerates tumorigenesis in a mouse model of breast cancer[43], and promotes late-onset liver cancer in mice[44].

In the brain, PKM2 has been reported to be induced by SHH in CGNPs and expressed in the *ND2:SmoA1* mouse model of medulloblastoma[12,45], suggesting a role in SHH-driven growth. PKM2 up-regulation has also been noted in MYC-amplified Group 3 medulloblastomas[46], suggesting a role for PKM2 in tumor growth across medulloblastoma subgroups. Here, we analyzed how conditional *Pkm2* deletion in CGNPs alters metabolism, proliferation, and medulloblastoma tumorigenesis. *Pkm2* deletion, like *Hk2*, decreased glycolysis. In contrast to *Hk2*-deleted mice, however, *Pkm2*-deleted animals showed increased CGNP growth and accelerated medulloblastoma formation. The differential effects of impeding aerobic glycolysis through deletion of *Hk2* or *Pkm2* point to the glycolytic steps upstream of pyruvate kinase as critical to promoting proliferation.

2.3 Results

2.3.1 Pkm isoform expression in the brain mirrors differentiation status

We found a dichotomous pattern of *Pkm* splicing in the postnatal brain, with PKM2 expressed by undifferentiated neural progenitors, and PKM1 expressed by neurons. Immunohistochemistry (IHC)

showed PKM1 expression in differentiated neurons throughout the brain and absence of PKM1 in progenitor regions, including the cerebellar external granule layer (EGL), the hippocampus, and the subventricular zone/rostral migratory stream (SVZ/RMS) (Fig. 2.1A). In contrast, the neural progenitors of the EGL, the hippocampus, and the SVZ/RMS specifically expressed PKM2 and not PKM1 (Fig. 2.1B).

In the postnatal cerebellum, neural progenitor proliferation peaks at P7 then wanes, ending by P15, as CGNPs exit the cell cycle, migrate to the internal granule layer (IGL), and differentiate into cerebellar granule neurons (CGNs)[4,11,47]. Western blot of whole cerebellum lysates showed that PKM2, like the proliferation marker Cyclin D2 (CCND2), decreased between P7 and P15, while PKM1 conversely increased (Fig. 2.1C). PKM2 expression, however, was not limited to proliferating cells; both proliferating PCNA+ CGNPs in the outer layer of the EGL (oEGL), and differentiating PCNA- CGNPs of the inner EGL (iEGL) expressed PKM2 (Fig. 2.1D). Similarly, in the SVZ/RMS, both PCNA+ and PCNA- progenitors expressed PKM2 (Fig. 2.1E). Thus, PKM2 marked undifferentiated brain progenitors, whether proliferating or quiescent, while PKM1 marked differentiated neurons.

To determine if medulloblastomas, like CGNPs, exclusively expressed PKM2, we analyzed PKM isoform expression in transgenic, medulloblastoma-prone *ND2:SmoA1* mice. *ND2:SmoA1* mice express a mutant, constitutively active allele of *Smo*, driven by the *NeuroD2* promoter. In CGNPs of *ND2:SmoA1* mice, cell autonomous SHH activation prolongs proliferation beyond P15. These mice develop medulloblastoma with incomplete penetrance after a variable latency[20]. During this latent period, CGNPs continue to proliferate as premalignant lesions within the EGL, generating progeny that differentiate, undergo apoptosis, or remain proliferative.

We found that CGNPs in the premalignant lesions of P60 *ND2:SmoA1* mice expressed PKM2 and not PKM1 (Fig. 2.1F). Similarly, medulloblastomas that arose from these premalignant lesions consistently and homogeneously expressed PKM2, while adjacent, normal brain expressed PKM1 (Fig. 2.1G). Thus, PKM2 expression persisted as undifferentiated CGNPs gave rise to SHH-driven medulloblastoma.

We compared the expression of PKM1 and PKM2 mRNA in human medulloblastoma samples analyze by RNA-seq. As in the mouse model, we found exclusive expression of PKM2, with minimal

expression of PKM1 in all four medulloblastoma subgroups (Fig. 2.1H). Together, our studies of mouse and human tumors show that PKM2 expression in the mouse model recapitulates the distinct pattern of PKM expression in medulloblastoma patients.

2.3.2 SHH stimulates PKM2 expression

To examine the effect of SHH signaling on PKM1/2 expression, we isolated CGNPs and compared PKM isoform expression in the presence or absence of SHH ligand. We identified cells at S-phase by adding 5-ethynyl-2'-deoxyuridine (EdU) to CGNP cultures 1h before fixation. EdU+ cells and PKM2+ cells were more numerous in SHH-treated wells (Fig. 2.2A; cyan arrows) compared SHH-deprived controls (Fig. 2.2B; arrows). In SHH-treated wells, PKM2 was detected in both EdU+ and EdU- cells (Figs. 2.2A,B; white arrowheads). Consistent with the absence of PKM1 expression in the EGL, no CGNPs in either condition showed a detectable level of PKM1; rare cells that were PKM1 positive did not have the size and shape characteristic of CGNPs (Figs. 2.2C,D). These data show that SHH sustained PKM2 expression in CGNPs, while PKM1 expression remained low as SHH-deprived CGNPs exited the cell cycle.

We used Western blot to compare PKM1 and PKM2 expression between CGNPs cultured with or without SHH ligand or with SHH ligand plus the *Smo* inhibitor vismodegib (vismo)[48]. As an indicator of SHH-driven proliferation, we also measured the expression of CCND2 protein. As expected, SHH-treated CGNPs expressed 5.5-fold more CCND2 compared to CGNPs without SHH (Fig. 2.2E). SHH-treated CGNPs expressed 2-fold more PKM2 (Fig. 2.2E). The low level of PKM1 expression that did not localize to CGNPs by immunostaining was also significantly increased by SHH (Fig. 2.2E). However, while SHH inhibition by vismo decreased CCND2 by 30%, the effects of vismo on PKM1 and PKM2 were relatively small and not statistically significant (Fig. 2.2E). These data show that the expression of both PKM2 and CCND2 was up-regulated by SHH. Compared to *CcnD2*, however, *Pkm* was markedly less responsive to changes in SHH signaling, suggesting that *Pkm*, unlike *CcnD2,* is not a direct SHH target[15].

2.3.3 Pyruvate kinase activity in CGNPs is increased by growth stimulation

SHH and IGF receptor (IGFR) signaling converge to regulate aerobic glycolysis in CGNPs[6]. Tyrosine kinase signaling, and specifically insulin signaling, can down-regulate the enzymatic activity of PKM2 in diverse cell lines[33,49,50]. While CGNPs are typically cultured with insulin-rich N2 supplement to improve cell viability[51], we have previously shown that CGNPs can be cultured in the absence of N2 for 24h, reducing IGFR activation without compromising survival[6]. We maintained CGNPs in the presence or absence of SHH or N2, to determine the effect of SHH and IGFR stimulation on CGNP pyruvate kinase activity.

We found that withholding either SHH[6] or N2 similarly reduced glycolysis, detected by reduced lactate production (Fig. 2.2F). We measured pyruvate kinase activity in lysates of CGNPs cultured with or without SHH or N2 by quantifying the conversion of exogenous PEP to pyruvate. CGNPs maintained with SHH + N2 showed significantly higher pyruvate kinase activity compared to either SHH without N2 or N2 without SHH (Figs. 2.2G,H). These findings show that CGNP pyruvate kinase activity, like PKM expression, was responsive to extracellular signaling, and was maximal with SHH/IGFR co-activation. While reduced pyruvate kinase activity has been correlated with growth factor stimulation in cancer cells[31,35,36], in CGNPs, developmentally-relevant growth factors increased pyruvate kinase expression, pyruvate kinase activity, and aerobic glycolysis.

2.3.4 *Pkm2* deletion is not replaced by *Pkm1* in brain progenitors

To determine the developmental significance of PKM function and splicing in CGNPs, we examined the effect of conditionally deleting *Pkm* exon 10, the exon that is differentially included in PKM2 and excluded from PKM1[27]. We crossed *Math1-Cre* mice, which express Cre recombinase in CGNPs[52,53], with $Pkm2^{fl}$ mice that harbor loxP sites flanking exon 10 of *Pkm*[43]. The resulting *Math1-Cre;* $Pkm2^{fl/fl}$ mice ($Pkm2^{cKO}$) mice were viable and fertile with no overt neurologic deficits. Examination of the $Pkm2^{cKO}$ cerebellum showed normal foliation and cellular organization, with an EGL that showed no detectable PKM2 (Fig. 2.3A,B). *Pkm2* deletion did not induce PKM1 in CGNPs, but increased PKM1 expression in

CGNs, the terminally differentiated CGNP progeny (Fig. 2.3A, inset). Consistent with these changes, Western blot of whole P7 cerebellum lysates showed reduced PKM2 and increased PKM1 in *Pkm2*^{cKO} mice compared to no-Cre littermate controls (Fig. 2.3C). In whole cerebellum lysates, pyruvate kinase activity was equivalent in *Pkm2*^{cKO} and littermate controls (Fig. 2.3D). In CGNPs, however, *Pkm2* deletion blocked all detectable PKM expression.

During the breeding of *Pkm2*^{cKO} mice, we noted an unanticipated tendency for germline recombination of the *Pkm2*^{fl} allele. This recombination event was detected as a smaller than expected PCR product when primers flanking *Pkm* exon 10 were used to amplify genomic DNA extracted from toe cuts. While these primers were separated by 605 bp in the *Pkm2*$^{fl/fl}$ allele and 560 bp in the *Pkm2*$^{+/+}$ allele, we found pups in several litters that generated 220 bp PCR products consistent with the recombined allele (Fig. 2.S1A). Sequencing of this band demonstrated that intron 9-10 and 10-11 were brought together, separated by a single loxP site, consistent with Cre-mediated excision of exon 10 from *Pkm*[43] (Fig. 2.S1B). Germline recombination has been observed when *Pkm2*^{fl} mice were crossed with other non-germline Cre drivers (M. Vander Heiden, unpublished), suggesting that *Pkm* exon 10 deletion may be positively selected in the germline. The recombined allele (*Pkm2*^{null}) was heritable and *Pkm2*$^{null/null}$ mice were viable and fertile without overt neurologic abnormalities, consistent with the published *Pkm2* null phenotype[44]. Although *Pkm2* null mice have been reported to develop spontaneous hepatocellular carcinoma after 55 weeks[44], we did not observe any spontaneous tumor formation in our *Pkm2*$^{null/null}$ aged for up to 1 year. In *Pkm2*$^{null/null}$ mice, PKM2 was absent from all brain progenitor regions and endothelial cells, while PKM1 was appropriately limited to differentiated neurons (Fig. 2.S1C,D). Like *Pkm2*^{cKO} mice, *Pkm2*$^{null/null}$ mice showed normal brain anatomy.

2.3.5 *Pkm2* deletion increases CGNP proliferation

Although *Pkm2*^{cKO} cerebella had normal organization, quantitative analysis showed that CGNP proliferation was increased compared to PKM2-intact littermate controls without Cre. We analyzed proliferation dynamics *in vivo*, by injecting EdU at P6 into *Pkm2*^{cKO} and *Pkm2*$^{fl/fl}$ littermates without Cre, then harvesting cerebella 24h later and staining tissue sections for EdU and the CGNP differentiation

marker $p27^{Kip1}$. Both genotypes showed EdU in p27+ and p27- cells in the EGL (Figs. 2.4A,B). While the fraction of EdU+ cells was similar between genotypes (Fig. 2.4C), we noted a trend toward reduced $p27^{Kip1}$+ cells in the EGL of *Pkm2*^{cKO} mice (Fig. 2.4D). Quantification of double labeling demonstrated that EdU+ CGNPs that were $p27^{Kip1}$-, and thus in a proliferative state, were more numerous in the EGL of *Pkm2*^{cKO} mice (Fig. 2.4E). Conversely, the fraction of $p27^{Kip1}$+ CGNPs that were EdU- was lower in the EGL of *Pkm2*^{cKO} mice, indicating that in these mice, a greater proportion of the differentiating CGNPs had been proliferating 24h earlier (Fig. 2.4F). *In vitro* studies provided additional evidence of increased proliferation with *Pkm2* deletion. CGNPs explanted from *Pkm2*^{cKO} mice showed a higher fraction of EdU+ cells after a 1h pulse, compared to CGNPs explanted from littermate controls (Fig. 2.4G).

Consistent with the increased proliferation of *Pkm2*^{cKO} CGNPs, analysis of equivalent midline cerebellar sections showed that *Pkm2*^{cKO} cerebella contained significantly more cells (CGNPs and CGNs) compared to littermate controls (Fig. 2.4H). We did not detect a significant difference in the ratio of EGL to IGL between the two genotypes however (Fig. 2.4I), indicating that *Pkm2* deletion did not prevent CGNPs from progressing through their normal differentiation trajectory. Taken together, our data show that *Pkm2* deletion blocks PKM expression in CGNPs, with the effects of increasing proliferation and reducing cell cycle exit, without altering cell fate.

2.3.6 *Pkm2* deletion inhibits the catabolism of glucose to lactate

We used a non-biased, metabolomic approach to determine the effect of *Pkm2* deletion and consequent loss of PKM function on CGNP metabolism. We isolated CGNPs from P5 *Pkm2*^{cKO} and littermate control pups and cultured them in three replicate wells *in vitro* for 24h in media in which [1,6-^{13}C] glucose was substituted for unlabeled glucose. We analyzed media metabolites from each replicate well for each condition at 0 and 24h using NMR spectroscopy followed by orthogonal partial least squares discriminant analysis to identify metabolites that varied consistently across genotypes (Table 1).

Lactate production was significantly reduced in *Pkm2*^{cKO} CGNPs compared to controls (Fig. 2.5A), and lactate was the only analyzed media metabolite that showed a change over time that was

significantly different between genotypes (Table 1). We confirmed that *Pkm2*^{cKO} CGNPs produced less lactate by measuring media lactate concentrations over time in a replicate set of wells by colorimetric assay (Fig. 2.5B). Thus *Pkm2* deletion, like *Hk2* deletion, impaired the conversion of glucose to lactate in CGNPs. Together with our findings that *Pkm2*^{cKO} CGNPs have increased proliferation and *Hk2*-deleted CGNPs have premature differentiation[6], these studies show that blocking glycolysis at different steps (hexokinase versus pyruvate kinase) produces markedly different developmental effects.

Pkm2^{cKO} CGNPs demonstrated detectable but decreased ^{13}C incorporation into lactate (Figs. 2.5C,D). The reduced fractional enrichment of lactate in *Pkm2*-deleted CGNPs is consistent with less efficient conversion of PEP to pyruvate. However, these data also demonstrate that glucose carbons can flow into lactate in the absence of PKM1 and PKM2.

To determine effect of *Pkm2* deletion on the intracellular disposition of glucose in CGNPs, we analyzed ^{13}C incorporation in cell extracts by liquid chromatography-mass spectrometry (LC-MS). LC-MS detected diverse small molecules that did not show significantly different distributions between genotypes, although we noted a trend toward increased choline in *Pkm2*^{cKO} CGNPs, consistent with their increased proliferation (Fig. 2.5E). We were able to detect ^{13}C-labeling in glutamate, indicative of flow through the Krebs cycle, and in the ribose component of ATP, ADP and AMP, indicative of flow through the pentose phosphate pathway (PPP) (Fig. 2.6).

Relative to *Pkm2*^{cKO} CGNPs, *Pkm2*-intact controls produced significantly more glutamate with 3 or more ^{13}C atoms incorporated (Fig. 2.6). The incorporation of multiple ^{13}C atoms from [1,6-^{13}C] glucose requires both conversion of pyruvate to acetyl-CoA and multiple turns of the Krebs cycle (Fig. 2.S2). The increased glutamate enrichment with 3 or 4 incorporated ^{13}C atoms in controls indicates that a higher proportion of glucose-derived metabolites remained in the Krebs cycle. In contrast, less glutamate labeling in *Pkm2*^{cKO} CGNPs demonstrates increased channeling of glucose-derived metabolites out of the Krebs cycle.

Both genotypes demonstrated ^{13}C incorporation into ribose. LC-MS demonstrated labeled parent masses of ATP, ADP, and AMP that fragmented into unlabeled adenine and ^{13}C-labeled ribose. These data demonstrate active flow through the PPP. However, we did not detect a robust difference in PPP flux

between genotypes (Fig. 2.6). These data show that the presence or absence of PKM2 did not profoundly alter the generation of ribose from glucose.

Our data do not identify the reactions that bypass the conversion of PEP to pyruvate catalyzed by pyruvate kinase. However, the incorporation of ^{13}C into glutamate and lactate shows that *Pkm2*-deleted CGNPs are able to metabolize glucose into 2- and 3- carbon species at a reduced but detectable rate, while maintaining comparable flow through the PPP. Thus *Pkm2* deletion impedes PEP dephosphorylation and redirects glucose-derived metabolites away from both lactate generation and retention in the Krebs cycle.

2.3.7 Medulloblastoma tumorigenesis is exacerbated by loss of PKM2

We examined the functional consequence of *Pkm2* deletion on SHH-driven medulloblastoma tumorigenesis by crossing *Pkm2*^{cKO} and *Pkm2*$^{null/null}$ mice with medulloblastoma-prone mouse lines. We generated tumor-prone mice using either the *SmoM2* allele that induces rapidly developing progressive medulloblastoma with 100% incidence by P20, or with the *ND2:SmoA1* allele that induces tumors more slowly. In contrast to the anti-tumor effect of *Hk2* deletion, we found that *Pkm2* deletion did not slow tumor progression in *Math1-Cre;SmoM2;Pkm2*$^{fl/null}$ mice (Fig. 2.7A) or *hGFAP-cre;SmoM2;Pkm2*$^{fl/null}$ mice (data not shown) compared to *Pkm2*-intact, littermate controls. In both of these models, however, rapid tumor growth limits the ability to determine whether the loss of PKM2 accelerates disease. To address this question, we examined *Pkm2* deletion in *ND2:SmoA1* mice.

We found that *ND2:SmoA1* mice with *Pkm2* deletion developed tumors more frequently than *Pkm2*-intact *ND2:SmoA1* controls and this difference became more pronounced over time. We compared *ND2:SmoA1* mice with two mutant copies of *Pkm2*, including *Math1-Cre;ND2:SmoA1;Pkm2*$^{fl/fl}$, *Math1-Cre;ND2:SmoA1;Pkm2*$^{fl/null}$, and *ND2:SmoA1;Pkm2*$^{null/null}$ genotypes to control *ND2:SmoA1* mice with two intact copies of *Pkm2*, including no-*Cre;ND2:SmoA1;Pkm2*$^{+/+}$, no-*Cre;ND2:SmoA1;Pkm2*$^{fl/+}$, and *Math1-Cre;ND2:SmoA1;Pkm2*$^{+/+}$ genotypes. We observed a trend toward increased tumor formation in *Pkm2*–deleted mice at P150, where the incidence was 37.5% with *Pkm2* deletion vs 15.8% for controls

(p=0.245, Fisher's Exact test). By 300, increased tumor formation in *Pkm2*–deleted mice was detectable with statistical significance, showing 100% incidence with *Pkm2* deletion vs 57.9% for controls (p=0.004, Fisher's Exact test). Consistent with increased tumor formation, *ND2:SmoA1* mice with *Pkm2* deletion demonstrated significantly shorter survival (Fig. 2.7B).

To determine if *Pkm2* deletion accelerated tumor growth through a cell autonomous process, we separately compared the *Math1-Cre;ND2:SmoA1;Pkm2*$^{fl/null}$ and *ND2:SmoA1;Pkm2*$^{null/null}$ subgroups to *Pkm2*-intact *ND2:SmoA1* controls. This analysis also showed significantly shorter survival for both *Math1-Cre;ND2:SmoA1;Pkm2*$^{fl/null}$ (Fig. 2.7C) and *ND2:SmoA1;Pkm2*$^{null/null}$ genotypes (Fig. 2.7D). We found no statistically significant difference between different *Pkm2*-deleted genotypes. The similar effect of *Pkm2* deletion in the *Math1-Cre;ND2:SmoA1;Pkm2*$^{fl/null}$ and *ND2:SmoA1;Pkm2*$^{null/null}$ subgroups shows that the effect of *Pkm2* deletion is cell autonomous.

Like *Pkm2*-deleted CGNPs, *Pkm2*-deleted medulloblastoma cells did not express PKM2 (Fig. 2.7E) or PKM1 (Fig. 2.7F). However, we noted scattered PKM1+ cells within *Pkm2*-deleted tumors (Fig. 2.7E'''). These cells were consistently PCNA- (Fig. 2.S3) and were also found in *Pkm2*-intact tumors. These non-proliferative, PKM1+ cells may be entrapped neurons or differentiated progeny of tumor cells. Similar PKM1+ stromal cells were previously observed in *Pkm2*-deleted breast tumors[43].

The slow process of tumor formation in *ND2:SmoA1* mice allowed us to analyze the effect of *Pkm2* deletion on the growth of premalignant lesions. We counted PCNA+ cells in cerebella of *ND2:SmoA1* mice with deleted or intact *Pkm2*, harvested at either P60 or P120 and normalized the number of PCNA+ cells to the total number of cells in each cerebellar section (Fig. 2.7G). In controls, the median fraction of PCNA+ cells in the cerebellum and the range of these values decreased over time, consistent with a dynamic balance between growth and growth suppression. In contrast, in *Pkm2*-deleted genotypes, the median and range of PCNA+ fractions increased over time, consistent with reduced growth suppression during the premalignant period. Altogether, *Pkm2* deletion increased SHH-driven CGNP proliferation during development, accelerated tumorigenesis in premalignant lesions in *Smo*-mutant mice, and increased the incidence of tumor formation from these lesions.

The more rapid progression of mouse tumors with *Pkm2* deletion was mirrored by a trend toward shorter survival in medulloblastoma patients with low PKM2 expression. We classified SHH-subgroup medulloblastoma patients as having either high or low PKM2 expressing tumors and compared their clinical outcomes. All patients were treated similarly with radiation and chemotherapy. While not statistically significant, we found that patients with low PKM2 expression trended toward shorter survival times (Fig. 2.7H). Together, these data confirm that PKM2 is not essential for tumor progression and suggest that low PKM2 expression, like *Pkm2* deletion, enhances medulloblastoma tumor growth.

2.4 Discussion

This study is the first to analyze the functional significance of pyruvate kinase isoform expression in the developing brain and in medulloblastoma. While aerobic glycolysis has been associated with proliferation in both development[6,54,55] and cancer[1,2], our data show that disrupting glycolysis at pyruvate kinase actually increases, rather than decreases both developmental proliferation and tumorigenesis. We show that within the neural lineage, *Pkm* is spliced into mutually exclusive expression patterns that correlate pyruvate kinase activity with differentiation state. In the postnatal brain, undifferentiated progenitors in the cerebellum, hippocampus, and SVZ expressed the less catalytically active PKM2 isoform, while differentiated neurons expressed the more active PKM1. The correlation of PKM2 with the undifferentiated state was maintained in medulloblastoma. Moreover, the PKM1:PKM2 dichotomy persisted after conditional or germline deletion of *Pkm2*, which increased PKM1 in differentiated cells but not in progenitors. The lack of compensatory up-regulation of PKM1 in brain progenitors contrasts with prior observations in MEFs and other tissues, where PKM1 expression increases when *Pkm* exon 10 is deleted[44,56]. In *Pkm2*-deleted MEFs, increased PKM1 caused nucleotide scarcity and cell cycle arrest. However, $Pkm2^{cKO}$ CGNPs expressed neither PKM isoform and showed decreased glycolysis and increased proliferation. *Pkm2* deletion also enhanced the growth of premalignant lesions and tumors in *ND2:SmoA1* mice. These findings demonstrate that PKM2 is not required for the physiologic or malignant proliferation of neural progenitors. Rather, the absence of detectable PKM in $Pkm2^{cKO}$ mice was associated with increased proliferation.

The different effects of *Pkm2* deletion in CGNPs and MEFs, taken together, argue that proliferation is restricted by PKM1, rather than enhanced by PKM2. We propose a model in which high pyruvate kinase activity inhibits proliferation and suppresses tumor formation; consistent with this model, splicing *Pkm* pre-mRNA to generate PKM2 has a permissive effect on proliferation and abrogation of PKM expression is more permissive. The finding that SHH and IGFR signaling increased maximal pyruvate kinase activity is not necessarily at odds with this model as growth factors are known to induce simultaneously both positive and negative regulation of proliferation. For example, mitogenic SHH activation up-regulates, Patched (Ptc), which negatively regulates SHH signaling[57–59]. Activating PKM2 may be a similar inhibitory element that is part of the normal regulation of SHH-induced growth. Alternatively, the normal regulation of PKM2 activity in CGNPs may not be fully recapitulated in lysates where the intracellular architecture is disrupted.

Our prior studies of *Hk2* deletion demonstrate that the initiation of glycolysis supports postnatal neurogenesis and sustains the malignant growth of medulloblastomas. In contrast, our present studies of *Pkm2* deletion show that impeding the flow of glucose to lactate increases CGNP proliferation and accelerates medulloblastoma tumorigenesis. Together, these deletion studies show that the pathways through which glucose is metabolized significantly influence the proliferative behavior of undifferentiated cells. The divergent effects of *Hk2* deletion versus *Pkm2* deletion establish the glycolytic steps upstream of pyruvate kinase as critical to promoting the proliferative phenotype.

Between the reactions catalyzed by HK2 and PKM2 are several reversible reactions that permit glycolytic intermediates to be shunted toward biosynthetic processes. We and others have previously proposed that low flow downstream of PEP, achieved by preferentially splicing PKM to generate PKM2, may support growth by diverting glycolytic intermediates away from lactate generation and towards the synthesis of macromolecules[28,60,61]. However, evidence for this was lacking in MEFs[56] and recent work found that the direct incorporation of glucose carbons is a minor component of the biomass of proliferating cells[62]. Working with explanted neural progenitors limited the range of metabolites we could detect, as the amount of material for analysis was quite small. However, we were able to detect ^{13}C label in extracellular lactate and in intracellular glutamate and ribose. *Pkm2* deletion decreased the

incorporation of glucose into lactate and decreased the repeated cycling of glucose-derived carbons through the Krebs cycle. These changes show that altering PEP metabolism decreases flow through the final step of aerobic glycolysis while increasing cataplerosis. *Pkm2* deletion did not produce a detectable effect on the incorporation of glucose into ribose, suggesting that PPP flux is not the major destination of glucose carbons redirected by low pyruvate kinase activity.

Our ^{13}C studies show that CGNPs lacking both PKM1 and PKM2 can metabolize glucose to pyruvate, raising the question of what alternative pathway metabolizes PEP. We were not able to detect changes in glycolytic intermediates that might indicate how PEP is processed in *Pkm2*^{cKO} CGNPs. However, prior studies have shown that PKM2-expressing cells with low pyruvate kinase activity can generate pyruvate by transferring the high-energy phosphate of PEP to the enzyme PGAM1[63]. This phosphorylation activates PGAM1, which may promote biosynthetic metabolism [64,65]. If PEP-PGAM1 phosphotransfer occurs in CGNPs, it may mediate the growth promoting effect of PKM2 splicing that is enhanced by *Pkm2* deletion.

The ubiquitous expression of PKM2 in cancer has suggested that this protein may be essential for tumorigenesis. The identified, nonmetabolic functions of PKM2 that could promote malignant growth include phosphorylating Histone H3[39,41], participating in cytokinesis[66], and regulating gene expression[37]. However, our data on the effects of *Pkm2* deletion in medulloblastoma together with previous findings in breast cancer[43] demonstrate that these nonmetabolic functions of PKM2 are not required for tumor growth.

Our work suggests that *Pkm* functions as a tumor suppressor. Identifying *Pkm* as a tumor suppressor has profound implications for aerobic glycolysis and may be effectively targeted in cancer treatment. Inhibiting PKM function as an anti-cancer therapy would be counterproductive while drugs that increase PKM catalytic activity may be of limited therapeutic value if tumors can thrive with low *Pkm* expression. The loss of tumor suppressor genes, however, may be targeted through alternative approaches that require defining the consequent changes in pathway regulation[67,68]. A detailed understanding of how low pyruvate kinase activity promotes proliferation may produce novel clinical strategies to treat tumor growth.

2.5 Materials and Methods

Animals

All wild-type and genetically engineered mice were maintained on the C57/Bl6 background with at least 5 backcrosses. ND2:SmoA1 mice were provided by Dr. James Olson (Fred Hutchinson Cancer Research Center, Seattle, WA, USA). Math1-Cre mice were provided by Dr. David Rowitch (UCSF, CA, USA) and Robert Wechsler-Reya (Sanford-Burnham Medical Research Institute, La Jolla, CA, USA). Eva Anton (UNC-CH, NC, USA) provided hGFAP-Cre mice. $Pkm2^{fl/fl}$ mice were generously shared by Dr. Matthew Vander Heiden (MIT, Cambridge, MA, USA). Medulloblastoma-prone mice were monitored daily for abnormalities of head shape and movement. At the onset of tumor symptoms, such as weight loss, ataxia, and impaired movement, animals were sacrificed and survival time to onset of symptoms was considered the event-free survival.

For EdU experiments, mice were IP injected with EdU (#A10044, Life Technologies, Grand Island, NY, USA) at 40 mg/kg in 50 µL of HBSS and dissected 24h later. Brains were fixed in 4% paraformaldehyde in 1X PBS for 24h at 4°C, then processed for histology. All animal handling and protocols were carried out in accordance with established NIH practices and approved under UNC IACUC #13-121.0 and 15-306.0.

Cell Culture Techniques

CGNPs were isolated and cultured as previously described[6,69]. Briefly, cerebella were dissected from P5 pups, dissociated, and allowed to adhere to coated culture wells in DMEM/F12 (#11320, Life Technologies, Grand Island, NY, USA) with 25 mM KCl, supplemented with FBS and N2. After 4h, media were replaced with identical serum-free media. Cells were maintained in 0.5 µg/mL SHH (#464SH, R&D Systems, Minneapolis, MN, USA) or vehicle (0.1% BSA in 1X PBS). Where indicated, vismo (#S1082, Selleck Chemicals, Houston, TX, USA) was added to cultures after the first 24h, at the specified concentration, with cells harvested 24h after drug treatment. In vitro CGNP proliferation was measured by EdU incorporation after a 1h exposure to 20 µM EdU. EdU was visualized following the manufacturer's

protocol (#C10337, Life Technologies). Cell counts were performed using Leica-Metamorph software (Molecular Devices, Sunnyvale, CA, USA).

In vitro metabolism studies

Briefly, CGNPs of each genotype were cultured in at least 3 replicate wells. Explanted CGNPs were maintained in [1,6-^{13}C] glucose media for 24h followed by media sampling and cell extraction for metabolomic analysis. For ^{1}H-NMR metabolomic analysis of the media, samples were processed as previously described[6,70]. Briefly, ^{1}H spectra were acquired at 25ºC on a 14.1T Varian INOVA spectrometer at 600 MHz ^{1}H frequency and equipped with a CapNMR™ microcoil (Magnetic Resonance Microsensors Corp, Savoy, MN, USA). The ^{1}H spectra were acquired using a one-pulse sequence with presaturation of the water resonance with a 90º flip angle and a total repetition time of 12.65 sec. For analysis, ^{1}H spectra were first zero-filled to 32,000 points and line broadened by applying a 0.5 Hz exponential Gaussian function using ACD Labs 12.0 1D NMR Processor (ACD Labs Toronto, Ontario, Canada). Metabolites were identified using Chenomx NMR processing software version 7.1 (Edmonton, Alberta, Canada) and the Human Metabolome Database[71] for chemical shifts.

For LC-MS metabolomic analysis of the cells, dried extract was resuspended in 60 µL of 1:1 acetonitrile: water, vortexed, and 10 µL was used for analysis. The HILIC column (Venusil HILIC Column, 3 µm, 100Å, 2.1 x 100 mm, Agela Technologies Inc., Wilmington, DE, USA) was used for liquid chromatography and optimized for both nucleotide and amino acid organic separation using the following solvent gradient requiring 10 min cycles. Solvent A: 100 mM ammonium acetate (Fisher Chemicals, Fair Lawn, NJ, USA) and 20 mM ammonium hydroxide (Fisher Chemicals) in HPLC grade water (Fluka, Sigma-Aldrich, St. Louis, MO, USA). Solvent B: 100% HPLC grade acetonitrile (Fluka). LC gradient: Starting with 98% Solvent B, 1 min – starting gradient, 6 min – 50% Solvent B, 6.01 min – 2% Solvent B, 7 min – 2% Solvent B, 8 min – 98% Solvent B, 10 min – stop, with a total binary flow of 0.4 mL/min. Mass spectrometry was performed in positive mode using an AB Sciex TripleTOF 5600 with the following parameters: Ion source gas 1 – 45, Ion source gas 2 – 30, Curtain gas – 20, Temperature – 450, Ion spray voltage – 4500 V, Declustering potential – 80 V, Collision energy 5 (35 – for phosphonucleotide

detection and product ion fragmentation, 25 – for amino acid detection and fragmentation). TOF mass detection at 5 to 1050 Da for phosphonucleotides and 43 to 155 Da for amino acids. MS-MS was performed for the 10 highest products. Where applicable, mass spectrometry data were corrected for the contribution of naturally abundant isotopes using IsoCor[72] (MetaSys, LISBP, Toulouse, France).

For the enzymatic measurement of lactate, media from at least three replicate wells were sampled at the specified time points and lactate was quantified using the L-Lactate Assay Kit (#1200011002, Eton Bioscience, San Diego, CA, USA) per manufacturer's protocol.

For pyruvate kinase activity assays, cells from at least three replicate wells per condition, or whole cerebella from at least three replicate mice per genotype, were lysed and processed for the colorimetric assay per manufacturer's protocol (#K709-100, BioVision Inc., Milpitas, CA, USA).

Histology and immunohistochemistry

Mouse brain and tumor tissues were processed for IHC as previously described[73] using antibodies from Cell Signaling Technology (Danvers, MA, USA): PKM1 (#7067), PKM2 (#4053), Proliferating cell nuclear antigen (PCNA; #2586), and $p27^{Kip1}$ (#3686). EdU was visualized per manufacturer's protocol. After IHC and EdU staining, where indicated, nuclei were counterstained with 200 ng/mL 4'6-diamidino-2-phenylindole (DAPI; #D1306, ThermoFisher Scientific, Waltham, MA, USA) in 1X PBS for 5 min. Stained slides were digitally acquired using an Aperio ScanScope XT (Aperio, Vista, CA, USA). Where indicated, maximum intensity projections of stained tissue sections were acquired on a Zeiss LSM 780 confocal microscope with a Plan-Apochromat 20x objective (NA 0.8). To quantify EdU, PCNA, and $p27^{Kip1}$ positive cells in the EGL, the EGL region was manually annotated on each section, which was then subjected to automated cell counting using Tissue Studio (Definiens, München, Germany) for fluorescent slides. For premalignant lesion analysis, the entire cerebellum was annotated and used for cell counts.

Western blot analysis

Cultured cells and whole cerebella were lysed by homogenization in RIPA buffer containing protease inhibitor cocktail, NaF, and sodium orthovanadate. Protein concentrations were quantified using the bicinchoninic acid (BCA) method (#23229, ThermoFisher Scientific) and equal concentrations of protein were resolved on SDS-polyacrylamide gels followed by transfer onto polyvinylidene difluoride membranes. Immunologic analysis was performed on the SNAP i.d. Protein Detection System (Millipore, Billerica, MA, USA) per manufacturer's protocol with antibodies from Cell Signaling Technology: β-actin (#4970), PKM1 (#7067), PKM2 (#4053), and Cyclin D2 (CCND2; #3741), anti-Rabbit IgG HRP (#7074) and anti-Mouse IgG HRP (#7076). Western blots were developed using the enhanced chemiluminescent SuperSignal West Femto Maximum Sensitivity Substrate (#34095, ThermoFisher Scientific) and digitized using the C-DiGit blot scanner (LI-COR, Lincoln, NE, USA). Quantification was performed using Image Studio Lite software (LI-COR).

Primers used for genotyping

Pkm2^{fl} were TAGGGCAGGACCAAAGGATTCCCT and CTGGCCCAGAGCCACTCACTCTTG, producing a ~605 bp band from the floxed allele and a ~560 bp band from the wildtype allele. *Cre* primers were GCGGTCTGGCAGTAAAAACTATC and GTGAAACAGCATTGCTGTCACTT, producing a ~200 bp band. *SmoM2* primers were AAGTTCATCTGCACCACCG and TCCTTGAAGAAGATGGTGCG, producing a ~200 bp band. *ND2:SmoA1* primers were AATCTCTGCTTTTCCTGCGTTGGG and CTCGGTCATTCTCACACTTG, producing a ~700 bp band.

DNA sequencing

DNA was lysed from toe cuttings and used to generate *Pkm2* PCR products. *Pkm2* PCR primers were F_ TAGGGCAGGACCAAAGGATTCCCT and R_CTGGCCCAGAGCCACTCACTCTTG. PCR products were extracted from a 0.8% agarose gel using the MinElute Gel Extraction Kit (#28604, Qiagen,

Valencia, CA, USA), cloned by TOPO TA Cloning (#K4575-J10, Life Technologies) and sequenced from the M13F and M13R primer sites by Sanger sequencing (Eton Bioscience).

Patients and samples

All patient samples were obtained with consent as outlined by individual institutional review boards. Written informed consent was obtained at the time of surgical resection. De-identified medulloblastoma tissues were obtained from Queensland Children's Tumor Bank (Brisbane, Australia), German Cancer Research Center (Heidelberg, Germany), Sanford-Burnham Medical Research Institute (La Jolla, USA), and Hospital for Sick Children (Toronto, Canada).

Differential Pkm isoform expression analysis of RNA-seq data

Library construction, sequencing, and alignment of RNA-seq data are described in detail in the Messenger RNA library construction and sequencing section. Transcriptome aligned binary alignment files (bams) were processed using RNA-Seq by Expectation Maximization (RSEM) software[74]. The reference for RSEM was built using the same GRCh37-lite assembly and GRCh37.75 GTF as used by STAR aligner[75]. This was followed by the calculation of PKM isoform level FPKM using RSEM with default parameters in 97 human tumors. The accession number for the RNA-seq data is European Genome-phenome Archive: EGAD00001001899.

Messenger RNA library construction and sequencing

Two micrograms of total RNA samples were arrayed into a 96-well plate and polyadenylated (PolyA+) messenger RNA (mRNA) was purified using the 96-well MultiMACS mRNA isolation kit on the MultiMACS 96 separator (Miltenyi Biotec, Bergisch Gladbach, Germany) with on-column DNase I-treatment per the manufacturer's instructions. The eluted polyA+ mRNA was ethanol precipitated and resuspended in 10 µL of DEPC treated water with 1:20 SuperaseIN (Life Technologies, Grand Island, NY,

USA). First-strand cDNA was synthesized from the purified polyA+ mRNA using the Superscript cDNA Synthesis kit (Life Technologies) and random hexamer primers at a concentration of 5 µM along with a final concentration of 1 µg/µL Actinomycin D, followed by Ampure XP SPRI beads on a Biomek FX robot (Beckman-Coulter, Brea, CA, USA). The second strand cDNA was synthesized following the Superscript cDNA Synthesis protocol by replacing the dTTP with dUTP in the dNTP mix, allowing the second strand to be digested using UNG (Uracil-N-Glycosylase, Life Technologies) in the post-adapter ligation reaction and thus achieving strand specificity. The cDNA was quantified in a 96-well format using PicoGreen (Life Technologies) and VICTOR3V Spectrophotometer (PerkinElmer, Inc., Waltham, MA, USA). The quality was checked on a random sampling using the High Sensitivity DNA chip Assay (Agilent, Santa Clara, CA, USA). The cDNA was fragmented by Covaris E210 (Covaris, Woburn, MA, USA) sonication for 55 seconds, using a Duty cycle of 20% and Intensity of 5. Plate-based libraries were prepared following the BC Cancer Agency's Michael Smith Genome Sciences Centre (BCGSC) paired-end (PE) protocol on a Biomek FX robot (Beckman-Coulter). Briefly, the cDNA was purified in 96-well format using Ampure XP SPRI beads, and was subject to end-repair and phosphorylation by T4 DNA polymerase, Klenow DNA Polymerase, and T4 polynucleotide kinase respectively in a single reaction, followed by cleanup using Ampure XP SPRI beads and 3’ A-tailing by Klenow fragment (3’ to 5’ exo minus). After cleanup using Ampure XP SPRI beads, picogreen quantification was performed to determine the amount of Illumina PE adapters used in the next step of adapter ligation reaction. The adapter-ligated products were purified using Ampure XP SPRI beads, then PCR-amplified with Phusion DNA Polymerase (Thermo Fisher Scientific Inc., Waltham, MA, USA) using Illumina’s PE primer set, with cycle conditions of 98°C 30sec followed by 10-15 cycles of 98°C 10 sec, 65°C 30 sec and 72°C 30 sec, and then 72°C 5 min. The PCR products were purified using Ampure XP SPRI beads, and checked with a Caliper LabChip GX for DNA samples using the High Sensitivity Assay (PerkinElmer, Inc.). PCR products with a desired size range were purified using a 96-channel size selection robot developed at the BCGSC, and the DNA quality was assessed and quantified using an Agilent DNA 1000 series II assay and Quant-iT dsDNA HS Assay Kit using Qubit fluorometer (Invitrogen, Carlsbad, CA, USA), then diluted to 8 nM. The final concentration was verified by Quant-iT dsDNA HS Assay. The libraries, 2 per 100 PE lane, were sequenced on the Illumina HiSeq 2000/2500 platform using v3 chemistry and HiSeq Control Software version 2.0.10.

Alignment of RNA-seq data

RNA sequencing data was aligned to GRCh37-lite genome-plus-junctions[76] using BWA (version 0.5.7)[77]. This reference is a combination of GRCh37-lite assembly and exon-exon junction sequences with coordinates defined based on transcripts in Ensembl (v61), Refseq and known genes from the UCSC genome browser (both were downloaded from UCSC in November 2011; The GRCh37-lite assembly is available at http://www.bcgsc.ca/downloads/genomes/9606/hg19/1000genomes/bwa_ind/genome. BWA was run with default parameters, except for the inclusion of the (-s) option to disable the Smith-Waterman alignment. Reads failing the Illumina chastity filter were flagged with a custom script, and duplicated reads were flagged with Picard Tools (version 1.31). After the alignment, the junction-aligned reads that mapped to exon-exon junctions were repositioned to the genome as large-gapped alignments and tagged with "ZJ:Z".

Aligned genome coordinates for the *Pkm* region where then extracted in fastq format and converted to transcriptome coordinates using the STAR aligner[75], to facilitate downstream processing. The reference for STAR was built using chromosome 15 of the GRCh37-lite assembly, the GRCh37.75 GTF file from Ensembl, and using parameters of --sjdbOverhang 99. STAR was then run with parameters --quantMode TranscriptomeSAM and SortedByCoordinate to generate the transcriptome aligned binary alignment files (bams).

Survival analysis of SHH-subgroup medulloblastoma patients

PKM2 FPKM expression was converted to a Z-score and used to segregate SHH patients into a high or low category with the criteria of being greater than 0.5 or smaller than -0.5 respectively. A cox proportional hazard model was used to determine the presence of a survival difference.

2.6 Figures and Legends

Figure 2.1 Mutually exclusive expression patterns of PKM1 and PKM2 correspond to differentiation state.

(A-A'') PKM1 (brown) demonstrated by IHC in differentiated neurons throughout the P7 brain, but excluded from progenitors. (B-B'') PKM2 (brown) demonstrated by IHC in neural progenitors of the SVZ, HC, and EGL. (C) Western blot and quantification of CCND2, PKM2, and PKM1 in whole cerebellum lysates harvested at the indicated age, normalized to β-actin. PKM2 decreases as proliferation wanes from P7 (n=4) to P15 (n=4), while PKM1 increases. Graph presents average ± s.e.m. (D) Immunofluorescence in P7 wildtype mice, shows PKM2 expressed in both the PCNA+ oEGL and the PCNA- iEGL. (E) P7 SVZ, stained as in D, demonstrates PKM2 in PCNA+ and PCNA- progenitors (arrowheads identify PCNA- cells). (F) Premalignant lesions in P60 *ND2:SmoA1* mice identified by PCNA staining, express PKM2 and not PKM1. High magnification of boxed area is shown in F'-F'''. (G) PKM2 and PCNA are expressed in a medulloblastoma in the cerebellum of a *ND2:SmoA1* mouse, while the adjacent normal tissue expresses PKM1. High magnification of boxed area is shown in G'-G'''. (H) RNA-seq analysis shows that PKM2 is preferentially expressed in all human medulloblastoma subgroups (total n=97). *P* values determined by Student's *t*-tests. SVZ, subventricular zone; HC, hippocampus; EGL, external granule layer; IGL, internal granule layer; PC, Purkinje cell layer; oEGL, outer EGL; iEGL, inner EGL; ML, molecular layer; FPKM, Fragments Per Kilobase of transcript per Million mapped reads. Scale bars: 2 mm (A,B,G); 600 μm (A',B'); 100 μm (A",B",E); 50 μm (D,E inset); 1 mm (F); 500 μm (F'-F'"); 300 μm (G'-G'").

Figure 2.1

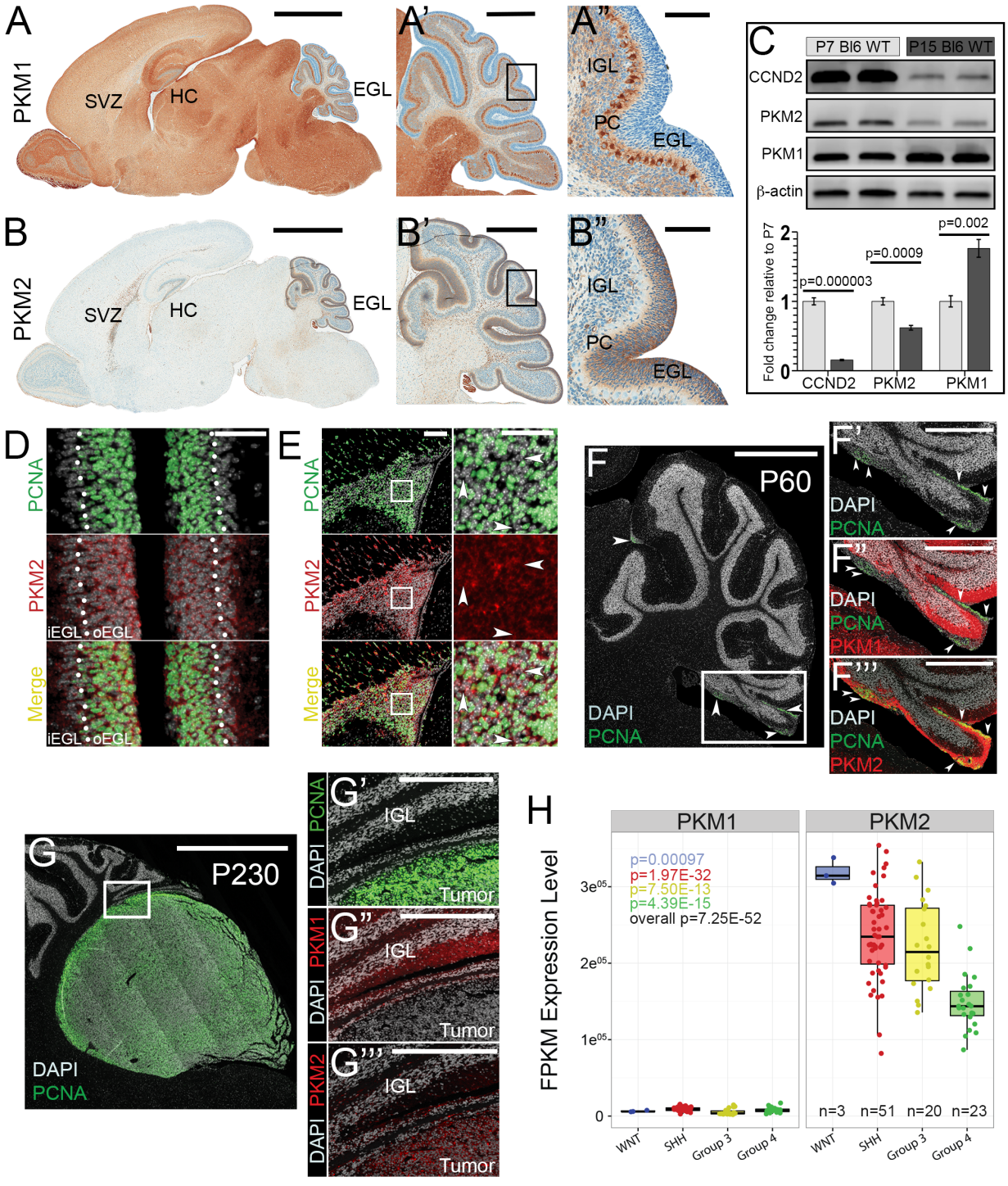
A
PKM1
SVZ
HC
EGL
A'
A''
IGL
PC
EGL
B
PKM2
SVZ
HC
EGL
B'
B''
IGL
PC
EGL
C
P7 Bl6 WT
P15 Bl6 WT
CCND2
PKM2
PKM1
β-actin
Fold change relative to P7
p=0.000003
p=0.0009
p=0.002
CCND2
PKM2
PKM1
D
PCNA
PKM2
Merge
iEGL
oEGL
E
PCNA
PKM2
Merge
F
P60
DAPI
PCNA
F'
DAPI
PCNA
F''
DAPI
PCNA
PKM1
F'''
DAPI
PCNA
PKM2
G
P230
DAPI
PCNA
G'
DAPI
PCNA
IGL
Tumor
G''
DAPI
PKM1
IGL
Tumor
G'''
DAPI
PKM2
IGL
Tumor
H
FPKM Expression Level
PKM1
PKM2
p=0.00097
p=1.97E-32
p=7.50E-13
p=4.39E-15
overall p=7.25E-52
3e05
2e05
1e05
0
n=3
n=51
n=20
n=23
WNT
SHH
Group 3
Group 4

Figure 2.2 Growth factor signaling regulates PKM expression and activity.

(A,B) Immunofluorescence on explanted wildtype CGNPs exposed to EdU for 1h in presence or absence of SHH. SHH increases both PKM2 and EdU staining. (C,D) Rare cells within CGNP explants expressed PKM1 (arrowheads) in both SHH- and vehicle-treated wells. (E) Western blot and quantification of CCND2, PKM2, and PKM1 in cell cultures, normalized to β-actin. SHH induces a 5.5-fold increase in CCND2 that is blocked by 1 μM vismodegib. Both PKM1 and PKM2 show statistically significant increase with SHH. However, vismodegib does not significantly alter PKM1 or PKM2. (F) N2-deprived CGNPs produce significantly less lactate detected by enzymatic assay. (G,H) Pyruvate kinase (PK) activity of CGNPs significantly increases with combined SHH and N2 supplementation. Graphs present average ± s.e.m. *P* values determined by Student's *t*-tests. Scale bars: 50 μm.

Figure 2.2

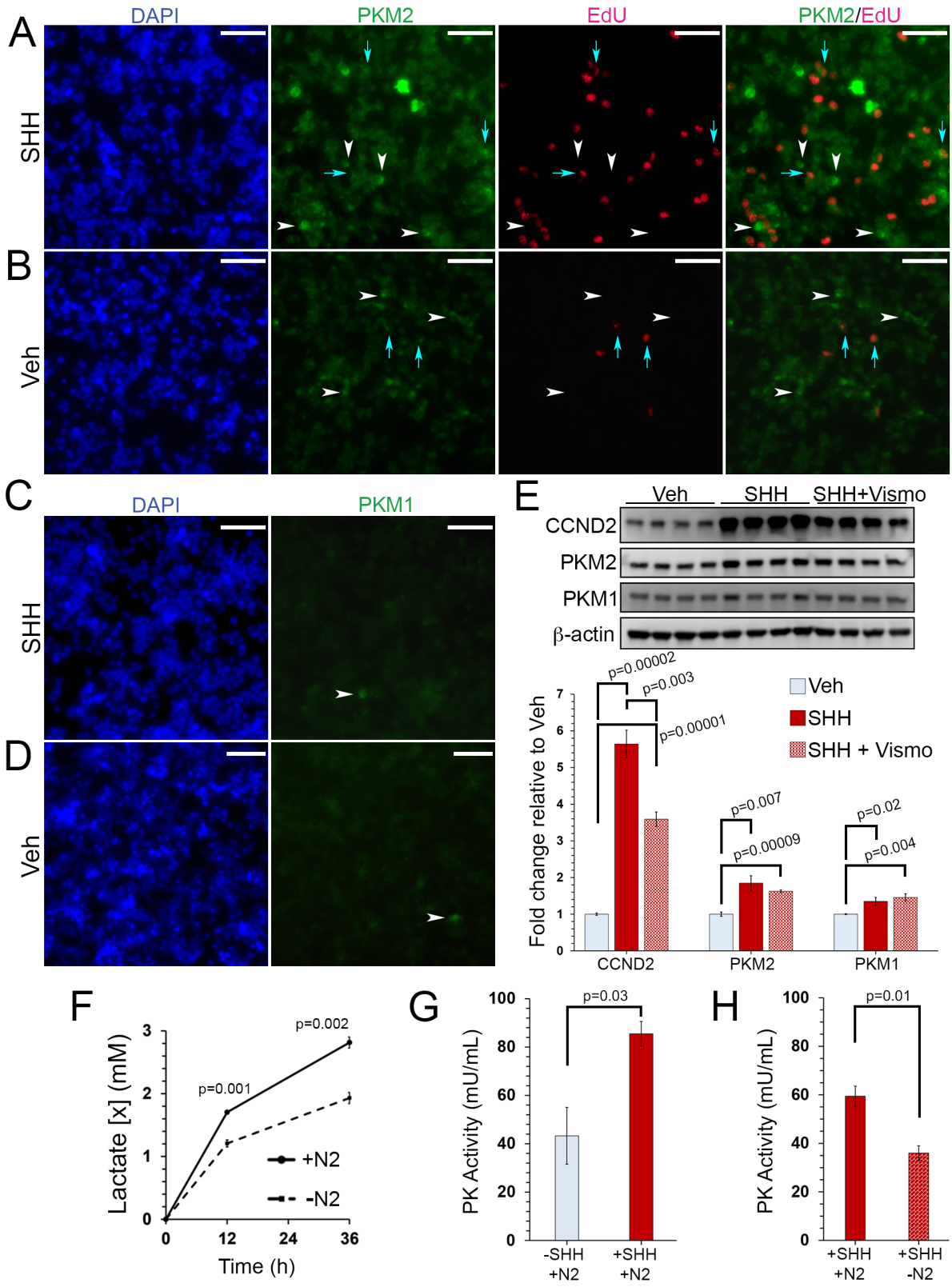
A
DAPI
PKM2
EdU
PKM2/EdU
SHH
B
Veh
C
DAPI
PKM1
SHH
D
Veh
E
Veh
SHH
SHH+Vismo
CCND2
PKM2
PKM1
β-actin
p=0.00002
p=0.003
p=0.00001
p=0.007
p=0.00009
p=0.02
p=0.004
Veh
SHH
SHH + Vismo
Fold change relative to Veh
CCND2
PKM2
PKM1
F
Lactate [x] (mM)
p=0.002
p=0.001
+N2
-N2
Time (h)
G
PK Activity (mU/mL)
p=0.03
-SHH +N2
+SHH +N2
H
PK Activity (mU/mL)
p=0.01
+SHH +N2
+SHH -N2

Figure 2.3 Conditional *Pkm2* deletion blocks all *Pkm* expression in CGNPs.

(A,B) IHC of PKM1 and PKM2 in representative sagittal cerebellar sections from P7 Ctrl and *Pkm2*^{cKO} mice. *Pkm2* deletion does not induce compensatory PKM1 expression in the EGL. High magnification of boxed area is shown on the right. (C) Western blot and quantification normalized to β-actin in whole P7 cerebellar lysates demonstrates significantly decreased PKM2 and increased PKM1. (D) Pyruvate kinase activity in lysates of whole, P7 cerebella is not significantly different between Ctrl and *Pkm2*^{cKO} genotypes. EGL, external granule layer; IGL, internal granule layer; ML, molecular layer. Graphs present average ± s.e.m. *P* values determined by Student's *t*-tests. Scale bars: 500 μm; 100 μm (inset).

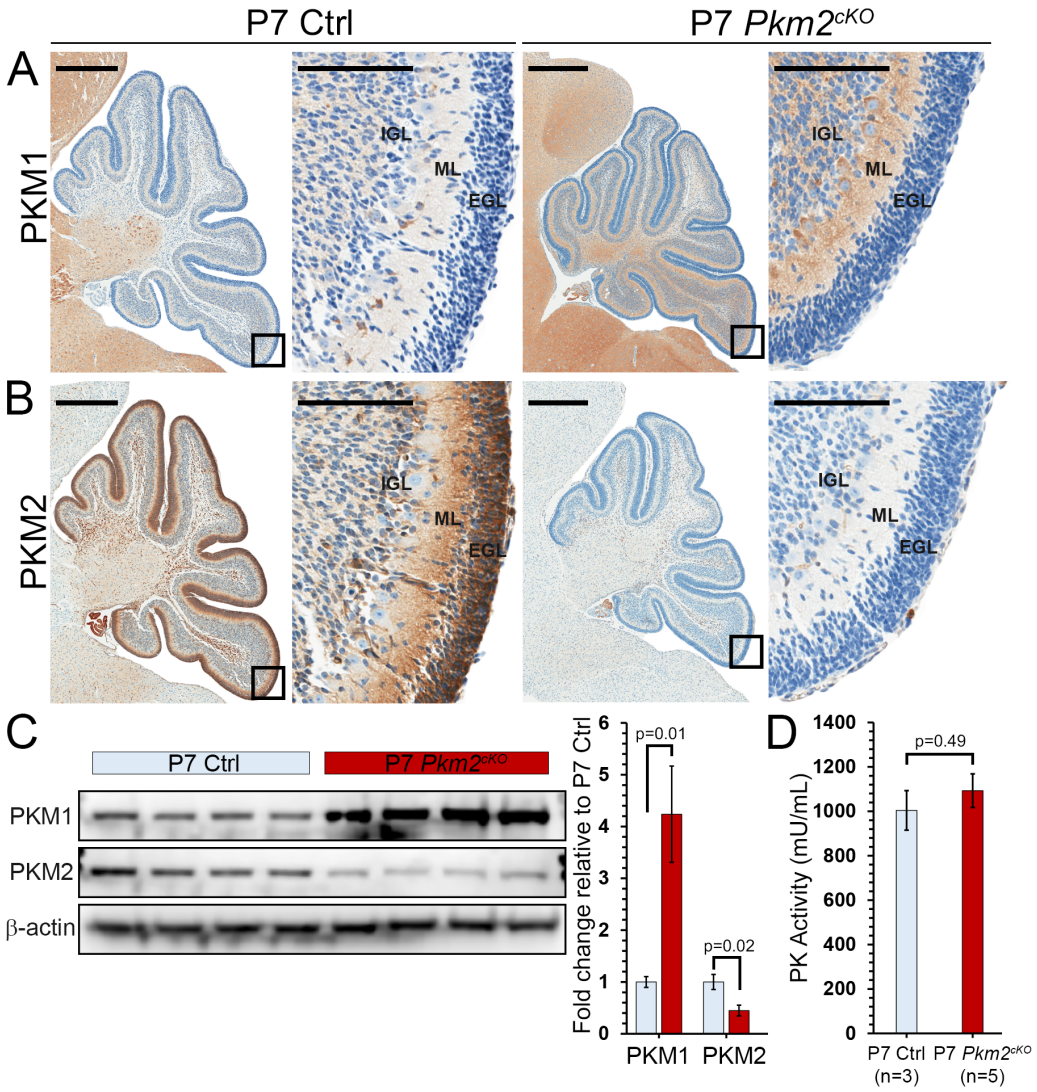

Figure 2.4 *Pkm2* deletion increases CGNP proliferation.

(A,B) Confocal images of P7 (A) Ctrl and (B) $Pkm2^{cKO}$ cerebellar sections, labeled for the differentiation marker $p27^{Kip1}$ and for EdU incorporation, 24h after EdU injection. High magnifications of boxed areas are shown on the right. (C) Quantification of EdU+ cells in the EGL from sections analyzed as in A and B, demonstrates comparable incorporation of EdU between genotypes. (D) Quantification of $p27^{Kip1}$+ cells in the EGL shows a trend towards decrease in the $Pkm2^{cKO}$ genotype. (E) Analysis of $p27^{Kip1}$ expression in the EdU+ population CGNPs shows reduced cell cycle exit by $Pkm2^{cKO}$ progenitors. (F) Decreased $p27^{Kip1}$+ EdU- cells in the $Pkm2^{cKO}$ EGL indicates that a greater fraction of differentiating CGNPs were in S-phase 24h earlier. (G) EdU incorporation after a 1h pulse *in vitro*. $Pkm2^{cKO}$ CGNPs demonstrate increased proliferation. (H) Analysis of midsagittal cerebellar sections shows significantly increased EGL and IGL populations in $Pkm2^{cKO}$ mice. (I) EGL:IGL ratio is similar between genotypes. Graphs present average ± s.e.m. *P* values determined by Student's *t*-tests. Scale bars: 500 μm (A,B); 50 μm (A,B, insets).

Figure 2.4

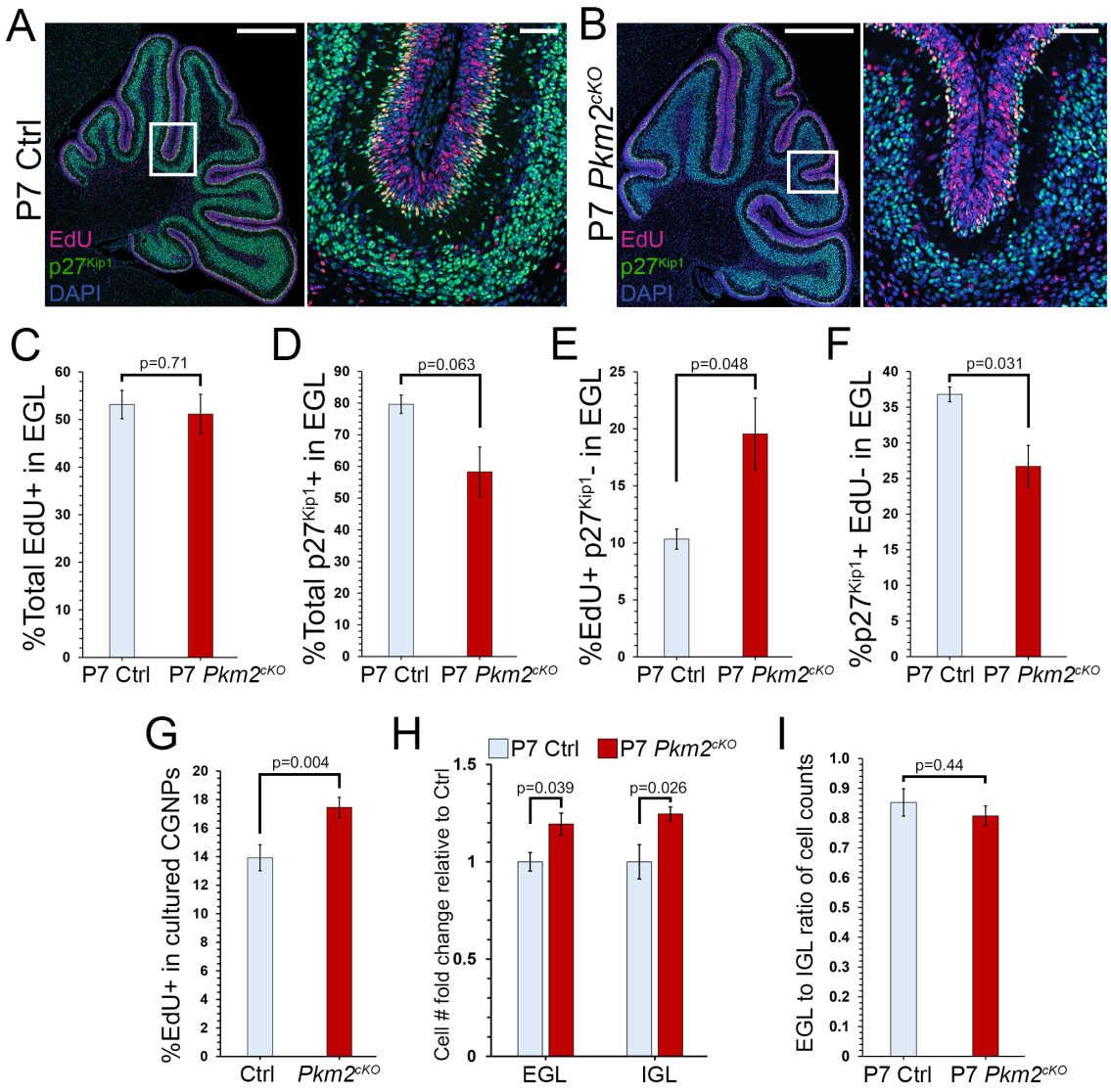
A
P7 Ctrl
EdU
p27Kip1
DAPI
B
P7 Pkm2cKO
EdU
p27Kip1
DAPI
C
%Total EdU+ in EGL
p=0.71
P7 Ctrl
P7 Pkm2cKO
D
%Total p27Kip1+ in EGL
p=0.063
P7 Ctrl
P7 Pkm2cKO
E
%EdU+ p27Kip1- in EGL
p=0.048
P7 Ctrl
P7 Pkm2cKO
F
%p27Kip1+ EdU- in EGL
p=0.031
P7 Ctrl
P7 Pkm2cKO
G
%EdU+ in cultured CGNPs
p=0.004
Ctrl
Pkm2cKO
H
P7 Ctrl
P7 Pkm2cKO
Cell # fold change relative to Ctrl
p=0.039
p=0.026
EGL
IGL
I
EGL to IGL ratio of cell counts
p=0.44
P7 Ctrl
P7 Pkm2cKO

Figure 2.5 *Pkm2* deletion reduces the conversion of glucose to lactate.

(A) ^{1}H NMR analysis of culture media at 24h demonstrates significantly decreased lactate production by *Pkm2*^{cKO} CGNPs compared to Pkm2-intact controls (**p=0.029). (B) Lactate concentration in culture media, measured by enzymatic assay, also show decreased production by *Pkm2*^{cKO} CGNPs. (C) Representative ^{1}H NMR spectra of Ctrl and *Pkm2*^{cKO} media at 24h demonstrate the doublet, satellite peaks generated by [3-^{13}C] lactate (dashed line) and by unlabeled lactate (solid line). The magnitudes of the peaks and the areas under the curve are lower in media from *Pkm2*^{cKO} CGNPs. (D) Quantification of NMR spectra demonstrates reduced fractional enrichment (FE) of lactate in media from *Pkm2*^{cKO} CGNPs. (E) LC-MS analysis of metabolites in cell extracts of explanted CGNPs demonstrates comparable levels between genotypes. A trend toward increased choline was noted in *Pkm2*^{cKO} CGNPs. Graphs present average ± s.e.m. *P* values determined by Student's *t*-tests.

Figure 2.5

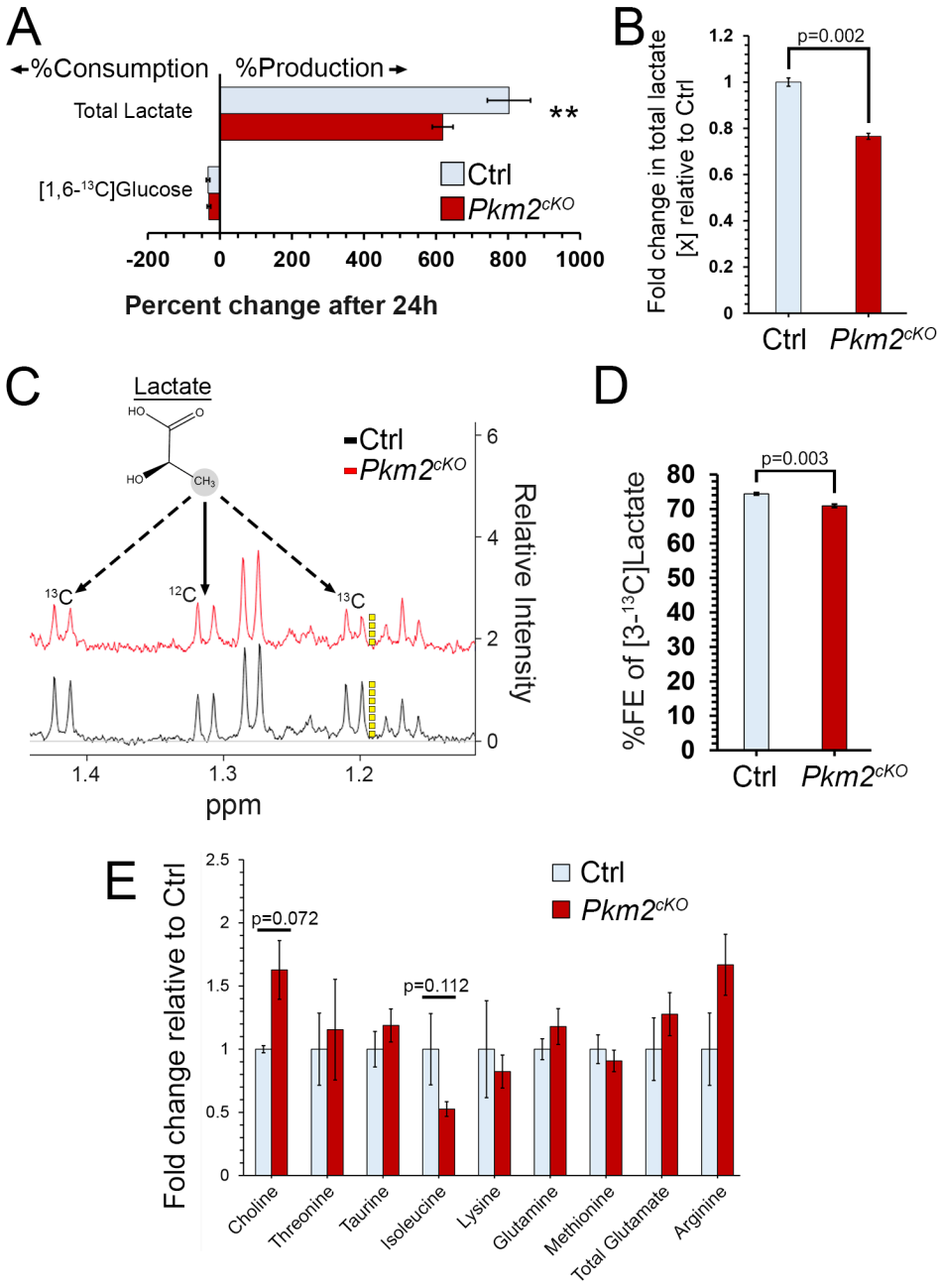
A
%Consumption
%Production
Total Lactate
**
[1,6-13C]Glucose
Ctrl
Pkm2cKO
-200
0
200
400
600
800
1000
Percent change after 24h
B
p=0.002
Fold change in total lactate [x] relative to Ctrl
1.2
1
0.8
0.6
0.4
0.2
0
Ctrl
Pkm2cKO
C
Lactate
Ctrl
Pkm2cKO
13C
12C
13C
Relative Intensity
6
4
2
0
1.4
1.3
1.2
ppm
D
p=0.003
%FE of [3-13C]Lactate
80
70
60
50
40
30
20
10
0
Ctrl
Pkm2cKO
E
Ctrl
Pkm2cKO
Fold change relative to Ctrl
2.5
2
1.5
1
0.5
0
p=0.072
p=0.112
Choline
Threonine
Taurine
Isoleucine
Lysine
Glutamine
Methionine
Total Glutamate
Arginine

Figure 2.6 *Pkm2*-deleted CGNPs show altered glutamate progression through the Krebs cycle but comparable PPP flux.

The canonical pathways through which [1,6-^{13}C] glucose can label glutamate and ribose are presented in schematic form. LC-MS analysis demonstrated reduced fractional enrichment of glutamate in *Pkm2*^{cKO} CGNPs, with a specific decrease in the fractional enrichment of glutamate molecules with 3 or 4 ^{13}C atoms, (m3, m4). Incorporation of ^{13}C into the ribose of adenine nucleotides was not significantly altered, indicating comparable flow through the PPP. Graphs present average ± s.e.m. *P* values determined by Student's *t*-tests. Ox*PPP*, oxidative phase of pentose phosphate pathway; Non-Ox*PPP*, non-oxidative phase of pentose phosphate pathway; GAP, glyceraldehyde 3-phosphate; X5P, xylulose 5-phosphate; E4P, erythrose 4-phosphate; F6P, fructose 6-phosphate; S7P, sedoheptulose 7-phosphate; R5P, ribose 5-phosphate; Ru5P, ribulose 5-phosphate; LDH, lactate dehydrogenase; PDH, pyruvate dehydrogenase; PC, pyruvate carboxylation.

Figure 2.6

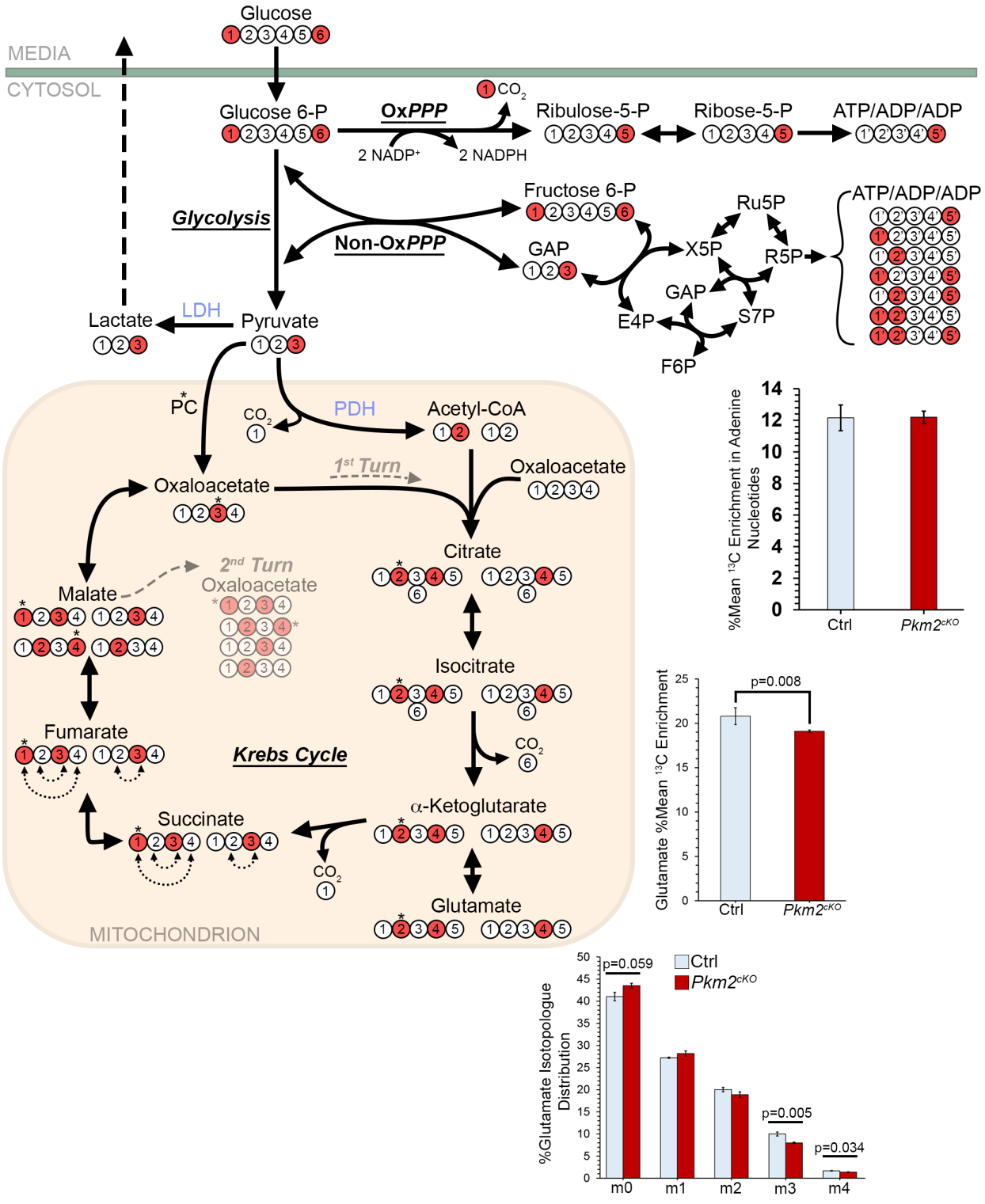
Glucose
MEDIA
CYTOSOL
Glucose 6-P
OxPPP
CO2
2 NADP+
2 NADPH
Ribulose-5-P
Ribose-5-P
ATP/ADP/ADP
Glycolysis
Non-OxPPP
Fructose 6-P
GAP
Ru5P
X5P
R5P
GAP
E4P
S7P
F6P
ATP/ADP/ADP
Lactate
LDH
Pyruvate
PC
CO2
PDH
Acetyl-CoA
1st Turn
Oxaloacetate
Oxaloacetate
2nd Turn
Oxaloacetate
Citrate
Malate
Isocitrate
Fumarate
Krebs Cycle
CO2
α-Ketoglutarate
Succinate
CO2
Glutamate
MITOCHONDRION
%Mean 13C Enrichment in Adenine Nucleotides
Ctrl
Pkm2cKO
Glutamate %Mean 13C Enrichment
p=0.008
Ctrl
Pkm2cKO
%Glutamate Isotopologue Distribution
p=0.059
Ctrl
Pkm2cKO
p=0.005
p=0.034
m0
m1
m2
m3
m4

Figure 2.7 *Pkm2* deletion accelerates medulloblastoma tumorigenesis

(A) Kaplan-Meier curves demonstrate no effect of *Pkm2* deletion on survival in the rapidly progressive *Math1-Cre;SmoM2* model of medulloblastoma. (B) In the slow growing *ND2:SmoA1* model, *Pkm2* deletion significantly accelerates tumorigenesis, reducing mouse survival. (C,D) Significantly reduced survival of *ND2:SmoA1* mice with (C) conditional *Pkm2* deletion or (D) global *Pkm2* deletion, compared to *Pkm2*-intact *ND2:SmoA1* controls. (E,F) A representative *Pkm2*-deleted *ND2:SmoA1* mouse brain with medulloblastoma at P147 shows (E) PKM1 (brown) in the normal brain adjacent to the tumor and (F) absence of PKM2 (brown). Within the *Pkm2*-deleted tumors, we noted scattered PKM1+ cells with relatively large cell bodies. The morphology of these cells suggests that they are differentiated cells entrapped within or generated by the tumor. (G) Comparison of premalignant lesions at P60 and P120 between genotypes. The proportion of PCNA+ cells to the total number of cells in the cerebellum increases over time in the *Pkm2* deleted genotypes. (H) Kaplan-Meier curve demonstrates a trend toward shorter survival in SHH medulloblastoma patients with low PKM2 expression. *P* values determined by log-rank test for Kaplan-Meier curves (A-D), cox proportional hazard model (H), and by Student's *t*-test (G). Scale bars: 2 mm (E,F); 100 μm (E'-E'", F'-F'").

Figure 2.7

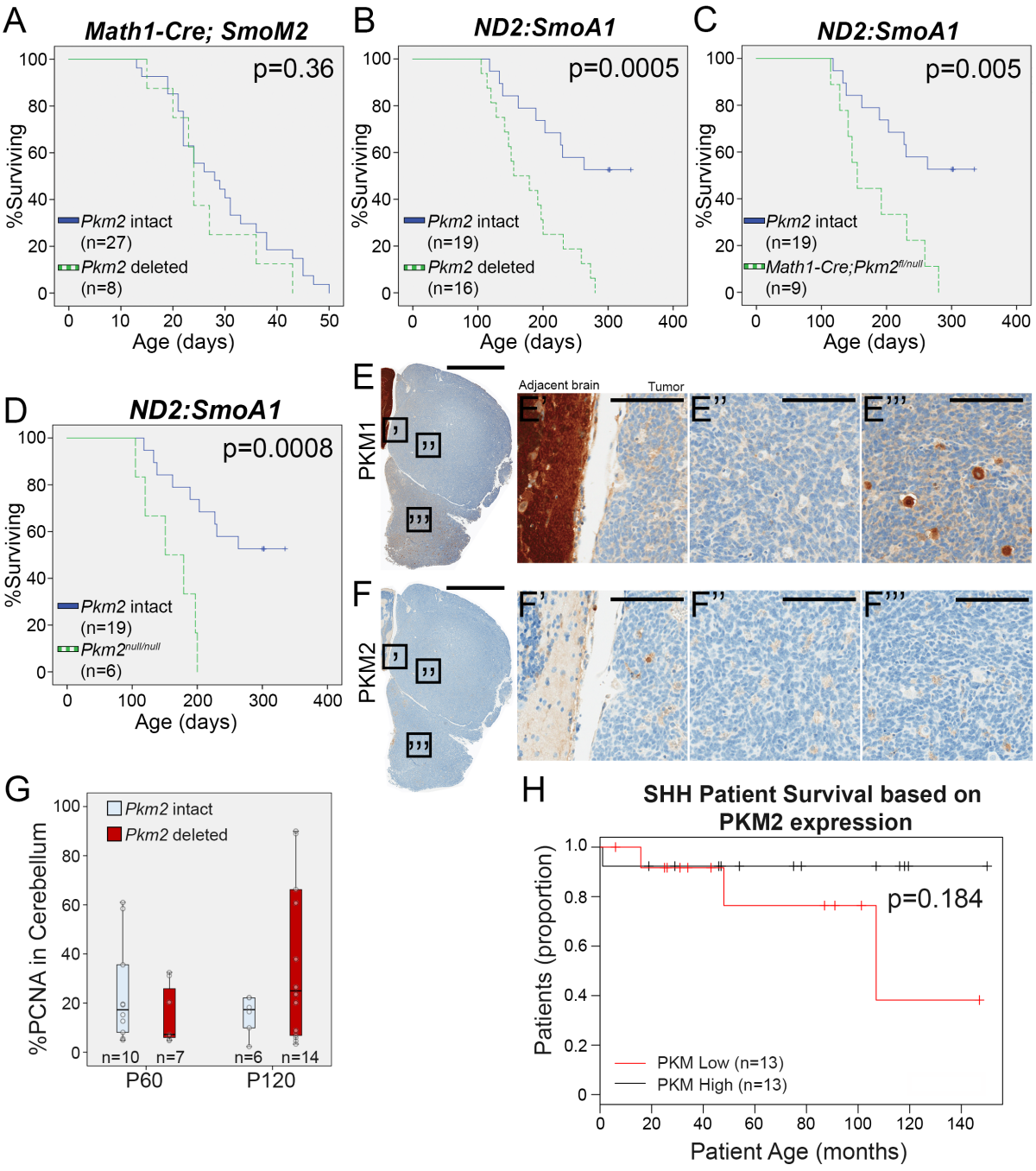
A
Math1-Cre; SmoM2
p=0.36
%Surviving
Pkm2 intact (n=27)
Pkm2 deleted (n=8)
Age (days)
B
ND2:SmoA1
p=0.0005
Pkm2 intact (n=19)
Pkm2 deleted (n=16)
C
ND2:SmoA1
p=0.005
Pkm2 intact (n=19)
Math1-Cre;Pkm2fl/null (n=9)
D
ND2:SmoA1
p=0.0008
Pkm2 intact (n=19)
Pkm2null/null (n=6)
E
PKM1
Adjacent brain
Tumor
E'
E''
E'''
F
PKM2
F'
F''
F'''
G
%PCNA in Cerebellum
Pkm2 intact
Pkm2 deleted
n=10
n=7
n=6
n=14
P60
P120
H
SHH Patient Survival based on PKM2 expression
Patients (proportion)
p=0.184
PKM Low (n=13)
PKM High (n=13)
Patient Age (months)

2.7 Tables

Table 2.1 Percent change of analyzed media metabolites.

	Δ24h Ctrl	Δ24h *Pkm2*^{cKO}	ΔCtrl vs Δ*Pkm2*^{cKO} *p value*
Acetate	-71.1 ± 2.2	-69.2 ± 3.7	0.700
Alanine	64.4 ± 17.1	68.4 ± 8.9	0.831
Arginine	-58.2 ± 2.4	-43.7 ± 4.5	0.053
Choline	-75.6 ± 12.9	-52.4 ± 8.8	0.182
[1,6-^{13}C]Glucose	-32.8 ± 4.7	-30.4 ± 4.9	0.739
Glutamine	6.1 ± 3.8	20.5 ± 7.8	0.199
Glycine	-71.9 ± 11.0	-71.0 ± 6.4	0.945
Isoleucine	-15.7 ± 1.7	-14.0 ± 1.2	0.409
Total Lactate	802.4 ± 60.0	618.4 ± 28.8	**0.029****
Lysine	-5.5 ± 2.3	3.2 ± 6.9	0.346
Methionine	-70.4 ± 0.9	-73.0 ± 2.1	0.353
Threonine	-63.3 ± 10.6	-73.1 ± 5.8	0.423
Tyrosine	-14.0 ± 13.8	13.4 ± 12.6	0.205

(**) Includes ^{13}C fractionally enriched lactate

Media from explanted CGNPs with intact or deleted *Pkm2* was sampled at 0 and 24h then subjected to ^{1}H NMR. Data presented are mean ± s.e.m. *P* values determined by Student's *t*-tests.

2.8 Supplemental Figures and Legends

Figure 2.S1 Germline deletion of *Pkm2*.

(A) PCR genotyping of genomic DNA from $Pkm2^{fl/fl}$, $Pkm2^{fl/null}$, $Pkm2^{null/null}$, and $Pkm2^{+/+}$ mice. Genotyping primers anneal outside of the loxP sites and produce amplicons of 560 bp from the $Pkm2^{+}$ allele, 605 bp from the $Pkm2^{fl}$ allele, and 220 bp from the $Pkm2^{null}$ allele. (B) Schematic of the $Pkm2^{null}$ allele with partial alignment (bold) between $Pkm2^{fl}$ and $Pkm2^{null}$ sequences shown below. (C,D) IHC demonstrates no overt malformation of the P8 $Pkm2^{null/null}$ brain. PKM1 expression (brown) is limited to differentiated neurons and PKM2 (brown) is absent from all brain regions. High magnification of boxed area is shown on the right. SVZ, subventricular zone; HC, hippocampus; EGL, external granule layer; IGL, internal granule layer; PC, Purkinje cell layer. Scale bars: 2 mm (C,D); 500 μm (C',D'); 100 μm (C",D").

Figure 2.S1

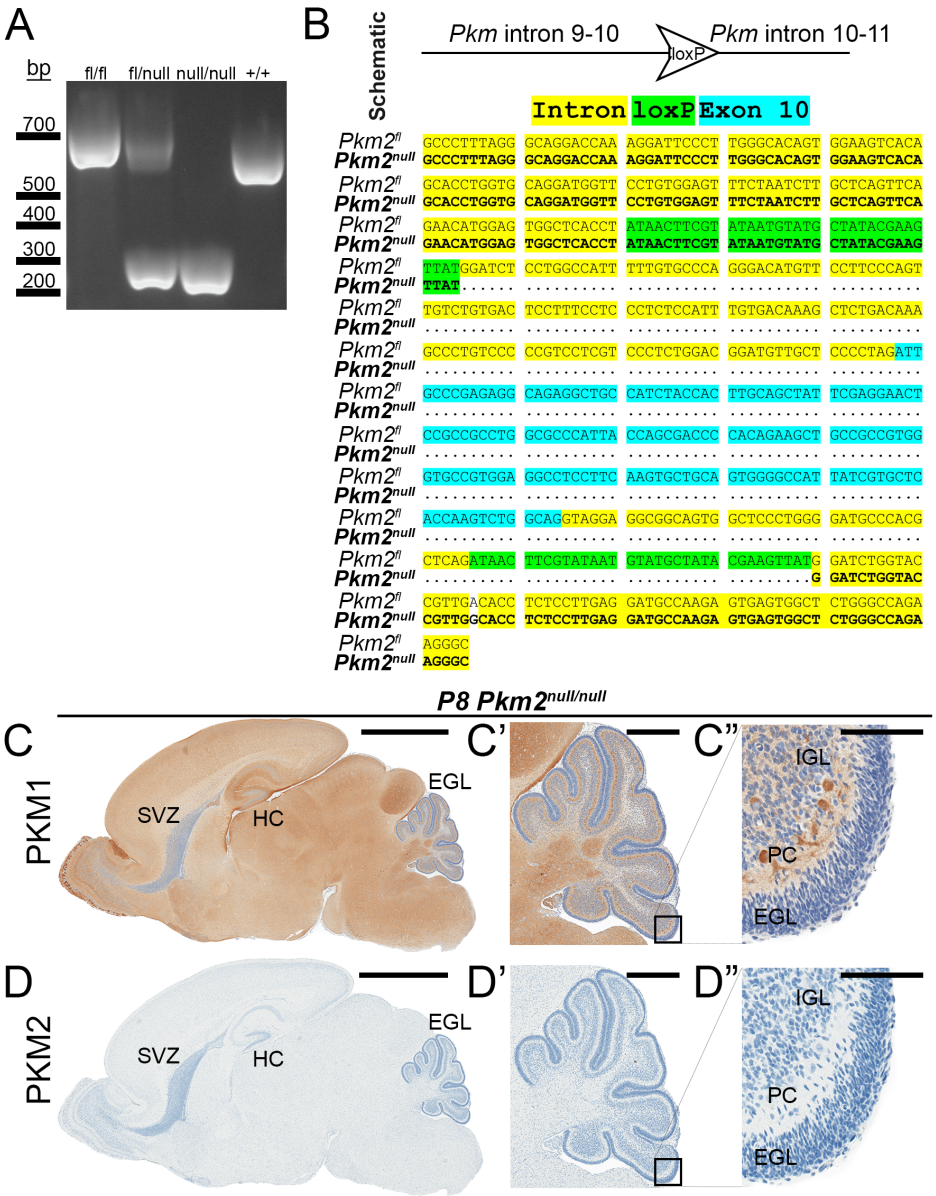
A
bp
fl/fl
fl/null
null/null
+/+
700
500
400
300
200
B
Schematic
Pkm intron 9-10
loxP
Pkm intron 10-11
Intron loxP Exon 10
Pkm2fl GCCCTTTAGG GCAGGACCAA AGGATTCCCT TGGGCACAGT GGAAGTCACA
Pkm2null GCCCTTTAGG GCAGGACCAA AGGATTCCCT TGGGCACAGT GGAAGTCACA
Pkm2fl GCACCTGGTG CAGGATGGTT CCTGTGGAGT TTCTAATCTT GCTCAGTTCA
Pkm2null GCACCTGGTG CAGGATGGTT CCTGTGGAGT TTCTAATCTT GCTCAGTTCA
Pkm2fl GAACATGGAG TGGCTCACCT ATAACTTCGT ATAATGTATG CTATACGAAG
Pkm2null GAACATGGAG TGGCTCACCT ATAACTTCGT ATAATGTATG CTATACGAAG
Pkm2fl TTATGGATCT CCTGGCCATT TTTGTGCCCA GGGACATGTT CCTTCCCAGT
Pkm2null TTAT
Pkm2fl TGTCTGTGAC TCCTTTCCTC CCTCTCCATT TGTGACAAAG CTCTGACAAA
Pkm2null
Pkm2fl GCCCTGTCCC CCGTCCTCGT CCCTCTGGAC GGATGTTGCT CCCCTAGATT
Pkm2null
Pkm2fl GCCCGAGAGG CAGAGGCTGC CATCTACCAC TTGCAGCTAT TCGAGGAACT
Pkm2null
Pkm2fl CCGCCGCCTG GCGCCCATTA CCAGCGACCC CACAGAAGCT GCCGCCGTGG
Pkm2null
Pkm2fl GTGCCGTGGA GGCCTCCTTC AAGTGCTGCA GTGGGGCCAT TATCGTGCTC
Pkm2null
Pkm2fl ACCAAGTCTG GCAGGTAGGA GGCGGCAGTG GCTCCCTGGG GATGCCCACG
Pkm2null
Pkm2fl CTCAGATAAC TTCGTATAAT GTATGCTATA CGAAGTTATG GATCTGGTAC
Pkm2null G GATCTGGTAC
Pkm2fl CGTTGACACC TCTCCTTGAG GATGCCAAGA GTGAGTGGCT CTGGGCCAGA
Pkm2null CGTTGGCACC TCTCCTTGAG GATGCCAAGA GTGAGTGGCT CTGGGCCAGA
Pkm2fl AGGGC
Pkm2null AGGGC
P8 Pkm2null/null
C
C'
C''
PKM1
SVZ
HC
EGL
IGL
PC
EGL
D
D'
D''
PKM2
SVZ
HC
EGL
IGL
PC
EGL

Figure 2.S2 Scrambling of ^{13}C glucose label in the Krebs cycle.

Incorporation ^{13}C from [1,6-^{13}C] glucose into glutamate starts with [3-^{13}C] pyruvate entering the Krebs cycle. Glutamate labeling at different carbons depends on whether [3-^{13}C] pyruvate enters the Krebs cycle through carboxylation, catalyzed by pyruvate carboxylase (*PC), to form [3-^{13}C] oxaloacetate or through decarboxylation, catalyzed by pyruvate dehydrogenase (PDH), to form [2-^{13}C] acetyl-CoA. In the first turn of the cycle, [4-^{13}C] glutamate is formed from [2-^{13}C] acetyl-CoA, while [2-^{13}C] glutamate is formed from [3-^{13}C] oxaloacetate. Additional ^{13}C atoms are incorporated on subsequent turns of the cycle as [2-^{13}C] acetyl-CoA joins with labeled oxaloacetate to form citrate. Decreased ^{13}C incorporation into glutamate in *Pkm2*-deleted CGNPs suggests increased cataplerosis of Krebs cycle intermediates.

Figure 2.S2

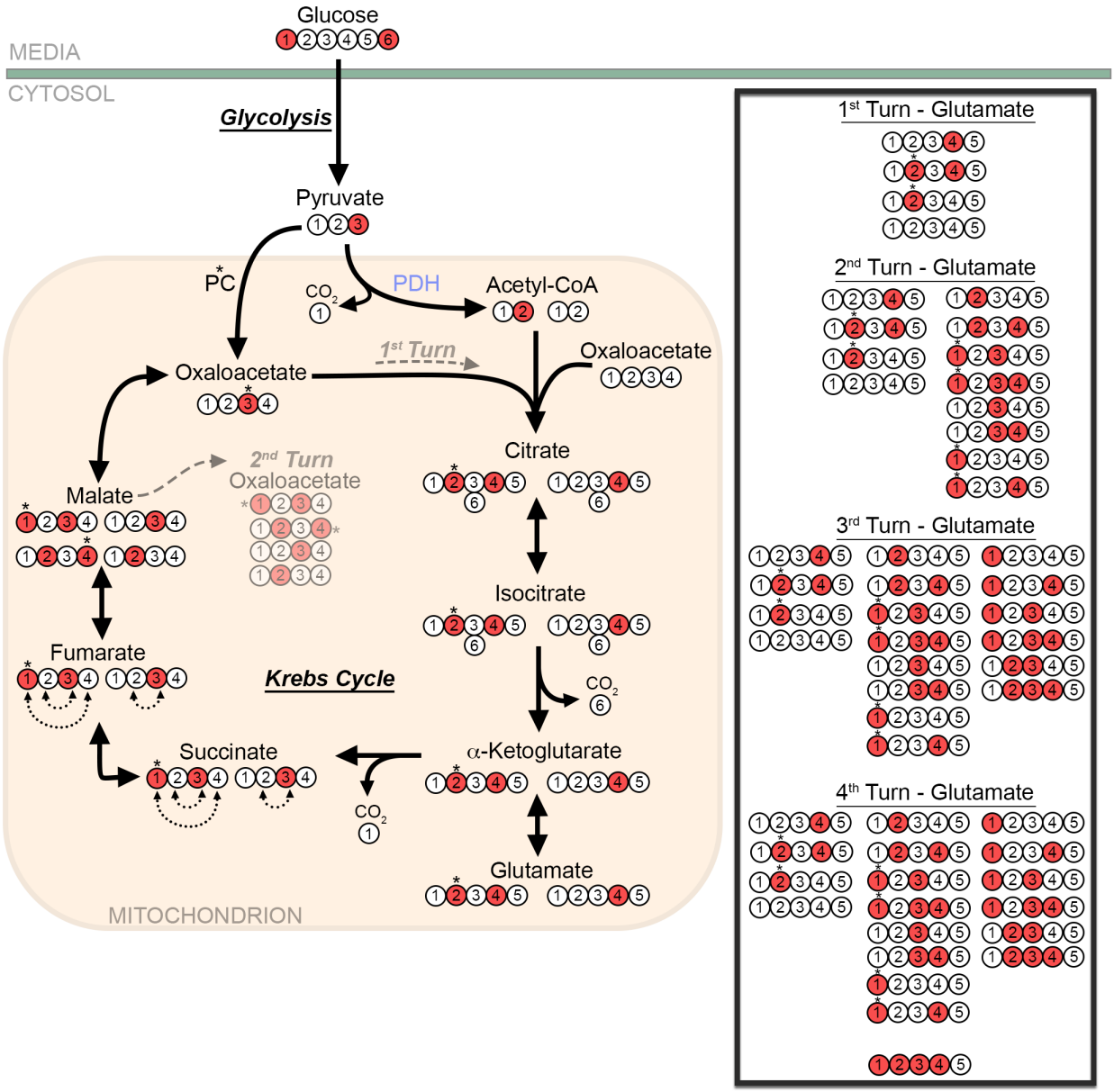
Glucose
MEDIA
CYTOSOL
Glycolysis
Pyruvate
PC
PDH
Acetyl-CoA
Oxaloacetate
1st Turn
Oxaloacetate
2nd Turn
Oxaloacetate
Citrate
Malate
Isocitrate
Fumarate
Krebs Cycle
Succinate
α-Ketoglutarate
Glutamate
MITOCHONDRION
1st Turn - Glutamate
2nd Turn - Glutamate
3rd Turn - Glutamate
4th Turn - Glutamate

Figure 2.S3 Entrapped PKM1+ cells in *Pkm2*-deleted tumors are not proliferating.

A representative *Pkm2*-deleted *ND2:SmoA1* mouse brain with medulloblastoma at P147 shows (A) PKM1 (red) in the normal brain adjacent to the tumor. (B-B") The scattered PKM1+ cells with relatively large cell bodies (arrowheads) noted in Fig. 7E are PKM1+ PCNA- cells. These differentiated cells were entrapped or generated by the tumor. Scale bars: 2 mm (A); 100 μm (B-B").

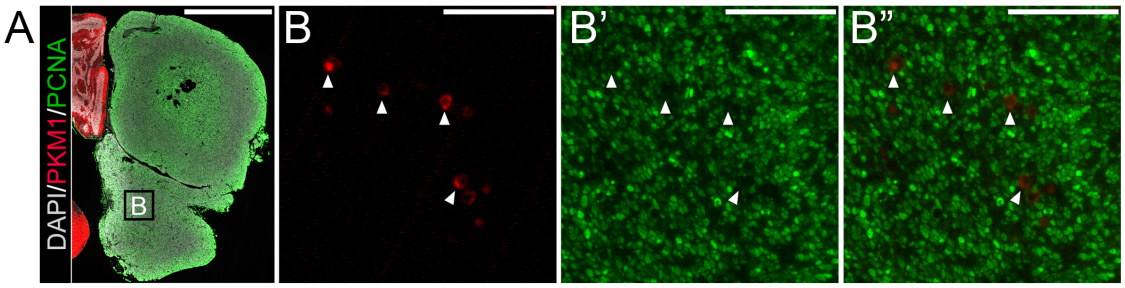

2.9 REFERENCES

1 Warburg O. On the Origin of Cancer Cells. *Science* 1956; **123**: 309–314.

2 Lunt SY, Vander Heiden MG. Aerobic Glycolysis: Meeting the Metabolic Requirements of Cell Proliferation. *Annu Rev Cell Dev Biol* 2011; **27**: 441–464.

3 Vander Heiden MG, Lunt SY, Dayton TL, Fiske BP, Israelsen WJ, Mattaini KR *et al.* Metabolic Pathway Alterations that Support Cell Proliferation. *Cold Spring Harb Symp Quant Biol* 2011; **76**: 325–334.

4 Hatten ME, Rifkin DB, Furie MB, Mason CA, Liem RK. Biochemistry of granule cell migration in developing mouse cerebellum. *Prog Clin Biol Res* 1982; **85**: 509–519.

5 Hatten ME, Alder J, Zimmerman K, Heintz N. Genes involved in cerebellar cell specification and differentiation. *Curr Opin Neurobiol* 1997; **7**: 40–47.

6 Gershon TR, Crowther AJ, Tikunov A, Garcia I, Annis R, Yuan H *et al.* Hexokinase-2-mediated aerobic glycolysis is integral to cerebellar neurogenesis and pathogenesis of medulloblastoma. *Cancer Metab* 2013; **1**: 1–17.

7 Grimmer MR, Weiss WA. Childhood tumors of the nervous system as disorders of normal development. *Curr Opin Pediatr* 2006; **18**: 634–638.

8 Schüller U, Heine VM, Mao J, Kho AT, Dillon AK, Han Y-G *et al.* Acquisition of granule neuron precursor identity is a critical determinant of progenitor cell competence to form Shh-induced medulloblastoma. *Cancer Cell* 2008; **14**: 123–134.

9 Yang Z-J, Ellis T, Markant SL, Read T-A, Kessler JD, Bourboulas M *et al.* Medulloblastoma can be initiated by deletion of Patched in lineage-restricted progenitors or stem cells. *Cancer Cell* 2008; **14**: 135–145.

10 Marino S. Medulloblastoma: developmental mechanisms out of control. *Trends Mol Med* 2005; **11**: 17–22.

11 Roussel MF, Hatten ME. Cerebellum: Development and Medulloblastoma. *Curr Top Dev Biol* 2011; **94**: 235–282.

12 Bhatia B, Potts CR, Guldal C, Choi S, Korshunov A, Pfister S *et al.* Hedgehog-mediated regulation of PPARγ controls metabolic patterns in neural precursors and shh-driven medulloblastoma. *Acta Neuropathol* 2012; **123**: 587–600.

13 Dahmane N, Ruiz i Altaba A. Sonic hedgehog regulates the growth and patterning of the cerebellum. *Development* 1999; **126**: 3089–3100.

14 Wechsler-Reya RJ, Scott MP. Control of Neuronal Precursor Proliferation in the Cerebellum by Sonic Hedgehog. *Neuron* 1999; **22**: 103–114.

15 Kenney AM, Rowitch DH. Sonic hedgehog Promotes G1 Cyclin Expression and Sustained Cell Cycle Progression in Mammalian Neuronal Precursors. *Mol Cell Biol* 2000; **20**: 9055–9067.

16 Vaillant C, Monard D. SHH pathway and cerebellar development. *Cerebellum* 2009; **8**: 291–301.

17 Kool M, Korshunov A, Remke M, Jones DTW, Schlanstein M, Northcott PA *et al.* Molecular subgroups of medulloblastoma: an international meta-analysis of transcriptome, genetic aberrations, and clinical data of WNT, SHH, Group 3, and Group 4 medulloblastomas. *Acta Neuropathol* 2012; **123**: 473–484.

18 Northcott PA, Korshunov A, Pfister SM, Taylor MD. The clinical implications of medulloblastoma subgroups. *Nat Rev Neurol* 2012; **8**: 340–351.

19 Northcott PA, Korshunov A, Witt H, Hielscher T, Eberhart CG, Mack S *et al.* Medulloblastoma comprises four distinct molecular variants. *J Clin Oncol* 2011; **29**: 1408–1414.

20 Hallahan AR, Pritchard JI, Hansen S, Benson M, Stoeck J, Hatton BA *et al.* The SmoA1 Mouse Model Reveals That Notch Signaling Is Critical for the Growth and Survival of Sonic Hedgehog-Induced Medulloblastomas. *Cancer Res* 2004; **21**: 7794–7800.

21 Mao J, Ligon KL, Rakhlin EY, Thayer SP, Bronson RT, Rowitch D *et al.* A Novel Somatic Mouse Model to Survey Tumorigenic Potential Applied to the Hedgehog Pathway. *Cancer Res* 2006; **66**: 10171–10178.

22 Hatton BA, Villavicencio EH, Tsuchiya KD, Pritchard JI, Ditzler S, Pullar B *et al.* The Smo/Smo model: Hedgehog-induced medulloblastoma with 90% incidence and leptomeningeal spread. *Cancer Res* 2008; **68**: 1768–1776.

23 Lin H, Zeng J, Xie R, Schulz MJ, Tedesco R, Qu J *et al.* Discovery of a Novel 2,6-Disubstituted Glucosamine Series of Potent and Selective Hexokinase 2 Inhibitors. *ACS Med Chem Lett* 2016; **7**: 217–222.

24 Mathupala SP, Ko YH, Pedersen PL. Hexokinase II: Cancer's double-edged sword acting as both facilitator and gatekeeper of malignancy when bound to mitochondria. *Oncogene* 2006; **25**: 4777–4786.

25 Lehninger AL. *Lehninger Principles of Biochemistry*. 4th ed. W.H. Freeman: New York, USA, 2005.

26 Imamura K, Tanaka T. Multimolecular Forms of Pyruvate Kinase from Rat and Other Mammalian Tissues. *J Biochem* 1972; **71**: 1043–1051.

27 Noguchi T, Inoue H, Tanaka T. The M1- and M2-type Isozymes of Rat Pyruvate Kinase Are Produced from the Same Gene by Alternative RNA Splicing. *J Biol Chem* 1986; **261**: 13807–13812.

28 Mazurek S. Pyruvate kinase type M2 : A key regulator of the metabolic budget system in tumor cells. *Int J Biochem Cell Biol* 2011; **43**: 969–980.

29 Israelsen WJ, Vander Heiden MG. Pyruvate kinase: Function, regulation and role in cancer. *Semin Cell Dev Biol* 2015; **43**: 43–51.

30 Yang W, Lu Z. Regulation and function of pyruvate kinase M2 in cancer. *Cancer Lett* 2013; **339**: 153–158.

31 Varghese B, Swaminathan G, Plotnikov A, Tzimas C, Yang N, Rui H *et al.* Prolactin Inhibits Activity of Pyruvate Kinase M2 to Stimulate Cell Proliferation. *Mol Endocrinol* 2010; **24**: 2356–2365.

32 Gui DY, Lewis CA, Vander Heiden MG. Allosteric regulation of PKM2 allows cellular adaptation to different physiological states. *Sci Signal* 2013; **6**: pe7.

33 Christofk HR, Vander Heiden MG, Wu N, Asara JM, Cantley LC. Pyruvate kinase M2 is a phosphotyrosine-binding protein. *Nature* 2008; **452**: 181–188.

34 Anastasiou D, Yu Y, Israelsen WJ, Jiang J-K, Boxer MB, Hong BS *et al.* Pyruvate kinase M2 activators promote tetramer formation and suppress tumorigenesis. *Nat Chem Biol* 2012; **8**: 839–847.

35 Hitosugi T, Kang S, Vander Heiden MG, Chung T-W, Elf S, Lythgoe K *et al.* Tyrosine phosphorylation inhibits PKM2 to promote the Warburg effect and tumor growth. *Sci Signal* 2009; **2**: 1–8.

36 Christofk HR, Vander Heiden MG, Harris MH, Ramanathan A, Gerszten RE, Wei R *et al.* The M2 splice isoform of pyruvate kinase is important for cancer metabolism and tumour growth. *Nature* 2008; **452**: 230–234.

37 Gao X, Wang H, Yang JJ, Liu X, Liu Z-R. Pyruvate kinase M2 regulates gene transcription by acting as a protein kinase. *Mol Cell* 2012; **45**: 598–609.

38 Yang W, Xia Y, Ji H, Zheng Y, Liang J, Huang W *et al.* Nuclear PkM2 regulates beta-catenin transactivation upon EGFR activation. *Nature* 2011; **480**: 118–122.

39 Yang W, Xia Y, Hawke D, Li X, Liang J, Xing D *et al.* PKM2 Phosphorylates Histone H3 and Promotes Gene Transcription and Tumorigenesis. *Cell* 2012; **150**: 685–696.

40 Ignacak J, Stachurska MB. The dual activity of pyruvate kinase type M2 from chromatin extracts of neoplastic cells. *Comp Biochem Physiol Part B Biochem Mol Biol* 2003; **134**: 425–433.

41 Lu Z. PKM2 functions as a histone kinase. *Cell cycle* 2012; **11**: 4101–4102.

42 Hosios AM, Fiske BP, Gui DY, Vander Heiden MG. Lack of Evidence for PKM2 Protein Kinase Activity. *Mol Cell* 2015; **59**: 850–857.

43 Israelsen WJ, Dayton TL, Davidson SM, Fiske BP, Hosios AM, Bellinger G *et al.* PKM2 isoform-specific deletion reveals a differential requirement for pyruvate kinase in tumor cells. *Cell* 2013; **155**: 397–409.

44 Dayton TL, Gocheva V, Miller KM, Israelsen WJ, Bhutkar A, Clish CB *et al.* Germline loss of PKM2 promotes metabolic distress and hepatocellular carcinoma. *Genes Dev* 2016; **30**: 1020–1033.

45 Di Magno L, Manzi D, D'Amico D, Coni S, Macone A, Infante P *et al.* Druggable glycolytic requirement for Hedgehog-dependent neuronal and medulloblastoma growth. *Cell Cycle* 2014; **13**: 3404–3413.

46 Staal JA, Lau LS, Zhang H, Ingram WJ, Hallahan AR, Northcott PA *et al.* Proteomic profiling of high risk medulloblastoma reveals functional biology. *Oncotarget* 2015; **6**: 14584–95.

47 Hibi M, Shimizu T. Development of the cerebellum and cerebellar neural circuits. *Dev Neurobiol* 2012; **72**: 282–301.

48 Rubin LL, de Sauvage FJ. Targeting the Hedgehog pathway in cancer. *Nat Rev Drug Discov* 2006; **5**: 1026–1033.

49 Salani B, Ravera S, Amaro A, Salis A, Passalacqua M, Millo E *et al.* IGF1 regulates PKM2 function through Akt phosphorylation. *Cell Cycle* 2015; **14**: 1559–1567.

50 Iqbal MA, Siddiqui FA, Gupta V, Chattopadhyay S, Gopinath P, Kumar B *et al.* Insulin enhances metabolic capacities of cancer cells by dual regulation of glycolytic enzyme pyruvate kinase M2. *Mol Cancer* 2013; **12**: 72–83.

51 Dudek H, Datta SR, Franke TF, Segal RA, Kaplan DR, Greenberg ME. Regulation of neuronal survival by the serine-threonine protein kinase Akt. *Science* 1997; **275**: 661–665.

52 Helms AW, Abney AL, Ben-Arie N, Zoghbi HY, Johnson JE. Autoregulation and multiple enhancers control Math1 expression in the developing nervous system. *Development* 2000; **127**: 1185–1196.

53 Machold R, Fishell G. Math1 is expressed in temporally discrete pools of cerebellar rhombic-lip neural progenitors. *Neuron* 2005; **48**: 17–24.

54 Goyal MS, Hawrylycz M, Miller JA, Snyder AZ, Raichle ME. Aerobic glycolysis in the human brain is associated with development and neotenous gene expression. *Cell Metab* 2014; **19**: 49–57.

55 Wolf A, Agnihotri S, Munoz D, Guha A. Developmental profile and regulation of the glycolytic enzyme hexokinase 2 in normal brain and glioblastoma multiforme. *Neurobiol Dis* 2011; **44**: 84–91.

56 Lunt SY, Muralidhar V, Hosios AM, Israelsen WJ, Gui DY, Newhouse L *et al.* Pyruvate Kinase Isoform Expression Alters Nucleotide Synthesis to Impact Cell Proliferation. *Mol Cell* 2015; **57**: 95–107.

57 Johnson RL, Grenier JK, Scott MP. Patched Overexpression Alters Wing Disc Size and Pattern: Transcriptional and Post-Transcriptional Effects on Hedgehog Targets. *Development* 1995; **121**: 4161–4170.

58 Goodrich L V., Jung D, Higgins KM, Scott MP. Overexpression of ptc1 inhibits induction of Shh target genes and prevents normal patterning in the neural tube. *Dev Biol* 1999; **211**: 323–334.

59 Taipale J, Cooper MK, Maiti T, Beachy PA. Patched acts catalytically to suppress the activity of Smoothened. *Nature* 2002; **418**: 892–897.

60 Eigenbrodt R, Reinacher M, Scheefers-Borchel U, Scheefers H, Friss R. Double role for pyruvate kinase type M2 in the expansion of phosphometabolite pools found in tumor cells. *Crit Rev Oncog* 1992; **3**: 91–115.

61 Tech K, Deshmukh M, Gershon TR. Adaptations of energy metabolism during cerebellar neurogenesis are co-opted in medulloblastoma. *Cancer Lett* 2014; **356**: 268–272.

62 Hosios AM, Hecht VC, Danai LV, Johnson MO, Rathmell JC, Steinhauser ML *et al.* Amino Acids Rather than Glucose Account for the Majority of Cell Mass in Proliferating Mammalian Cells. *Dev Cell* 2016; **36**: 540–549.

63 Vander Heiden MG, Locasale JW, Swanson KD, Sharfi H, Heffron GJ, Amador-Noguez D *et al.* Evidence for an alternative glycolytic pathway in rapidly proliferating cells. *Science* 2010; **329**: 1492–1499.

64 Hitosugi T, Zhou L, Fan J, Elf S, Zhang L, Xie J *et al.* Tyr26 phosphorylation of PGAM1 provides a metabolic advantage to tumours by stabilizing the active conformation. *Nat Commun* 2013; **4**: 1–10.

65 Hitosugi T, Zhou L, Elf S, Fan J, Kang H-B, Seo JH *et al.* Phosphoglycerate Mutase 1 Coordinates Glycolysis and Biosynthesis to Promote Tumor Growth. *Cancer Cell* 2012; **22**: 585–600.

66 Jiang Y, Wang Y, Wang T, Hawke DH, Zheng Y, Li X *et al.* PKM2 phosphorylates MLC2 and regulates cytokinesis of tumour cells. *Nat Commun* 2014; **5**: 1–14.

67 Morris LGT, Chan TA. Therapeutic targeting of tumor suppressor genes. *Cancer* 2015; **121**: 1357–1368.

68 Liu Y, Hu X, Han C, Wang L, Zhang X, He X *et al.* Targeting tumor suppressor genes for cancer therapy. *BioEssays* 2015; **37**: 1277–1286.

69 Kenney AM, Cole MD, Rowitch DH. Nmyc upregulation by sonic hedgehog signaling promotes proliferation in developing cerebellar granule neuron precursors. *Development* 2003; **130**: 15–28.

70 Tikunov AP, Johnson CB, Lee H, Stoskopf MK, Macdonald JM. Metabolomic investigations of American oysters using 1H-NMR spectroscopy. *Mar Drugs* 2010; **8**: 2578–2596.

71 Human Metabolome Database. http://www.hmdb.ca.

72 Millard P, Letisse F, Sokol S, Portais JC. IsoCor: Correcting MS data in isotope labeling experiments. *Bioinformatics* 2012; **28**: 1294–1296.

73 Garcia I, Crowther AJ, Gama V, Miller CR, Deshmukh M, Gershon TR. Bax deficiency prolongs cerebellar neurogenesis, accelerates medulloblastoma formation and paradoxically increases both malignancy and differentiation. *Oncogene* 2013; **32**: 2304–2314.

74 Li B, Dewey CN. RSEM: accurate transcript quantification from RNA-Seq data with or without a reference genome. *BMC Bioinformatics* 2011; **12**: 323.

75 Dobin A, Davis CA, Schlesinger F, Drenkow J, Zaleski C, Jha S *et al.* STAR: Ultrafast universal RNA-seq aligner. *Bioinformatics* 2013; **29**: 15–21.

76 Morin RD, Bainbridge M, Fejes A, Hirst M, Krzywinski M, Pugh TJ *et al.* Profiling the HeLa S3 transcriptome using randomly primed cDNA and massively parallel short-read sequencing. *Biotechniques* 2008; **45**: 81–94.

77 Li H, Durbin R. Fast and accurate short read alignment with Burrows-Wheeler transform. *Bioinformatics* 2009; **25**: 1754–1760.

CHAPTER III: VISMODEGIB TREATMENT AND *HK2* DELETION ACT IN CONCERT TO RESTRICT MEDULLOBLASTOMA GROWTH

3.1 Overview

Medulloblastoma accounts for 18% of all malignant pediatric brain tumors as the most common malignant brain tumor in children[1]. Of the four subgroups, Wnt, SHH, Group 3, and Group 4, the SHH subgroup represents a third of all medulloblastoma cases. The SHH subgroup is driven by aberrant activation of the SHH signaling pathway. In CGNPs, SHH binds to the Patched1 (PTC) receptor, releasing the transmembrane protein Smoothened (SMO) from inhibition, and ultimately dissociates the SUFU-GLI complex to promote proliferation. Genetic and molecular alterations in *Ptc*, *Sufu*, and other downstream effectors of the SHH pathway activation lead to uncontrolled CGNP growth and medulloblastoma tumorigenesis. One strategy in the targeted treatment of SHH medulloblastoma is SMO inhibition. The competitive antagonist vismodegib binds to SMO to block downstream SHH signaling. While vismodegib has demonstrated safety and efficacy in the treatment of SHH medulloblastoma, acquired resistance is common. To identify vismodegib-resistance mechanisms, collaborators used the Sleeping Beauty mutagenesis screen in a SHH-driven medulloblastoma model. In a subset of resistant medulloblastomas, Hexokinase-2 (HK2) expression was increased independently of *Gli2* amplification. In collaboration with the Michael D. Taylor lab at The Hospital for Sick Children in Toronto, I investigated the effects of vismodegib treatment on *Hk2*-deleted medulloblastomas. *Hk2* deletion sensitized SHH tumors to vismodegib, promoting differentiation, reducing tumor growth, but did not prolong survival when compared to vehicle-treated counterparts. In all, these studies suggest that *Hk2* activation is a new mechanism of resistance to SMO inhibition such that the inhibition of both HK2 and the SHH pathway may be a novel, potent treatment for SHH-driven medulloblastoma.

3.2 Introduction

Medulloblastoma was universally fatal until the advent of craniospinal radiation therapy in 1953[2]. Decades of empirical trials have led to optimized regimens using surgical resection, radiation to the entire brain and spinal cord, followed by a year of chemotherapy. The conventional treatment, however, is unable to specifically target cancer cells resulting in damage to normal cells and untoward injuries. While 80% of medulloblastoma patients become long-term survivors, this treatment causes significant adverse effects, including cognitive impairment, strokes at a young age, hearing loss, and other toxicities. Moreover, the risk of recurrence looms over survivors as recurrent medulloblastoma is almost universally fatal[3]. Further research into medulloblastoma will contribute to the understanding of the disease and lead to novel treatments for both primary and recurrent tumors.

Genomic analyses has demonstrated that medulloblastoma is comprised of four distinct molecular variants defined by alterations in the wingless pathway (Wnt), sonic hedgehog pathway (SHH), *MYC*-amplification (Group 3), and heterogeneity (Group 4)[4–6]. SHH-driven medulloblastoma comprises about a third of all patient cases and predominately affects infants and adults[6]. Activating mutations in SMO and inactivating mutations in negative pathway regulators PTC and SUFU result in aberrant SHH pathway activation[5,7–9]. While this subgroup is defined by the SHH pathway, other genetic alterations contribute to subgroup heterogeneity which may affect drug response. Germline *TP53* mutations, in addition to MYCN and GLI2 co-amplifications, add to the complexity of SHH-driven medulloblastoma and its targeted treatment[1,10]. A better understanding of SHH signaling and its alterations in medulloblastoma may produce new anti-cancer strategies and provide insight to drug response.

Vismodegib is a competitive antagonist of SMO used in the treatment of SHH-driven medulloblastoma. While vismodegib treatment can prolong progression-free survival and induce tumor regression, the effects vary across SHH medulloblastoma patients[11,12] and are transient[13]. Within the SHH subgroup are vismodegib non-responders who have pathway-activating mutations downstream of SMO in SUFU and GLI2[11,12]. Likewise, SHH patients with pathway alterations upstream of SMO, such as loss-of-heterozygosity and loss-of-function PTC1 mutations, had longer progression-free survival with vismo treatment. Thus, SMO inhibitors are only clinically significant for medulloblastomas with genetic mutations

upstream of *Smoothened*[11,12]. Moreover, the initial success of vismodegib and other SMO inhibitors[14], however, is now overshadowed by drug resistance. In a single adult male medulloblastoma patient, vismodegib treatment induced robust tumor regression followed by relapse and death from disease progression. Subsequent analysis showed that this specific relapse was associated with a single amino acid substitution in SMO that impaired vismodegib binding[15]. Other mechanisms of vismodegib-resistance include SMO point mutations[16], amplification of SHH pathway effectors downstream of SMO (*Gli2*, *Ccnd1*)[17], loss-of-function mutations in SUFU[18], and phosphoinositide 3-kinase (PI3K) pathway activation[17,19]. Identifying additional mechanisms of resistance would provide ways sensitize tumors to current treatments and critical information for the development of second-generation SMO inhibitors. Unfortunately, the vismodegib-resistant human medulloblastomas essential for these studies are rarely biopsied, requiring the use of animal models.

To identify mechanisms of resistance to vismodegib, the Michael D. Taylor lab at The Hospital for Sick Children used an unbiased, genome-wide approach in a mouse model of SHH-driven medulloblastoma. The highly active Sleeping Beauty (SB) insertional mutagenesis system is used for functional genomic screens as an unbiased tool for the identification of genes and pathways involved in cancer[20–22]. Specifically, the transposition events in the SB system can mediate loss-of-function or gain-of-function mutations in somatic tissues and accelerate solid tumor formation in tumor-prone mice[23,24] (Fig. 3.1). To examine the genomic changes facilitating vismodegib-resistance, the $Ptc^{+/-}$ mouse model of SHH medulloblastoma was integrated with the SB system (Ptc-SB)[25]. In the Ptc-SB model, the *Math1* enhancer limits SB11 transposase expression to CGNPs and is in the presence of the mutagenic transposon vector T2/Onc on the $Ptc^{+/-}$ background[25]. The SB system increases the penetrance of $Ptc^{+/-}$ medulloblastoma, drives metastatic dissemination, and decreases latency from 8[26] to 2.5 months[25], making it the ideal system to study drug resistance.

Transposition events that confer vismodegib-resistance are expected to generate a clonal advantage in vismo-treated mice. Likewise, our collaborators found that relapsed, vismo-treated Ptc-SB mice up-regulated Hexokinase-2 (HK2) expression and activity. These findings were validated by re-analyzing a published gene expression profile of medulloblastomas from $Ptc^{+/-}$;$p53^{-/-}$ mice[19] treated with

the SMO inhibitor NVP-LDE225[27]. *Hk2* was initially down-regulated with NVP-LDE225 treatment and then restored when the tumor developed resistance[19]. Importantly, these changes in *Hk2* were independent of *Gli2* amplification, a known mechanism of SMO-resistance in medulloblastoma[17,19,28]. Together, these data suggest that HK2 activation is a novel driver of resistance to SMO inhibition, conferring a growth advantage through increased aerobic glycolysis. Here, I examine if *Hk2* deletion sensitizes primary, SHH-driven medulloblastomas to SMO inhibition. *Hk2* deletion and vismodegib treatment act in concert to restrict tumor growth but do not prolong survival compared to vehicle-treated counterparts. In all, these studies further emphasize the importance of aerobic glycolysis to SHH-driven medulloblastoma and its potential as a targeted cancer treatment.

3.3 Results

3.3.1 Vismodegib reduces proliferation in cultured, *Hk2*-deleted SHH-driven medulloblastomas

To examine the functional importance of HK2 in sensitizing SHH-driven medulloblastoma to SMO inhibition, I analyzed the anti-tumor effect of vismodegib treatment in *Hk2*-deleted tumors. The Gershon lab has previously shown that *Hk2* drives aerobic glycolysis and supports growth in SHH medulloblastomas of *hGFAP-Cre*;*SmoM2* mice[29]. In the Cre-driven SmoM2 model, the activating point mutation W529L in SMO induces the rapid development of progressive SHH-driven medulloblastoma with 100% incidence by P20. The mutation changes the binding pocket to block PTC binding and repression[30,31]. Because the oncogenic mutant SmoM2 is known to attenuate the effects of other SMO antagonists[32–34] and vismodegib binding is sensitive to SMO domain changes such as D473H[15], I first tested the effects of vismodegib in cultured medulloblastomas.

I cultured freshly isolated medulloblastoma cells from P12 *hGFAP-Cre*;*SmoM2*;$Hk2^{fl/+}$ ($Hk2^{fl/+}$) and *hGFAP-Cre*;*SmoM2*;$Hk2^{fl/fl}$ ($Hk2^{cKO}$) mice with and without vismodegib. Western blot and quantification confirmed *Hk2* deletion and showed that HK2 expression was not altered by 24 hours of vismodegib treatment in $Hk2^{fl/+}$ mice (Figs. 3.2A,B). In *Hk2*-deleted medulloblastoma cells, vismodegib treatment significantly decreased the proliferation marker CCDN2 (Fig. 3.2C) with no significant change in

apoptosis marker cleaved caspase-3 (Fig. 3.2D). In contrast, CCND2 and cC3 were not altered by vismodegib treatment in *Hk2*$^{fl/+}$ tumor cells. These data demonstrate that vismodegib decreases the proliferation of *Hk2*-deleted SmoM2-driven medulloblastomas, supporting the potential for vismodegib to inhibit SmoM2. My methods, however, did not demonstrate an effect of *in vitro* vismodegib on *Hk2*-intact tumor cells.

3.3.2 Injectable vismodegib maintains anti-tumor effects *in vivo*

Following the promising *in vitro* data, I then examined if *Hk2* deletion sensitizes medulloblastoma to short vismodegib treatment *in vivo*. As *hGFAP-Cre*;*SmoM2* mice develop medulloblastomas and succumb to disease by P20, I designed a short regimen to determine the effects of bolus vismodegib dosing delivered by intraperitoneal injection (IP). Starting at P12, *hGFAP-Cre*;*SmoM2* mice with and without *Hk2* deletion, were treated once a day for three days with either vehicle, 10% N-Methyl-2-pyrrolidone (NMP) in PEG200 (polyethylene glycol 200), or 100 mg/kg of vismodegib dissolved in 10% NMP in PEG 200. At P15, animals and tissues were collected for analysis.

Representative H&E stains of the four conditions, tumors with and without *Hk2* deletion treated with vismodegib or vehicle, are shown in Fig. 3.3A. IHC demonstrates that SMO inhibition reduces tumor size in both *Hk2*-intact and deleted mice. Subsequent immunohistochemistry stains for the proliferation marker proliferating cell nuclear antigen (PCNA) and the differentiation marker p27^{Kip1} are shown in Fig. 3.3B. After three days, the bolus vismodegib dose significantly decreased PCNA expression and increased p27^{Kip1} expression in both genotypes. There were no detectable differences in the response to drug treatment between genotypes over the short period of the experiment. Together, I demonstrate a novel, injectable formulation of vismodegib that inhibits proliferation and increases differentiation in SHH pathway-driven medulloblastoma. This work provided the experimental foundation for determining the survival benefit of blocking aerobic glycolysis by *Hk2* deletion in tandem with SMO inhibition by vismodegib treatment.

3.3.3 *Hk2* deletion and IP vismodegib treatment restrict tumor growth

To determine the survival benefit of simultaneously decreasing aerobic glycolysis and impeding the SHH signaling pathway, *hGFAP-Cre*;*SmoM2* mice with and without *Hk2* deletion were injected with vehicle or 100 mg/kg vismodegib every other day starting at P12. Similar to the previous *Hk2* deletion survival study[29], vehicle-treated *Hk2*-deleted mice survived significantly longer than vehicle-treated *Hk2*-intact controls (Fig. 3.4A). Vismodegib treatment provided a statistically significant survival benefit to the $Hk2^{fl/+}$ group (Fig. 3.4B). In the $Hk2^{cKO}$ group, where survival was longer and more heterogeneous, there was no statistically significant benefit of vismodegib (Fig. 3.4C). Comparing the two vismodegib-treated groups, the statistical significance of the benefit of *Hk2* deletion decreased to p=0.098, as vismodegib increased the relatively short survival of *Hk2*-intact controls but did not measurably increase the relatively long survival of *Hk2*-deleted mice (Fig. 3.4D). The overall survival data, however, were significant (Fig. 3.4E), likely due to the effect of *Hk2* deletion.

While treatment did not prolong the already extended survival of *Hk2*-deleted mice, vismodegib significantly reduced tumor size compared to vehicle-treated counterparts (Fig. 3.4F). Toxicity from chronic vismodegib is likely to have contributed to some of the deaths in the vismodegib-treated $Hk2^{cKO}$ group, as several mice died without large tumors. These findings demonstrate that both genotypes respond to vismodegib treatment and that survival may not be an ideal endpoint to determine treatment effect. The strong suppression of tumor growth by vismodegib in the longest surviving mice in the $Hk2^{cKO}$ group argues for a decreased rate of vismodegib resistance, compared to the *Hk2*-intact mice, where 100% of the animals developed tumor progression on vismodegib.

3.3.4 Oral vismodegib does not prevent toxicity or prolong survival in *Hk2*-deleted mice

Vismodegib is typically delivered orally in humans[11] and in mice[35]. For my initial *in vivo* drug experiments, I dissolved vismodegib in NMP[36], a common drug vehicle, for IP delivery. Although the final injection volume only contained NMP at the routine 10% v/v, there were concerns about NMP-induced toxicity and PEG200 accumulation. Specifically, the surviving vismo-treated, *Hk2*-deleted mice tended to

develop abdominal abnormalities and did not survive longer than vehicle-treated counterparts despite a clear decrease in tumor size (Fig. 3.4F). To further parse the survival benefit of vismodegib treatment in *Hk2*-deleted medulloblastomas, I conducted another survival study where vismodegib was delivered orally.

Consistent with prior work[35], vismodegib was formulated as a suspension in 0.5% methylcellulose, 0.2% Tween-80 (MCT) and administered orally at 100 mg/kg. As oral gavage is typically performed on adult mice, wildtype animals were first used to determined if ~P10 pups could endure MCT vehicle or vismodegib oral gavage every other day. After determining that healthy ~P10 pups can withstand oral gavage (data not shown), I started the oral gavage survival study on medulloblastoma-bearing mice. Starting at P12, *hGFAP-Cre*;*SmoM2* mice with and without *Hk2* deletion, were dosed four days a week with MCT vehicle or vismodegib. Similar to previous findings, *Hk2* deletion prolonged survival compared to *Hk2* intact controls in both vehicle- (Fig. 3.5A) and vismo-treated (Fig. 3.5B) groups. The oral gavage study again found a survival benefit of vismodegib only in *Hk2*-intact mice (Fig. 3.5C,D) with a similar overall significant difference (Fig. 3.5E). Oral gavage vismodegib treatment also reduced tumor size in *Hk2*-deleted mice compared to vehicle-treated counterparts (data not shown). Together, these data demonstrate that vismodegib prolongs survival in *Hk2* intact mice. While this survival benefit did not extend to *Hk2*-deleted mice, tumor size comparison showed that SMO inhibition works in tandem with blocked aerobic glycolysis to reduce tumor growth.

3.4 Discussion

Cancer chemotherapies have become increasingly targeted, and yet no anti-cancer treatment is 100% effective. Moreover, acquired resistance to these targeted, small molecule therapeutics in cancer is now common. SMO inhibition was once a promising anti-cancer strategy against SHH-driven medulloblastoma. Now, identifying and targeting the mechanisms of resistance to SMO inhibition is a requirement for the advancement of targeted SHH-medulloblastoma treatments. Using the Sleeping Beauty mutagenesis screen in the $Ptc^{+/-}$ model of SHH-driven medulloblastoma, our collaborators identified *Hk2* up-regulation as a potential driver of resistance to SMO inhibition. Here, I demonstrate that

blocking aerobic glycolysis at the start and SMO inhibition work in concert to further restrict tumor growth. Thus, HK2 inhibition in tandem with SHH-targeted therapies is a novel approach to disrupting SMO inhibitor-resistance.

Resistance to SMO inhibition in medulloblastoma is mostly independent of SMO mutations and is partly driven by *Gli2* amplification[23]. Our collaborators found that Ptc-SB medulloblastomas that recur after vismodegib treatment increase aerobic glycolysis through insertional mutagenic events that activate *Hk2* and do not have concurrent *Gli2* insertions. This metabolic rewiring in response to treatment was independent of *Gli2* activation, suggesting that *Hk2* activation is a *Gli2*- and *Smo*-independent, novel driver of SMO inhibitor-resistance. The Gershon lab has previously shown that *Hk2* drives aerobic glycolysis in primary medulloblastomas[29]. Together, these data support a role for *Hk2*-mediated aerobic glycolysis in conferring a growth advantage in both primary and recurrent medulloblastomas.

My work demonstrates that blocking aerobic glycolysis during SMO inhibition decreases proliferation without changing the rate of apoptosis in cultured medulloblastoma cells. The decrease in proliferation was mirrored by *in vivo* studies where short treatment of vismodegib reduced PCNA and increased $p27^{Kip1}$ expression. The short regimen study is the first to demonstrate that vismodegib maintains anti-tumor effects in both *Hk2*-intact and -deleted mice when delivered as an injectable solution. This additional delivery route has implications for preclinical and clinical studies in which oral delivery of vismodegib is not an option.

Hk2-deleted medulloblastomas responded similarly to vismodegib treatment when delivered by IP and by oral gavage. Compared to vehicle-treated counterparts, SMO inhibition significantly decreases tumor size in *Hk2*-deleted mice but does not prolong the already extended survival of these mice. My data demonstrate that *Hk2* deletion is twice more effective in extending survival than vismodegib treatment alone (Fig. 3.4A versus 3.4B; Fig. 3.5A versus 3.5C). Thus, *Hk2* deletion may mask the survival benefit of vismodegib treatment in SHH-driven medulloblastoma. An alternative endpoint in these preclinical studies is the measurement of tumor volume differences in medulloblastoma-bearing mice, with and without *Hk2* deletion, treated with vehicle or vismodegib.

In the clinic, combination therapy of HK2 and SMO inhibition has the potential to improve toxicity and efficacy in SHH-driven medulloblastoma patients. As HK2 inhibition sensitizes medulloblastoma to SMO inhibition, HK2 inhibitors could be used subvert acquired SMO-resistance or used prophylactically to circumvent the recurrent disease altogether. However, this novel anti-cancer strategy is limited by the absence of HK2 inhibitors. The intrinsic properties of the HK2 enzyme have stifled the development of selective HK2 small molecule inhibitors, that is, until recently[37]. In all, dual HK2/SMO inhibition is a novel strategy in the treatment of SHH-driven medulloblastoma that can now be explored.

3.5 Materials and Methods

Animals

All wildtype and genetically engineered mice were maintained on the C57/Bl6 background with at least 5 backcrosses. Eva Anton (UNC-CH, NC, USA) provided *hGFAP-Cre* mice and *SmoM2* mice on a Bl6 background were purchased from Jackson Laboratories (Bar Harbor, ME, USA). *Hk2*$^{fl/fl}$ mice were obtained from the European Mouse Mutant Archive (EMMA; Munchen, Germany). Medulloblastoma-bearing mice were monitored daily for abnormalities of head shape and movement. At the onset of tumor symptoms, such as ataxia, weight loss, and impaired movement, animals were sacrificed and survival time to onset of symptoms was considered the event-free survival. Animals were IP injected or oral gavaged with a final volume of 50 to 100 µL based on age and weight. Doses were updated every two weeks for changes in weight. All animal handling and protocols were carried out in accordance with established NIH practices and approved under UNC IACUC #13-121.0 and 15-306.0.

Drug formulation

Vismodegib (GDC-0449) was purchased from Selleckchem (#S1082; Houston, TX, USA). For the injectable drug solution, vismodegib was reconstituted in 100% NMP (#494496; Sigma-Aldrich, St. Louis, MO, USA) and diluted with PEG 200 (#P3015, Sigma-Aldrich). The final injection volume contained no

more than 10% NMP. For oral gavage, vismodegib suspension was prepared in 0.5% (w/v) methylcellulose (#274429, Sigma-Aldrich) and 0.2% (w/v) Tween-80 (#P1754, Sigma-Aldrich).

PCR

Cre primers were GCGGTCTGGCAGTAAAAACTATC and GTGAAACAGCATTGCTGTCACTT, producing a ~200 bp band. *hGFAP-Cre* primers were ACTCCTTCATAAAGCCCTCG and ATCACTCGTTGCATCGACCG, producing a ~190 bp band. *Hk2*^{fl} primers were CCCCTTCGCTTGCCATTAC and TGTCTTGGCTCAGATGTGAC, producing a ~450 bp band from the floxed allele and a ~400 bp band from the wildtype allele. *SmoM2* primers were AAGTTCATCTGCACCACCG and TCCTTGAAGAAGATGGTGCG, producing a ~200 bp band.

Cell culture

Medulloblastoma cells were isolated and cultured as previously described[29,38]. Tumors were harvested from P12 *hGFAP-Cre*;*SmoM2*;*Hk2*$^{fl/+}$ and *hGFAP-Cre*;*SmoM2*;*Hk2*$^{fl/fl}$ mice followed by trypsin digestion and trituration. Cells were maintained in DMEM/F12 (#11330-032; Thermo Fisher Scientific, Waltham, MA, USA) containing 25 mM KCl, Pen-Strep, and supplemented with N-2 (#17502048; Thermo Fisher Scientific) and 5% HI-FBS for 4 hours. After 4 hours, media were replaced with identical, serum-free media containing DMSO, 0.5, 1, or 2 μM vismodegib. Cells were lysed and collected after 24 hours.

Western blot analysis

Cultured cells were homogenized in RIPA lysis buffer supplemented protease inhibitor cocktail, NaF, and sodium orthovanadate. Protein concentrations were determined by Bicinchoninic acid (BCA) assay per manufacturer's protocol (#23229, Thermo Fisher Scientific). Equal concentrations of protein were resolved on SDS-Polyacrylamide gels followed by transfer onto polyvinylidene difluoride membranes (#IPSN07852; MilliporeSigma, Billerica, MA, USA). Immunologic analysis was performed on

the SNAP i.d. Protein Detection System (MilliporeSigma) per manufacturer's protocol using the following antibodies from Cell Signaling Technology (Danvers, MA, USA): β-actin (#4970), HK2 (#2867), Cyclin D2 (CCND2; #3741), cleaved Caspase-3 (cC3; #9661), anti-Rabbit IgG HRP (#7074) and anti-Mouse IgG HRP (#7076). Western blots were developed using the enhanced chemiluminescent SuperSignal West Femto Maximum Sensitivity Substrate (#34095, Thermo Fisher Scientific) and digitized using the C-DiGit blot scanner (LI-COR, Lincoln, NE, USA). Quantification was performed using Image Studio Lite software (LI-COR).

Histology and immunohistochemistry

Brain tissues were processed for H&E staining and IHC as previously described[39] and the following antibodies from Cell Signaling Technology were used: Proliferating cell nuclear antigen (PCNA; #2586) and $p27^{Kip1}$ (#3686). After immunofluorescent staining, nuclei were counterstained with 200 ng/mL 4'6-diamidino-2-phenylindole (DAPI; #D1306, Thermo Fisher Scientific) in 1X PBS for 5 min. Stained slides were digitally acquired using an Aperio ScanScope XT (Aperio, Vista, CA, USA).

Statistical analysis

SPSS software (IBM, Armonk, NY, USA) was used to generate Kaplan-Meier curves and perform the log-rank test. Excel was used to calculate Student's *t*-test.

3.6 Figures and Legends

Figure 3.1 Multiple ways Sleeping Beauty mutagenesis can occur

The Sleeping Beauty system is a powerful tool in identifying the genes involved in cancers. SB system transposons can randomly integrate at a TA dinucleotide junction anywhere in the genome and does not show affinity for hot or cold spots in the genome. Superior to retroviral infection, SB transposition can be controlled to mutagenize any target tissue and without extracellular signals for transposition activity. In the SB system, a mutagenic transposon vector (A) is used to increase SB transposition frequency and induce mutations. Containing a murine stem cell virus (MSCV) and a splice donor (SD), the transposon can promote gene expression when incorporated upstream or within a gene. It also contains two splice acceptors (SA) and a bi-directional polyA that can end transcription when incorporated in either orientation in a gene. As shown in B and C, the transposon can induce gain-of-function mutations in oncogenes when integrated within the promoter region (B) or transcription unit (C), driving overexpression of the full or truncated oncogene transcript. In tumor suppressor genes, transposon integration within the transcription unit can induce loss-of-function mutations. The SA and polyA signals can trap the promoter of a tumor suppressor gene in either orientation (D,E).

Figure 3.1

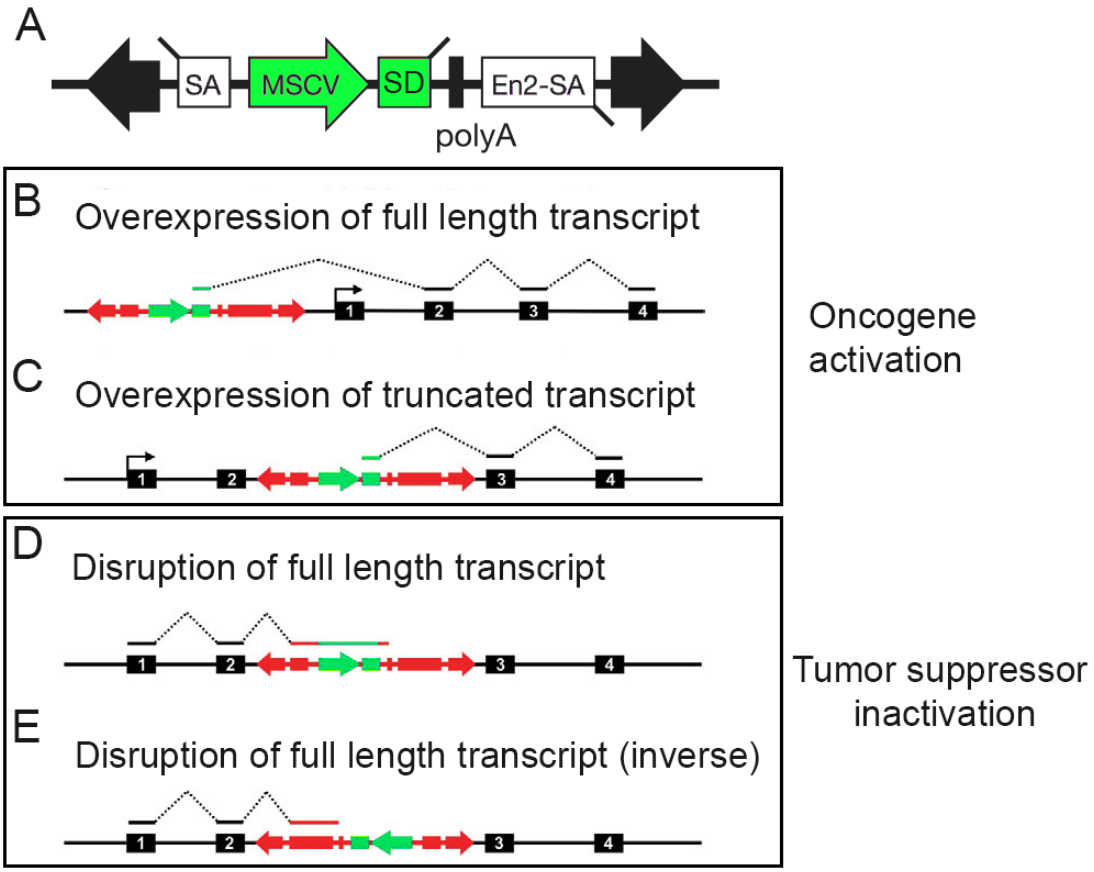

Adapted from Dupuy et al[20,24].

Figure 3.2 Vismodegib decreases proliferation in cultured *Hk2*-deleted medulloblastoma cells

Hk2 ablation sensitizes cultured medulloblastoma cells to vismodegib by decreasing proliferation. (A) Western Blot showing HK2, Cyclin D2 (CCND2) and cleaved Caspase-3 (cC3) protein expression levels in untreated and vismodegib-treated tumor cells from P12 *hGFAP-Cre*;*SmoM2*;*Hk2*$^{fl/+}$ (*Hk2*$^{fl/+}$) and *hGFAP-Cre*;*SmoM2*;*Hk2*$^{fl/fl}$ (*Hk2*^{cKO}) mice. Protein quantification normalized to β-actin shows that (B) *Hk2* deletion ablates HK2 expression compared to *Hk2* intact controls and that (C) vismodegib treatment decreases proliferation marked by CCND2 levels in *Hk2*-deleted mice with (D) no changes in apoptosis marker cC3 across the board. Graphs are averages ± s.e.m. *P* values were determined by Student's *t*-test. n=3 per condition.

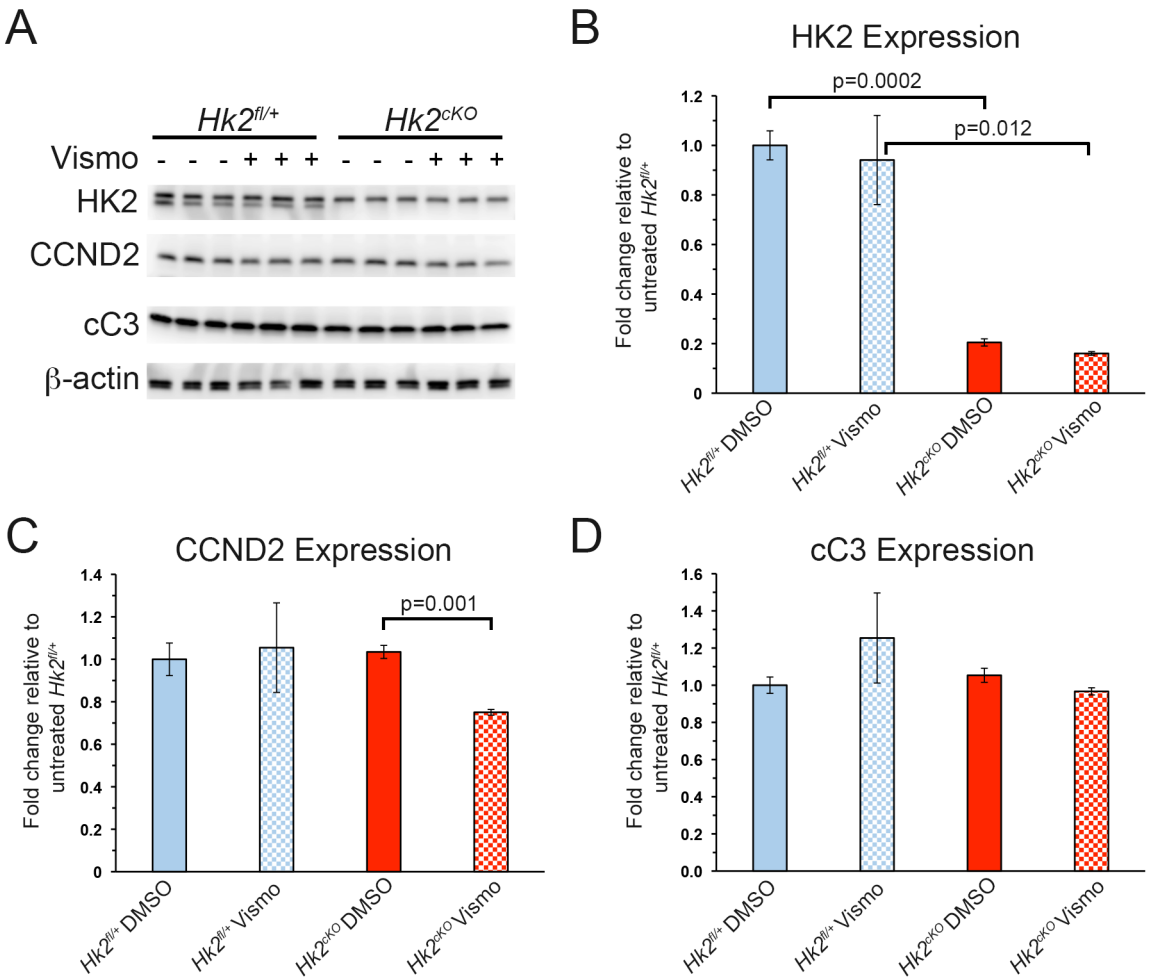

Figure 3.3 Vismodegib increased differentiation and decreased proliferation *in vivo*

P12 *hGFAP-Cre*;*SmoM2;Hk2*$^{fl/+}$ (*Hk2*$^{fl/+}$) and *hGFAP-Cre*;*SmoM2;Hk2*$^{fl/fl}$ (*Hk2*^{cKO}) mice were injected with 100 mg/kg of vismodegib once a day for three days and collected at P15. (A) Representative H&E stains demonstrate that medulloblastomas maintained typical pathology while decreasing in overall size with vismodegib treatment. (B) Immunohistochemistry stains for PCNA (red) and p27^{Kip1} (green) show a significant decrease in PCNA+ and an increase in p27^{Kip1}+ regions with vismodegib treatment in both *Hk2*$^{fl/+}$ and *Hk2*^{cKO} mice. All scale bars are 2 mm. PCNA, Proliferation cell nuclear antigen.

Figure 3.3

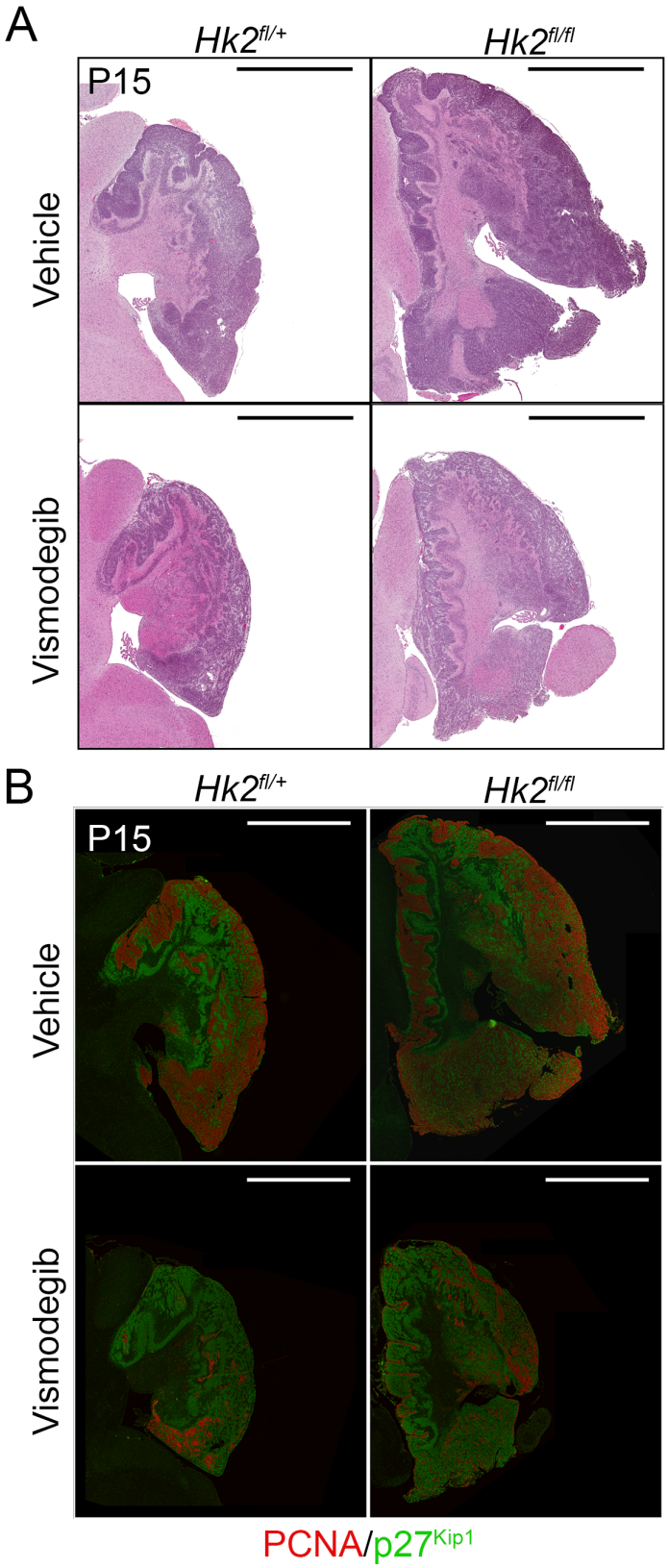
A
Hk2fl/+
Hk2fl/fl
P15
Vehicle
Vismodegib
B
Hk2fl/+
Hk2fl/fl
P15
Vehicle
Vismodegib
PCNA/p27Kip1

Figure 3.4 Vismodegib has anti-tumor effects in *Hk2*-intact and -deleted mice

In vehicle-treated mice, (A) *Hk2* deletion significantly prolonged survival compared to *Hk2*-intact controls. Vismodegib treatment significantly prolonged survival in (B) *Hk2*-intact mice and not in (C) *Hk2*-deleted mice. Vismo treatment also increased the (D) short survival of *Hk2*-intact mice but did not extend the long survival of *Hk2*-deleted mice. In all, the survival curves were significantly different (E). Representative (F) H&E stains demonstrate that vismodegib treatment significantly decreases tumor size in *Hk2*-deleted mice. *P* values were determined by log-rank test. All scale bars are 2 mm.

Figure 3.4

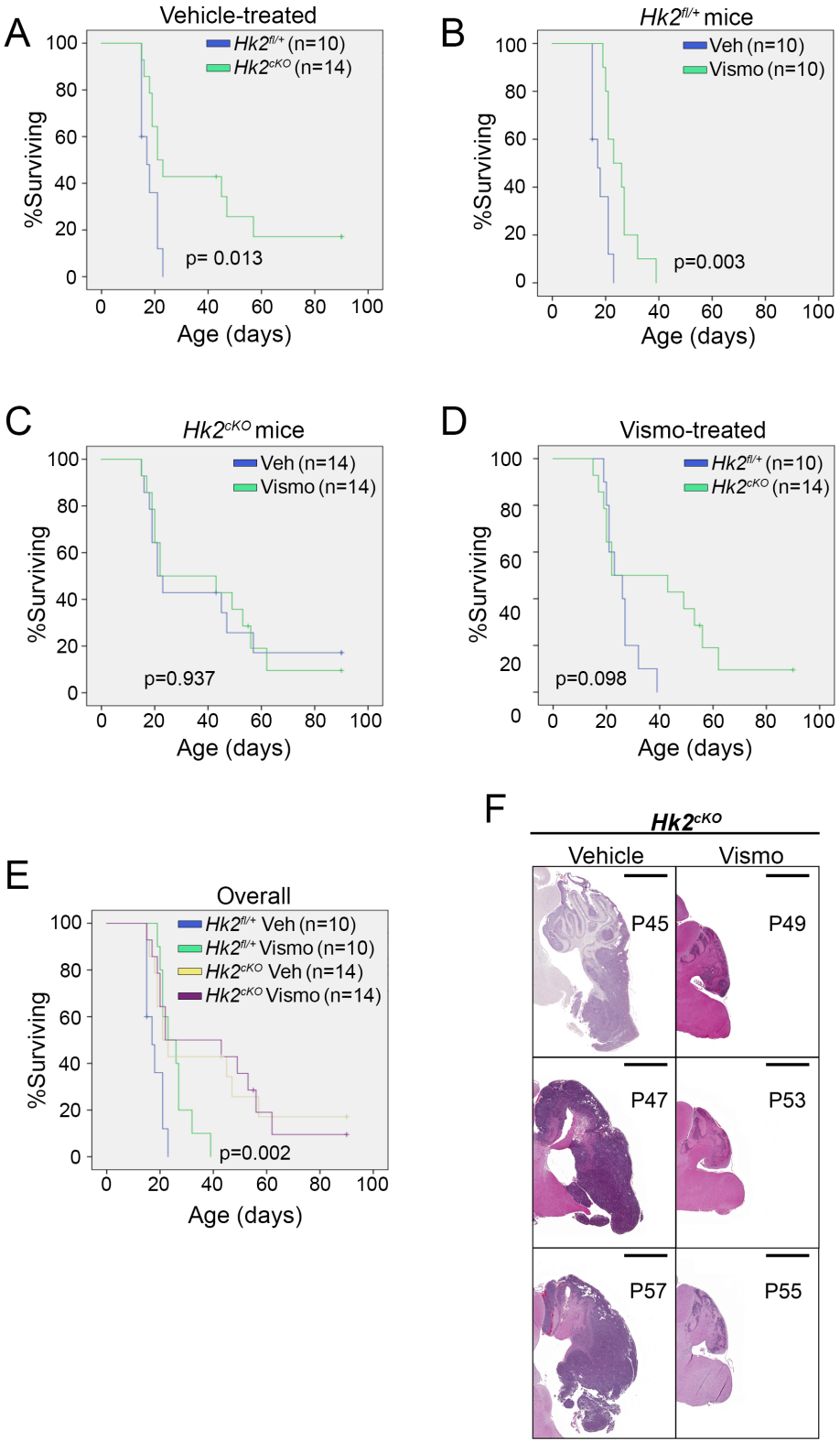
A
Vehicle-treated
Hk2fl/+ (n=10)
Hk2cKO (n=14)
p= 0.013
%Surviving
Age (days)
B
Hk2fl/+ mice
Veh (n=10)
Vismo (n=10)
p=0.003
%Surviving
Age (days)
C
Hk2cKO mice
Veh (n=14)
Vismo (n=14)
p=0.937
%Surviving
Age (days)
D
Vismo-treated
Hk2fl/+ (n=10)
Hk2cKO (n=14)
p=0.098
%Surviving
Age (days)
E
Overall
Hk2fl/+ Veh (n=10)
Hk2fl/+ Vismo (n=10)
Hk2cKO Veh (n=14)
Hk2cKO Vismo (n=14)
p=0.002
%Surviving
Age (days)
F
Hk2cKO
Vehicle
Vismo
P45
P49
P47
P53
P57
P55

Figure 3.5 Oral vismodegib does not prolong survival in *Hk2*-deleted animals

Kaplan-Meier curves show that *Hk2* deletion prolonged survival in both (A) MCT vehicle- and (B) vismo-treated groups. Vismodegib treatment significantly prolonged survival in (C) *Hk2*-intact mice but not in (D) *Hk2*-deleted mice when compared to MCT vehicle-treated counterparts. Overall, there is a significant difference in survival curves (E). *P* values were determined by log-rank test.

Figure 3.5

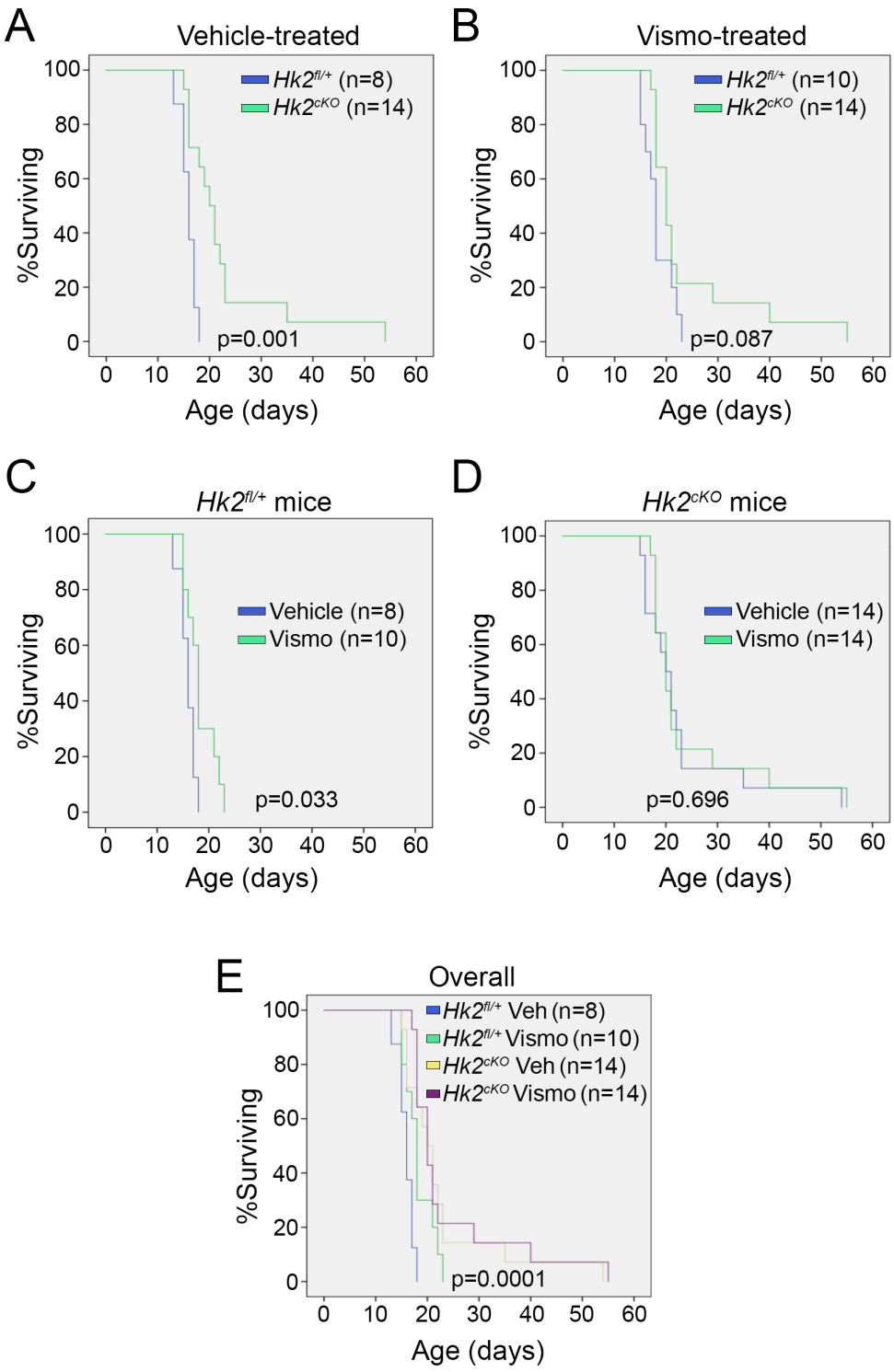
A
Vehicle-treated
Hk2fl/+ (n=8)
Hk2cKO (n=14)
p=0.001
%Surviving
Age (days)
B
Vismo-treated
Hk2fl/+ (n=10)
Hk2cKO (n=14)
p=0.087
%Surviving
Age (days)
C
Hk2fl/+ mice
Vehicle (n=8)
Vismo (n=10)
p=0.033
%Surviving
Age (days)
D
Hk2cKO mice
Vehicle (n=14)
Vismo (n=14)
p=0.696
%Surviving
Age (days)
E
Overall
Hk2fl/+ Veh (n=8)
Hk2fl/+ Vismo (n=10)
Hk2cKO Veh (n=14)
Hk2cKO Vismo (n=14)
p=0.0001
%Surviving
Age (days)

3.7 REFERENCES

1 Taylor MD, Northcott P a, Korshunov A, Remke M, Cho Y-J, Clifford SC *et al.* Molecular subgroups of medulloblastoma: the current consensus. *Acta Neuropathol* 2012; **123**: 465–72.

2 Paterson E, Farr RF. Cerebellar Medulloblastoma: Treatment by Irradiation of the whole central nervous system. *Acta radiol* 1952; **39**: 323–336.

3 Ramaswamy V, Remke M, Bouffet E, Faria CC, Perreault S, Cho YJ *et al.* Recurrence patterns across medulloblastoma subgroups: An integrated clinical and molecular analysis. *Lancet Oncol* 2013; **14**: 1200–1207.

4 Kool M, Korshunov A, Remke M, Jones DTW, Schlanstein M, Northcott PA *et al.* Molecular subgroups of medulloblastoma: an international meta-analysis of transcriptome, genetic aberrations, and clinical data of WNT, SHH, Group 3, and Group 4 medulloblastomas. *Acta Neuropathol* 2012; **123**: 473–484.

5 Thompson MC, Fuller C, Hogg TL, Dalton J, Finkelstein D, Lau CC *et al.* Genomics identifies medulloblastoma subgroups that are enriched for specific genetic alterations. *J Clin Oncol* 2006; **24**: 1924–1931.

6 Northcott P a, Dubuc AM, Pfister S, Taylor MD. Molecular subgroups of medulloblastoma. *Expert Rev Neurother* 2012; **12**: 871–884.

7 Northcott P a., Shih DJH, Peacock J, Garzia L, Sorana Morrissy a., Zichner T *et al.* Subgroup-specific structural variation across 1,000 medulloblastoma genomes. *Nature* 2012; **488**: 49–56.

8 Liu Y, Hu X, Han C, Wang L, Zhang X, He X *et al.* Targeting tumor suppressor genes for cancer therapy. *BioEssays* 2015; **37**: 1277–1286.

9 Reifenberger J, Wolter M, Weber RG, Megahed M, Ruzicka T, Lichter P *et al.* Missense mutations in SMOH in sporadic basal cell carcinomas of the skin and primitive neuroectodermal tumors of the central nervous system. *Cancer Res* 1998; **58**: 1798–1803.

10 Rausch T, Jones DTW, Zapatka M, Stütz AM, Zichner T, Weischenfeldt J *et al.* Genome sequencing of pediatric medulloblastoma links catastrophic DNA rearrangements with TP53 mutations. *Cell* 2012; **148**: 59–71.

11 Robinson GW, Orr BA, Wu G, Gururangan S, Lin T, Qaddoumi I *et al.* Vismodegib exerts targeted efficacy against recurrent sonic hedgehog - Subgroup medulloblastoma: Results from phase II Pediatric Brain Tumor Consortium studies PBTC-025B and PBTC-032. *J Clin Oncol* 2015; **33**: 2646–2654.

12 Ransohoff KJ, Sarin KY, Tang JY. Smoothened inhibitors in sonic hedgehog subgroup medulloblastoma. *J Clin Oncol* 2015; **33**: 2692–2694.

13 Rudin CM, Hann CL, Laterra J, Yauch RL, Callahan C a, Fu L *et al.* Treatment of medulloblastoma with hedgehog pathway inhibitor GDC-0449. *N Engl J Med* 2009; **361**: 1173–1178.

14 Rodon J, Tawbi HA, Thomas AL, Stoller RG, Turtschi CP, Baselga J *et al.* A phase I, multicenter, open-label, first-in-human, dose-escalation study of the oral smoothened inhibitor sonidegib (LDE225) in patients with advanced solid tumors. *Clin Cancer Res* 2014; **20**: 1900–1909.

15 Yauch RL, Dijkgraaf GJP, Alicke B, Januario T, Ahn CP, Holcomb T *et al.* Smoothened Mutation Confers Resistance to a Hedgehog Pathway Inhibitor in Medulloblastoma. *Science* 2009; **326**: 572–574.

16 Pricl S, Cortelazzi B, Dal Col V, Marson D, Laurini E, Fermeglia M *et al.* Smoothened (SMO)

receptor mutations dictate resistance to vismodegib in basal cell carcinoma. *Mol Oncol* 2015; **9**: 389–397.

17 Dijkgraaf GJP, Alicke B, Weinmann L, Januario T, West K, Modrusan Z *et al.* Small Molecule Inhibition of GDC-0449 Refractory Smoothened Mutants and Downstream Mechanisms of Drug Resistance. *Cancer Res* 2011; **71**: 435–444.

18 Kool M, Jones DTW, Jäger N, Northcott PA, Pugh TJ, Hovestadt V *et al.* Genome sequencing of SHH medulloblastoma predicts genotype-related response to smoothened inhibition. *Cancer Cell* 2014; **25**: 393–405.

19 Buonamici S, Williams J, Morrissey M, Wang A, Guo R, Vattay A *et al.* Interfering with resistance to smoothened antagonists by inhibition of the PI3K pathway in medulloblastoma. *Sci Transl Med* 2010; **2**: 51ra70.

20 Dupuy AJ, Akagi K, Largaespada DA, Copeland NG, Jenkins NA. Mammalian mutagenesis using a highly mobile somatic Sleeping Beauty transposon system. *Nature* 2005; **436**: 221–226.

21 Fischer SE, Wienholds E, Plasterk RH. Regulated transposition of a fish transposon in the mouse germ line. *Proc Natl Acad Sci U S A* 2001; **98**: 6759–64.

22 Dupuy AJ, Fritz S, Largaespada DA. Transposition and gene disruption in the male germline of the mouse. *Genesis* 2001; **30**: 82–88.

23 Collier LS, Carlson CM, Ravimohan S, Dupuy AJ, Largaespada DA. Cancer gene discovery in solid tumours using transposon-based somatic mutagenesis in the mouse. *Nature* 2005; **436**: 272–276.

24 Dupuy AJ, Jenkins NA, Copeland NG. Sleeping beauty: a novel cancer gene discovery tool. *Hum Mol Genet* 2006; **15**: 75–79.

25 Wu X, Northcott PA, Dubuc A, Dupuy AJ, Shih DJH, Witt H *et al.* Clonal selection drives genetic divergence of metastatic medulloblastoma. *Nature* 2012; **482**: 529–533.

26 Goorich L V, Milenkovic L, Higgins KM, Scott M. Altered neural cell fates and medulloblastoma in mouse patched mutants. *Science* 1997; **277**: 1109–1113.

27 Pan S, Wu X, Jiang J, Gao W, Wan Y, Cheng D *et al.* Discovery of NVP-LDE225, a potent and selective smoothened antagonist. *ACS Med Chem Lett* 2010; **1**: 130–134.

28 Metcalfe C, De Sauvage FJ. Hedgehog fights back: Mechanisms of acquired resistance against smoothened antagonists. *Cancer Res* 2011; **71**: 5057–5061.

29 Gershon TR, Crowther AJ, Tikunov A, Garcia I, Annis R, Yuan H *et al.* Hexokinase-2-mediated aerobic glycolysis is integral to cerebellar neurogenesis and pathogenesis of medulloblastoma. *Cancer Metab* 2013; **1**: 1–17.

30 Jeong J, Mao J, Tenzen T, Kottmann AH, Mcmahon AP. Hedgehog signaling in the neural crest cells regulates the patterning and growth of facial primordia. *Genes Dev* 2004; **18**: 937–951.

31 Mao J, Ligon KL, Rakhlin EY, Thayer SP, Bronson RT, Rowitch D *et al.* A Novel Somatic Mouse Model to Survey Tumorigenic Potential Applied to the Hedgehog Pathway. *Cancer Res* 2006; **66**: 10171–10178.

32 Taipale J, Chen JK, Cooper MK, Wang B, Mann RK, Milenkovic L *et al.* Effects of oncogenic mutations in Smoothened and Patched can be reversed by cyclopamine. *Nature* 2000; **406**: 1005–1009.

33 Chen JK, Taipale J, Cooper MK, Beachy P a. Inhibition of Hedgehog signaling by direct binding of cyclopamine to Smoothened service Inhibition of Hedgehog signaling by direct binding of cyclopamine to Smoothened. *Genes Dev* 2002; : 2743–2748.

34 Tao H, Jin Q, Koo DI, Liao X, Englund NP, Wang Y *et al.* Small molecule antagonists in distinct binding modes inhibit drug-resistant mutant of smoothened. *Chem Biol* 2011; **18**: 432–437.

35 Wong H, Alicke B, West KA, Pacheco P, La H, Januario T *et al.* Pharmacokinetic-pharmacodynamic analysis of vismodegib in preclinical models of mutational and ligand-dependent Hedgehog pathway activation. *Clin Cancer Res* 2011; **17**: 4682–4692.

36 Shortt J, Hsu AK, Martin BP, Doggett K, Matthews GM, Doyle MA *et al.* The drug vehicle and solvent N-Methylpyrrolidone is an immunomodulator and antimyeloma compound. *Cell Rep* 2014; **7**: 1009–1019.

37 Lin H, Zeng J, Xie R, Schulz MJ, Tedesco R, Qu J *et al.* Discovery of a Novel 2,6-Disubstituted Glucosamine Series of Potent and Selective Hexokinase 2 Inhibitors. *ACS Med Chem Lett* 2016; **7**: 217–222.

38 Kenney AM, Rowitch DH. Sonic hedgehog Promotes G1 Cyclin Expression and Sustained Cell Cycle Progression in Mammalian Neuronal Precursors. *Mol Cell Biol* 2000; **20**: 9055–9067.

39 Garcia I, Crowther AJ, Gama V, Miller CR, Deshmukh M, Gershon TR. Bax deficiency prolongs cerebellar neurogenesis, accelerates medulloblastoma formation and paradoxically increases both malignancy and differentiation. *Oncogene* 2013; **32**: 2304–2314.

CHAPTER IV: ADAPTATIONS OF ENERGY METABOLISM DURING CEREBELLAR NEUROGENESIS ARE CO-OPTED IN MEDULLOBLASTOMA

4.1 Overview

Recent studies show that metabolic patterns typical of cancer cells, including aerobic glycolysis and increased lipogenesis, are not unique to malignancy, but rather originate in physiologic development. In the postnatal brain, where sufficient oxygen for energy metabolism is scrupulously maintained, neural progenitors nevertheless metabolize glucose to lactate and prioritize lipid synthesis over fatty acid oxidation. Medulloblastoma, a cancer of neural progenitors that is the most common malignant brain tumor in children, recapitulates the metabolic phenotype of brain progenitor cells. During the physiologic proliferation of neural progenitors, metabolic enzymes generally associated with malignancy, including Hexokinase-2 (HK2) and Pyruvate kinase M2 (PKM2) configure energy metabolism to support growth. In these non-malignant cells, expression of HK2 and PKM2 is driven by transcriptional regulators that are typically identified as oncogenes, including N-myc. Importantly, N-myc continues to drive HK2 and PKM2 in medulloblastoma. Similarly E2F transcription factors and PPARγ function in both progenitors and medulloblastoma to optimize energy metabolism to support proliferation. These findings show that the ‘‘metabolic transformation’’ that is a hallmark of cancer is not specifically limited to cancer. Rather, metabolic transformation represents a co-opting of developmental programs integral to physiologic growth. Despite their physiologic origins, the molecular mechanisms that mediate metabolic transformation may nevertheless present ideal targets for novel anti-tumor therapy.

4.2 Introduction

Many cancers demonstrate metabolic transformation, configuring cellular metabolism to support malignant growth[1]. Metabolic patterns commonly observed in cancer include increased lipogenesis[2–4] and

aerobic glycolysis, the metabolism of glucose to lactate, despite the availability of oxygen for oxidative phosphorylation[5,6]. Up-regulation of aerobic glycolysis in cancer is known as the Warburg effect and is understood to be a malignant adaptation that allows continued proliferation in diverse microenvironments. The importance of metabolic transformation to cancer pathogenesis, however, raises important questions: Are these metabolic programs unique to cancer cells? If not, what might be their physiologic origins? Recent studies of postnatal neurogenesis have identified a physiological role in neural development for metabolic patterns typically associated with cancer, including both increased lipogenesis[7,8] and aerobic glycolysis[9,8]. In contrast to the production of aberrant onco-metabolites such as 2-hydroxyglutarate, which requires IDH mutation[10–12], the lipogenic and glycolytic phenotypes frequently observed in cancer originate in the normal metabolic repertoire of neural progenitor cells. Neurogenesis, like cancer, involves rapid proliferation and these studies show that metabolic pathways in neural progenitors, as in cancer cells, are optimized for cell division. The pattern of increased lipogenesis and aerobic glycolysis that manifests in neural progenitors is maintained in the progenitor-derived brain tumor medulloblastoma; in this cancer, developmentally-regulated metabolism is co-opted to support malignant growth. These studies provide a developmental perspective on the origins of cancer cell metabolism.

Medulloblastoma is the most common malignant brain tumor in children, and presents an ideal opportunity to examine cancer arising as a disruption of developmentally-regulated growth[13]. Medulloblastomas originate from the cerebellum, which is the most prominent site of neural progenitor proliferation in early postnatal life. Several lines of evidence link cerebellar neural progenitor proliferation to medulloblastoma pathogenesis. In the first year of life in humans, or the first 15 days of life in mice, cerebellar granule neuron progenitors (CGNPs) proliferate in a germinal matrix along the outside of the cerebellum called the external granule cell layer (EGL). This period of rapid proliferation is triggered by activation of the Sonic Hedgehog (Shh) signaling pathway[14]. While proliferation of cerebellar progenitors is virtually shut down once cerebellar development is complete, mutations in humans that aberrantly activate the Shh pathway predispose individuals to medulloblastoma formation; importantly, this process is recapitulated in transgenic mice[15–17]. Thus mice with conditional deletion of Patched (Ptc) or constitutively active alleles of Smoothened (Smo) allow the process of medulloblastoma tumorigenesis process to be examined prospectively, from CGNP proliferation forward to cancer[17,18].

4.3 Metabolism and medulloblastoma

4.3.1 Lipid metabolism

Along with induction of proliferation in the postnatal cerebellum, Shh signaling induces characteristic metabolic patterns in CGNPs, including decreased fatty acid oxidation[7], increased lipogenesis[7] and aerobic glycolysis[9,8]. Despite the normoxic environment of the postnatal brain, Shh drives a shift in energy production away from oxidative reactions. This developmentally-programmed metabolic configuration of CGNPs persists in primary medulloblastoma in transgenic mice[7–9]. Studies of human patients, moreover, show that the glycolytic phenotype of the model is shared by the actual disease; medulloblastomas are readily detected by clinical ^{18}FDG-PET studies[19,20] and glucose uptake correlates inversely with patient survival[19]. Thus understanding the cellular and molecular mechanisms of metabolic configuration of neural progenitors places the metabolic patterns of medulloblastoma into a developmental context and may provide key insight in tumor pathogenesis.

Bhatia et al demonstrated that Shh induced a metabolic switch from lipid consumption to lipid production[7]. After observing abundant lipid deposition in Shh-driven medulloblastomas in transgenic mice, the investigators examined whether fatty acid metabolism was altered by Shh in CGNPs, the normal cells from which these tumors originate. Bhatia et al found that CGNPs explanted into media containing Shh up-regulated key lipid synthesis enzymes, including Fatty Acid Synthase (FASN) and Acetyl-CoA Carboxylase (Acc1). Shh also caused down-regulation of enzymes required for lipid catabolism, including Acyl-CoA Oxidase 1 (Acox1) and Medium Chain Acyl-CoA Dehydrogenase (MCAD)[7]. These transcriptional changes seemed to be coupled with proliferation as they depended on the activity of the Rb-E2F axis; E2F1 knockdown blocked the induction of FASN and the suppression MCAD in Shh-treated CGNPs. Direct measurement of palmitate oxidation demonstrated that these transcriptional changes potently altered lipid metabolism; Shh reduced palmitate oxidation, which could be restored by the subsequent addition of E2F1 shRNA. Thus, as depicted in Fig. 4.1, Shh shifted the lipid metabolism of CGNPs from catabolic to synthetic, and this shift was mediated by E2F1 and negatively regulated by Rb[7].

Importantly, this metabolic switch was maintained in medulloblastoma, where it promoted tumor growth[7]. Treatment of medulloblastoma-bearing mice with inhibitors of either FASN or the CDK-Rb-E2F

signaling pathway slowed medulloblastoma progression and prolonged mouse survival. Bhatia et al used the transgenic *ND2:SmoA1* mouse line to generate animals with primary medulloblastoma. After tumor formation, these mice were injected daily for 2 weeks with either the CDK inhibitor olomoucine or with the FASN inhibitor C75. Both agents significantly extended animal survival by slowing tumor growth. Within treated tumors, C75 reduced lipid synthesis as expected. Similarly, olomoucine reduced intratumoral abundance of FASN[7]. Thus, direct inhibition of fatty acid synthesis exerted a significant anti-tumor effect and this effect was duplicated through CDK inhibition. Together these data show that lipogenic metabolism is both essential to tumor growth and derives from developmental physiology[7].

4.3.2 Aerobic glycolysis

The same group, in a follow up investigation, demonstrated that the metabolic regulator, Peroxisome Proliferator-Activated Receptor-γ (PPARγ) plays a key role in shaping the metabolic response of CGNPs to Shh stimulation in a manner that persists after medulloblastoma formation[8]. The investigators show that E2F1 up-regulates PPARγ and that PPARγ in turn causes up-regulation of key glycolytic enzymes, Hexokinase-2 (HK2) and Pyruvate Kinase M2 (PKM2), and of the glucose transporter Glut4. Inhibiting PPARγ in medulloblastoma-bearing *ND2:SmoA1* mice decreased the expression of both HK2 and PKM2, and reduced tumor glucose uptake, measured in vivo by ^{18}FDG-PET scan. Similar to the inhibition of CDK and FASN, PPARγ inhibition reduced the rate of tumor growth and extended survival[8]. These findings further demonstrate that the proliferative and metabolic functions of neural progenitors are interconnected and jointly become subverted in medulloblastoma tumorigenesis. Moreover, as shown in Fig. 4.1, this investigation demonstrates that changes in lipid and carbohydrate metabolizing enzymes occur in concert, jointly regulated by common intracellular signals.

A non-biased metabolomic analysis determined the functional significance of Shh-mediated changes in the expression of metabolic enzymes. CGNPs were explanted into media with or without Shh and changes in media metabolite concentrations were measured over time. Shh increased lactate production and glucose utilization of CGNPs, without causing additional changes in nutrient utilization and metabolite production. Continuous, real-time measurement of media oxygen content showed that Shh did

not increase the CGNP oxygen consumption rate, and that Shh-treated CGNPs retained significant unused capacity for mitochondrial respiration. *In vivo* studies, including quantitative measurement of ^{18}FDG uptake and MR spectroscopy, further showed that glucose utilization and lactate production in the cerebellum were highest during the period of CGNP proliferation. ^{18}FDG-PET also demonstrated that the glycolytic phenotype of CGNPs is preserved in *ND2:SmoA1* medulloblastoma. These studies confirmed that Shh signaling increased aerobic glycolysis in CGNPs and that Shh-driven medulloblastomas inherited the metabolic phenotype of their progenitor cells of origin[9].

Importantly, these studies revealed that hexokinase isoforms HK1 and HK2 were expressed in mutually exclusive domains in the postnatal brain, defined by the presence or absence of proliferating progenitors. While proliferating CGNPs up-regulated HK2, HK1 was expressed by differentiated neurons throughout the brain. HK1 was notably absent from the sites of postnatal progenitor proliferation, including the hippocampus, the subventricular zone, and the external granule layer of the cerebellum, the site of CGNP proliferation. These non-overlapping patterns suggested that the selective expression of HK2, rather than HK1, was integral to neural progenitor proliferation[9].

Insight into the functional significance of HK2 expression in neural progenitors came from studies that conditionally deleted HK2 in the brain. Mice with a floxed allele of *Hk2* (*Hk2*$^{f/f}$) were crossed with *hGFAP-Cre* mice that express Cre recombinase in brain stem cells during early brain development. While HK2 was deleted throughout the cerebellum, only CGNPs were directly affected because CGNPs are the primary source of HK2 in the postnatal cerebellum[21]. Metabolomic analysis showed that CGNPs in *hGFAP-Cre*;*Hk2*$^{f/f}$ mice generated markedly less lactate when exposed to Shh, confirming that *Hk2* deletion blocked the induction of aerobic glycolysis by Shh[9].

Genetic deletion of *Hk2* enabled functional studies to determine the role of aerobic glycolysis in both CGNP development and medulloblastoma tumorigenesis. Mice with conditional deletion of *Hk2* were viable and fertile and had no overt neurologic deficits. Inspection of the cerebellar microanatomy, however, revealed disruption of the typically regular pattern of cell layering, and increased capillary formation disrupting the EGL. CGNPs typically migrate along a predictable route as they differentiate into neurons; in focal areas, HK2-deficient CGNPs differentiated without completing migration, resulting in

granule neurons positioned aberrantly on both sides of the Purkinje cell layer. The increased vascularity of the cerebellum in *hGFAP-Cre*;*Hk2*$^{f/f}$ mice suggested that HK2-deficient CGNPs were increasingly dependent on oxidative metabolism and local tissue oxygenation, while the aberrant migration suggested disrupted timing of CGNP differentiation.

Further evidence that aerobic glycolysis negatively regulates terminal differentiation came from conditional deletion of *Hk2* in medulloblastoma-prone mice. These mice were generated by crossing *hGFAP-Cre*, *Hk2*$^{f/f}$ and *SmoM2* mouse lines. Mice heterozygous for *hGFAP-Cre* and *SmoM2* alleles develop medulloblastoma with 100% frequency by P12 and typically die from tumor progression by P20[22,23]. In these mice, cerebellar development is profoundly altered as the posterior fossa becomes filled with rapidly growing tumor. Tumors with homozygous conditional deletion of *Hk2* occurred in *hGFAP-*Cre;*SmoM2*;*Hk2*$^{f/f}$ with similar incidence, but were markedly less malignant. Deletion of *Hk2* significantly increased median survival from 18 to 30 days and in contrast to the 100% mortality of mice with medulloblastoma with intact *Hk2*, allowed 30% of tumor-bearing mice to survive long-term and to breed[9]. Similar survival benefits were demonstrated when *Hk2* was deleted in mouse models of glioblastoma[24], and more recently, lung and breast cancer, confirming the broad relevance of *Hk2* to solid tumors beyond developmental brain tumors[25].

Histologic examination of *Hk2*-deleted medulloblastomas showed that *Hk2*-deficiency dramatically increased the proportion of *SmoM2*-expressing CGNPs that differentiated appropriately, leading to relative normalization of cerebellar architecture. Staining for endothelial marker CD31 demonstrated increased vascularization in *Hk2*-deficient tumors. Proliferating cells localized predominantly in the perivascular regions; between regions of perivascular proliferation tumor cells exited the cell cycle and up-regulated the differentiation marker p27. The increased angiogenesis of *Hk2*-deficient tumors and the increased dependence of proliferative behavior on vascular proximity, suggested that growth restriction occurred when these *Hk2*-deficient tumors exceeded the limits of the compensatory effect of neovascularization. The presence of energy scarcity in *Hk2*-deficient tumors was assessed by studies of the phosphorylation of the intracellular energy sensor, AMP-activated Kinase (AMPK).

Consistent with energy scarcity, in *Hk2*-deficient tumors AMPK was consistently phosphorylated, as was the AMPK target, Acc1[9].

4.3.3 Metabolic switches

How does AMPK activation in *Hk2*-deficient tumors impair malignant growth? As shown in Fig. 4.1, the metabolic switch from lipid catabolism to lipid synthesis, identified by Bhatia et al as required for tumor growth[7,8], may be the underlying mechanism that is targeted by AMPK. While Bhatia et al showed that lipogenesis is regulated in CGNPs by E2F1 and PPARγ, AMPK-Acc1 signaling has been shown to down-regulate lipid production in diverse cell types[26] and may similarly affect the lipid metabolism of CGNPs. AMPK activation in *Hk2*-deletion medulloblastoma increased the inhibitory phosphorylation of Acc1[9], which would be predicted to block lipogenesis by inhibiting production of malonyl-CoA[27], leading to increased fatty acid oxidation[28]. Thus lipogenic metabolism may be a key mechanism of tumor pathogenesis that is supported by *Hk2*-dependent glycolysis. By preventing AMPK activation, *Hk2*-mediated aerobic glycolysis may enhance tumor growth not only by generating energy with less oxygen, but also by allowing lipogenesis to proceed. If so, pharmacologic agents that directly activate AMPK may be able to exploit this mechanism to inhibit tumor growth.

The induction of PKM2 by Shh, noted by Bhatia et al may be another critical link between Shh-driven glycolysis and Shh-driven lipid synthesis. We have recently found that *Smo*-driven medulloblastomas in mice, like CGNPs, up-regulate PKM2 (unpublished data). While pyruvate kinase plays an essential role in glucose metabolism, there are key differences in the activity of the PKM1 and PKM2 isoforms. In contrast to PKM1, the PKM2 isoform is subject to down-regulation of enzymatic activity and this regulation may be essential to its growth promoting effect[29]. By poorly catalyzing the conversion of phosphoenolpyruvate into pyruvate, PKM2 may increase the supply of glycolytic intermediaries up-stream of phosphoenolpyruvate that can be diverted into alternative fates, including lipid production and nucleotide biosynthesis[30,31].

The expression of the less active PKM2 isoform rather than the constitutively active PKM1, in both Shh-stimulated CGNPS and medulloblastoma suggests that pyruvate kinase activity may have an inhibitory effect on growth. Recent work by Anastasiou et al demonstrated that PkM2 activators, DASA-58 and TEPP-46, can block lipogenesis and inhibit the growth of PkM2-expressing cancers[32]. Unlike the activation of PKM2 by endogenous FBP, the activating effect of these agents could not be inhibited by phosphotyrosine signaling. Cells treated with DASA-58 reduced the flux of glucose-derived carbons into acetyl-CoA and generally lowered *de novo* lipid synthesis. Similarly, TEPP-46 treatment reduced the intracellular concentrations of acetyl-CoA, lactate, ribose phosphate, and serine, important precursors for lipid metabolism. Moreover, xenograft tumors from TEPP-46-treated mice recapitulated the metabolic profile found in vitro and exhibited delayed latency and smaller size than vehicle-treated mice. These findings show that increasing PKM2 activity alters glucose and lipid metabolism and reduces tumor growth. Conversely, Israelsen et al showed that conditional deletion of PKM2 actually accelerates tumorigenesis in an *in vivo* model of breast cancer[33]. Within *Pkm2*-deficient tumors, a subpopulation of non-proliferating cells expressed PKM1. Proliferative tumor cells, however, expressed no PKM1 and completely lacked PKM2. Together these studies show that pyruvate kinase activity correlates inversely with malignant growth.

The switch to PKM2 expression in CGNPs may similarly promote neural progenitor growth, again demonstrating a developmental origin for a metabolic pattern typically associated with cancer. As depicted in Fig. 4.2, in Shh-stimulated CGNPs, low PKM2 activity, operating downstream of high HK2-driven glycolytic flux, may divert glycolytic intermediates from lactate generation, into lipogenesis. PKM2 activation may reduce this diversion of glycolytic intermediates, reducing lipid synthesis required for growth. As medulloblastomas up-regulate PKM2, agents that increase PKM2 enzymatic activity may be able to block the lipogenic metabolism of these tumors. Through this mechanism, PKM2 activation, like AMPK activation, may offer a novel approach to medulloblastoma therapy by disrupting metabolic patterns that support tumor growth.

By up-regulating glycolytic enzymes HK2 and PKM2, and lipid synthesis enzymes FASN and Acc1, while down-regulating lipid catabolizing enzymes including Acox1, Shh configures CGNPs for both

aerobic glycolysis and lipid synthesis. These processes operate in tandem to satisfy the ATP needs of the cell while carrying out a net conversion of glucose into lactate and lipids. CGNPs integrate developmental regulation of lipid synthesis and aerobic glycolysis in order to support physiological proliferation during brain development. These same metabolic patterns become activated in medulloblastoma tumorigenesis and function similarly to support malignant growth.

4.4 Discussion

An important question is the relevance of these findings beyond cerebellar development and its disruption in medulloblastoma tumorigenesis. Transcriptional analyses of patient-derived samples demonstrate that medulloblastoma is a heterogeneous group of tumors, with at least 4 molecular subtypes[34–38]. The SHH sub-group of medulloblastoma makes up approximately 25% of the cases of this rare tumor. Do observations of metabolic regulation in cerebellar progenitors and medulloblastoma have relevance for other cell types during development and for other cancers?

Rather than being unique to CGNPs, aerobic glycolysis is likely to be a common feature of neural progenitors throughout the neuraxis. While Shh-dependent proliferation is unique to cerebellar progenitors, HK1 is absent in all progenitor regions of the postnatal brain[9], suggesting a molecular switch to HK2 may be activated by diverse growth factors. Similarly, PKM2 is known to integrate diverse growth factor signaling pathways into a common output of reduced PK activity[39,40]. Thus the activation of aerobic glycolysis by CGNPs in response to Shh may be a general response of progenitor cells to the specific growth factors that drive them to proliferate. As a group, tumors of neural progenitors, including retinoblastoma, Ewing sarcoma and neuroblastoma comprise the largest set of solid tumors in children; the set of tumors recapitulating the metabolism of their cells of origin is thus likely to be broad.

The role of N-Myc in mediating Shh-induced glycolysis in CGNPs supports the general relevance of metabolic configuration to progenitor function. N-Myc, and the homolog C-Myc, are essential regulators of neural and hematopoietic progenitor function[41,42]. They are also among the common oncogenes activated in human cancer[43,44], including all 4 medulloblastoma subtypes[45]. Disruption of Myc-Max

interaction in CGNPs treated with the inhibitor 10058-F4 blocked the induction of aerobic glycolysis by Shh and prevented Shh-induced proliferation[9]. These findings are consistent with the documented role of c-Myc in up-regulating glycolysis in both normal tissues and in cancer[46,47]. Moreover, disruption of N-Myc-Max interaction with the same agent in neuroblastoma reduced tumor growth while altering metabolism[48]. Thus while the metabolic and proliferative behaviors induced by Shh may be specific to CGNPs, the pattern of growth factor-induced metabolic configuration may be generalizable to diverse progenitors and progenitor-derived cancers. N-Myc and C-Myc proteins may be common effectors of metabolic transformation that operate downstream of diverse mitogenic signals, typified by Shh, that are cell-type specific.

The phenomenon of postnatal cerebellar neurogenesis degenerating into medulloblastoma in mice presents an ideal system in which to study the developmental origins of cancer metabolism. Because the cells of origin of these tumors are identifiable and accessible, the molecular regulation of energy metabolism in these progenitors can be discerned in detail. Moreover, the patterns of metabolism in cells of origin and in resulting tumors can be compared. Importantly, Shh-pathway activation drives medulloblastoma tumorigenesis through downstream oncogenes, including N-myc, that are relevant to diverse cancers in both children and adults. Understanding the mechanisms that regulate the metabolism of cerebellar progenitors during development may thus lead to novel, metabolic approaches to anti-cancer therapy.

4.5 Figures and Legends

Figure 4.1 Shh signaling regulates lipid metabolism and glycolysis in an integrated manner.

Regulatory genes and effector proteins are denoted by ovals and rounded rectangles, respectively, whereas inhibitors are in hexagons. Entities involved in lipid or glucose metabolism are in blue or red. AMPK may switch-off lipogenesis when aerobic glycolysis is blocked and energy scarcity results. Acc1, Acetyl-CoA carboxylase 1; Acox1, Acyl-CoA oxidase 1; AMPK, 5' adenosine monophosphate-activated protein kinase; E2F1, E2F transcription factor 1; FASN, Fatty acid synthase; Hk2, Hexokinase 2; PPARγ, Peroxisome proliferator-activated receptor-γ; PkM2, Pyruvate kinase isoform M2; Shh, Sonic hedgehog.

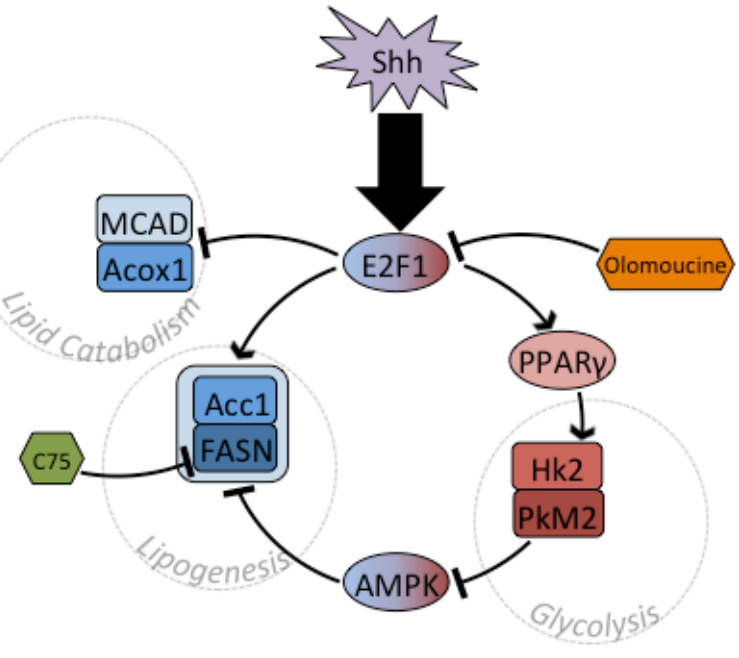

Figure 4.2 Changing the flow of glycolytic intermediates through HK2 and PKM2 regulation

By providing variable resistance to glycolytic flux, PkM2, induced by Shh, is ideally positioned to divert glycolytic intermediates, generated downstream of Shh-induced Hk2, to alternate metabolic pathways, such as lipogenesis, that support developmental and malignant growth. (A) Low PkM2 activity may channel glycolytic intermediates to alternate fates while allowing some production of lactate. (B) Hk2 deletion reduces glycolytic flux upstream of PkM2, preventing both lactate generation and alternate uses of glycolytic intermediates. (C) Pharmacologic activation of PkM2 activation may increase lactate generation while acting like Hk2 deletion to block the growth-promoting effects of aerobic glycolysis.

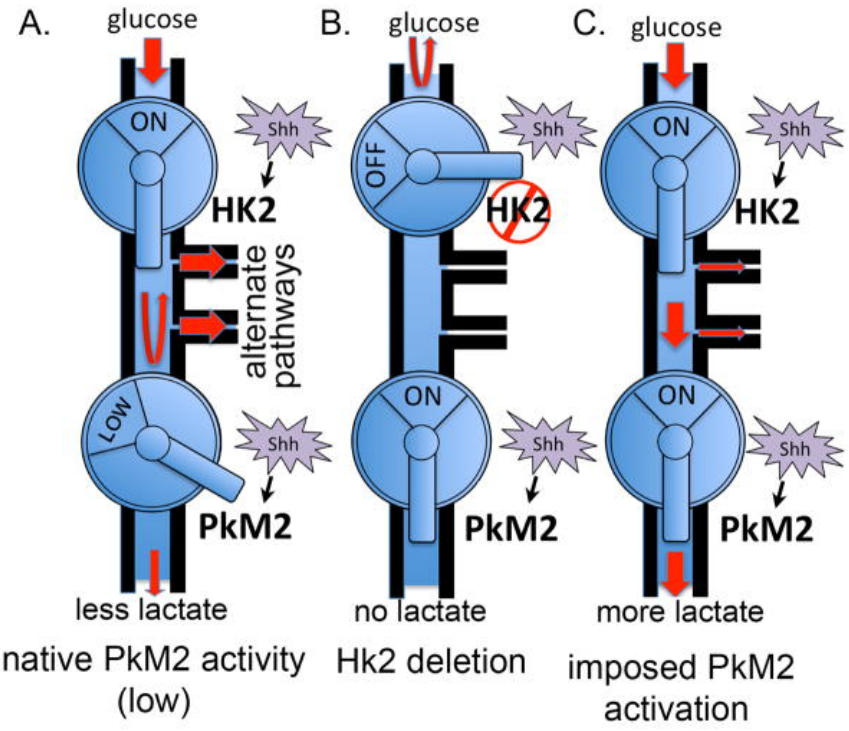

4.6 REFERENCES

1 Hanahan D, Weinberg RA. Hallmarks of cancer: The next generation. Cell. 2011; **144**: 646–674.

2 Mashima T, Seimiya H, Tsuruo T. De novo fatty-acid synthesis and related pathways as molecular targets for cancer therapy. *Br J Cancer* 2009; **100**: 1369–1372.

3 Menendez JA, Lupu R. Fatty acid synthase and the lipogenic phenotype in cancer pathogenesis. *Nat Rev Cancer* 2007; **7**: 763–777.

4 Abramson HN. The lipogenesis pathway as a cancer target. *J Med Chem* 2011; **54**: 5615–5638.

5 Vander Heiden MG, Cantley LC, Thompson CB. Understanding the Warburg Effect: The Metabolic Requirements of Cell Proliferation. *Science* 2009; **324**: 1029–1033.

6 Dang C V. Links between metabolism and cancer. *Genes Dev* 2012; **26**: 877–890.

7 Bhatia B, Hsieh M, Kenney a M, Nahlé Z. Mitogenic Sonic hedgehog signaling drives E2F1-dependent lipogenesis in progenitor cells and medulloblastoma. *Oncogene* 2011; **30**: 410–422.

8 Bhatia B, Potts CR, Guldal C, Choi S, Korshunov A, Pfister S *et al.* Hedgehog-mediated regulation of PPARγ controls metabolic patterns in neural precursors and shh-driven medulloblastoma. *Acta Neuropathol* 2012; **123**: 587–600.

9 Gershon TR, Crowther AJ, Tikunov A, Garcia I, Annis R, Yuan H *et al.* Hexokinase-2-mediated aerobic glycolysis is integral to cerebellar neurogenesis and pathogenesis of medulloblastoma. *Cancer Metab* 2013; **1**: 1–17.

10 Yang H, Ye D, Guan KL, Xiong Y. IDH1 and IDH2 mutations in tumorigenesis: Mechanistic insights and clinical perspectives. *Clin Cancer Res* 2012; **18**: 5562–5571.

11 Dang L, White DW, Gross S, Bennett BD, Bittinger MA, Driggers EM *et al.* Cancer-associated IDH1 mutations produce 2-hydroxyglutarate. *Nature* 2009; **462**: 739–744.

12 Xu W, Yang H, Liu Y, Yang Y, Wang P, Kim SH *et al.* Oncometabolite 2-hydroxyglutarate is a competitive inhibitor of alpha-ketoglutarate-dependent dioxygenases. *Cancer Cell* 2011; **19**: 17–30.

13 Grimmer MR, Weiss WA. Childhood tumors of the nervous system as disorders of normal development. *Curr Opin Pediatr* 2006; **18**: 634–638.

14 Wechsler-Reya RJ, Scott MP. Control of Neuronal Precursor Proliferation in the Cerebellum by Sonic Hedgehog. *Neuron* 1999; **22**: 103–114.

15 Zurawel RH, Allen C, Chiappa S, Cato W, Biegel J, Cogen P *et al.* Analysis of PTCH/SMO/SHH pathway genes in medulloblastoma. *Genes Chromosomes Cancer* 2000; **27**: 44–51.

16 Zurawel RH, Allen C, Wechsler-Reya R, Scott MP, Raffel C. Evidence that haploinsufficiency of Ptch leads to medulloblastoma in mice. *Genes Chromosomes Cancer* 2000; **28**: 77–81.

17 Hallahan AR, Pritchard JI, Hansen S, Benson M, Stoeck J, Hatton BA *et al.* The SmoA1 Mouse Model Reveals That Notch Signaling Is Critical for the Growth and Survival of Sonic Hedgehog-Induced Medulloblastomas. *Cancer Res* 2004; **21**: 7794–7800.

18 Oliver TG, Read TA, Kessler JD, Mehmeti A, Wells JF, Huynh TT *et al.* Loss of patched and disruption of granule cell development in a pre-neoplastic stage of medulloblastoma. *Development* 2005; **132**: 2425–2439.

19 Gururangan S, Hwang E, Herndon JE, Fuchs H, George T, Coleman RE. [18F]Fluorodeoxyglucose-Positron Emission Tomography in Patients with Medulloblastoma. *Neurosurgery* 2004; **55**: 1280–1289.

20 Tripathi M, Jain N, Jaimini A, Garg G, D'souza MM, Sharma R *et al.* Demonstration of diffuse leptomeningeal metastasis in a treated case of medulloblastoma with F-18 FDG PET/CT. *Clin Nucl Med* 2009; **34**: 530–532.

21 Gershon TR, Crowther AJ, Liu H, Miller CR, Deshmukh M. Cerebellar granule neuron progenitors are the source of Hk2 in the postnatal cerebellum. *Cancer Metab* 2013; **1**: 15–16.

22 Schüller U, Heine VM, Mao J, Kho AT, Dillon AK, Han Y-G *et al.* Acquisition of granule neuron precursor identity is a critical determinant of progenitor cell competence to form Shh-induced medulloblastoma. *Cancer Cell* 2008; **14**: 123–134.

23 Mao J, Ligon KL, Rakhlin EY, Thayer SP, Bronson RT, Rowitch D *et al.* A Novel Somatic Mouse Model to Survey Tumorigenic Potential Applied to the Hedgehog Pathway. *Cancer Res* 2006; **66**: 10171–10178.

24 Wolf A, Agnihotri S, Micallef J, Mukherjee J, Sabha N, Cairns R *et al.* Hexokinase 2 is a key mediator of aerobic glycolysis and promotes tumor growth in human glioblastoma multiforme. *J Exp Med* 2011; **208**: 313–326.

25 Patra KC, Wang Q, Bhaskar PT, Miller L, Wang Z, Wheaton W *et al.* Hexokinase 2 is required for tumor initiation and maintenance and its systemic deletion is therapeutic in mouse models of cancer. *Cancer Cell* 2013; **24**: 213–228.

26 Hardie DG. Minireview: The AMP-Activated Protein Kinase Cascade: The Key Sensor of Cellular Energy Status. *Endocrinology* 2003; **144**: 5179–5183.

27 Ruderman NB, Saha AK, Kraegen EW. Minireview: Malonyl CoA, AMP-Activated Protein Kinase, and Adiposity. *Endocrinology* 2003; **144**: 5166–5171.

28 Foster DW. Malonyl-CoA: The regulator of fatty acid synthesis and oxidation. *J Clin Invest* 2012; **122**: 1958–1959.

29 Christofk HR, Vander Heiden MG, Harris MH, Ramanathan A, Gerszten RE, Wei R *et al.* The M2 splice isoform of pyruvate kinase is important for cancer metabolism and tumour growth. *Nature* 2008; **452**: 230–234.

30 Eigenbrodt R, Reinacher M, Scheefers-Borchel U, Scheefers H, Friss R. Double role for pyruvate kinase type M2 in the expansion of phosphometabolite pools found in tumor cells. *Crit Rev Oncog* 1992; **3**: 91–115.

31 Mazurek S. Pyruvate kinase type M2 : A key regulator of the metabolic budget system in tumor cells. *Int J Biochem Cell Biol* 2011; **43**: 969–980.

32 Anastasiou D, Yu Y, Israelsen WJ, Jiang J-K, Boxer MB, Hong BS *et al.* Pyruvate kinase M2 activators promote tetramer formation and suppress tumorigenesis. *Nat Chem Biol* 2012; **8**: 839–847.

33 Israelsen WJ, Dayton TL, Davidson SM, Fiske BP, Hosios AM, Bellinger G *et al.* PKM2 isoform-specific deletion reveals a differential requirement for pyruvate kinase in tumor cells. *Cell* 2013; **155**: 397–409.

34 Jones DT, Jager N, Kool M, Zichner T, Hutter B, Sultan M *et al.* Dissecting the genomic complexity underlying medulloblastoma. *Nature* 2012; **488**: 100–105.

35 Northcott P a., Shih DJH, Peacock J, Garzia L, Sorana Morrissy a., Zichner T *et al.* Subgroup-specific structural variation across 1,000 medulloblastoma genomes. *Nature* 2012; **488**: 49–56.

36 Kool M, Korshunov A, Remke M, Jones DTW, Schlanstein M, Northcott PA *et al.* Molecular subgroups of medulloblastoma: an international meta-analysis of transcriptome, genetic aberrations, and clinical data of WNT, SHH, Group 3, and Group 4 medulloblastomas. *Acta Neuropathol* 2012; **123**: 473–484.

37 Ellison DW, Dalton J, Kocak M, Nicholson SL, Fraga C, Geoff N *et al.* Medulloblastoma: clinicopathological correlates of SHH, WNT, and non-SHH/WNT molecular subgroups. *Acta Neuropathol* 2011; **121**: 381–396.

38 Thompson MC, Fuller C, Hogg TL, Dalton J, Finkelstein D, Lau CC *et al.* Genomics identifies medulloblastoma subgroups that are enriched for specific genetic alterations. *J Clin Oncol* 2006; **24**: 1924–1931.

39 Hitosugi T, Kang S, Vander Heiden MG, Chung T-W, Elf S, Lythgoe K *et al.* Tyrosine phosphorylation inhibits PKM2 to promote the Warburg effect and tumor growth. *Sci Signal* 2009; **2**: 1–8.

40 Christofk HR, Vander Heiden MG, Wu N, Asara JM, Cantley LC. Pyruvate kinase M2 is a phosphotyrosine-binding protein. *Nature* 2008; **452**: 181–188.

41 Laurenti E, Varnum-Finney B, Wilson A, Ferrero I, Blanco-Bose WE, Ehninger A *et al.* Hematopoietic Stem Cell Function and Survival Depend on c-Myc and N-Myc Activity. *Cell Stem Cell* 2008; **3**: 611–624.

42 Knoepfler PS, Cheng PF, Eisenman RN. N- myc is essential during neurogenesis for the rapid expansion of progenitor cell populations and the inhibition of neuronal differentiation. *Genes Dev* 2002; **16**: 2699–2712.

43 Meyer N, Penn LZ. Reflecting on 25 years with MYC. *Nat Rev Cancer* 2008; **8**: 976–990.

44 Eilers M, Eisenman RN. Myc 's broad reach. *Genes Dev* 2008; **22**: 2755–2766.

45 Roussel MF, Robinson GW. Role of MYC in medulloblastoma. *Cold Spring Harb Perspect Med* 2013; **3**: 1–16.

46 Miller DM, Thomas SD, Islam A, Muench D, Sedoris K. c-Myc and cancer metabolism. *Clin Cancer Res* 2012; **18**: 5546–5553.

47 Dang C V. MYC, metabolism, cell growth, and tumorigenesis. *Cold Spring Harb Perspect Med* 2013; **5**: 1–15.

48 Zirath H, Frenzel A, Oliynyk G, Segerström L, Westermark UK, Larsson K *et al.* MYC inhibition induces metabolic changes leading to accumulation of lipid droplets in tumor cells. *Proc Natl Acad Sci U S A* 2013; **110**: 10258–10263.

CHAPTER V: CONCLUSIONS

5.1 Overview

The work presented here contributes to the understanding of aerobic glycolysis and its role in cerebellar development and medulloblastoma tumorigenesis. I approached medulloblastoma as a disorder of normal cerebellar development. Elucidating the developmental programs of proliferating CGNPs and how they are co-opted during tumorigenesis can lead to more targeted clinical interventions. Currently, targeted therapies against SHH-driven medulloblastoma have had potent, but limited clinical success. While SHH subgroup patients initially respond with dramatic tumor regression to direct inhibitors of the SHH signaling pathway, their medulloblastomas inevitably adapt and become drug-resistant. In drug-treated tumors, clonal genetic events mediate resistance to SHH pathway inhibition. Clonal selection, however, is unlikely to mediate concurrent genetic alterations to both the SHH pathway and a pathway that interacts with SHH signaling to acquire dual resistance. Thus, dual targeting of SHH pathway effectors and an interacting pathway is a potential clinical strategy in the treatment of SHH-driven medulloblastoma to circumvent and subvert drug resistance.

CGNPs and medulloblastomas both exhibit increased aerobic glycolysis, a metabolic program initiated by SHH signaling. To target aerobic glycolysis in the clinic, a better understanding of the metabolic program is required. SHH signaling increases the expression of two key glycolytic enzymes, Hexokinase-2 (HK2) and Pyruvate kinase M2 (PKM2). Previous work has demonstrated that inhibiting aerobic glycolysis at the start by *Hk2* deletion promotes CGNP differentiation, blunts medulloblastoma growth, and prolongs survival. In contrast, work presented here demonstrates that inhibiting aerobic glycolysis at the end by *Pkm2* deletion has opposite effects. *Pkm2* deletion supports CGNP proliferation, accelerates tumor growth, and shortens survival. These animal model findings were validated by SHH subgroup patient data, showing that low PKM2 expression was associated with decreased survival. Thus, *Pkm2* activation, rather than inhibition, may be a new treatment against SHH-driven medulloblastoma.

Together, these studies demonstrate that targeting aerobic glycolysis as an anti-cancer strategy must be sensitive to the location of therapeutic inhibition or activation. As a monotherapy, however, targeting aerobic glycolysis would not be effective because the cancer would adapt and undergo metabolic reprogramming, using alternate metabolic pathways to maintain aberrant growth. Glycolysis-based therapies could potentiate the cytotoxic effects of other treatments by disabling the downstream metabolic response to pro-survival mechanisms. Thus, dual targeting of SHH pathway effectors and aerobic glycolysis is a potential clinical strategy for medulloblastoma treatment.

In a preclinical model of SHH-driven medulloblastoma, I demonstrate that aerobic glycolysis inhibition by *Hk2*-deletion and SHH pathway inhibition by vismodegib treatment act in concert to reduce tumor growth. Vismodegib inhibits the Smoothened mutant allele SMO-W539L in tumor-bearing, *Hk2*-intact mice, demonstrated by a small, but statistically significant, reproducible increase in mouse survival. The anti-tumor effects of vismodegib treatment were also detected in *Hk2*-deleted mice as drastically reduced tumor growth compared to vehicle-treated counterparts. The robust survival benefit of *Hk2* deletion, however, obscured the survival benefit of vismodegib treatment. In all, these data suggest that dual inhibition of HK2 and the SHH pathway is a novel therapy against SHH-driven medulloblastoma.

The present work has implications for the SHH subgroup of medulloblastoma and cancer biology as whole. SHH pathway activation has been reported in other cancers including, basal cell carcinoma, gastric, pancreatic, and colorectal cancer. The insight demonstrated here might have parallel effects in these diverse cancers. However, additional studies are needed before these findings can be translated to the clinic.

5.2 Future studies

A new study of PKM2 activation in a preclinical model of SHH-driven medulloblastoma would provide further insight into the potential efficacy of therapeutically increasing the activity of PKM2. PKM2 activators are currently available for research use and are reported to cross the blood brain barrier after IP injection[1]. My unpublished *in vitro* studies with the PKM2 activator TEPP-46 have demonstrated that

CGNPs increase pyruvate kinase activity with treatment as measured by enzymatic assay. EdU proliferation studies with TEPP-46 will determine if PKM2 activation slows CGNP proliferation. These initial *in vitro* studies may lead to similar findings *in vivo*, using both normal and medulloblastoma-prone mice. Small molecule activation of PKM2 *in vivo*, however, has its limitations. While a short bolus dose of TEPP-46 may activate PKM2 and promote differentiation, treated tumors may develop resistance after chronic use. In response to prolonged PKM2 activation, medulloblastomas may reprogram their metabolism and stop expressing PKM2 to maintain rapid growth. In this regard, an alternative to small molecule activation of PKM2 is overexpression of PKM1 in the system. Studying pyruvate kinase activation with SHH inhibition in medulloblastoma would further elucidate the efficacy of simultaneously targeting aerobic glycolysis and the SHH pathway.

Hk2 deletion with vismodegib treatment demonstrated that dual targeting is a potential clinical strategy for the treatment of SHH-driven medulloblastoma. There are several compounds currently available that generally target hexokinases, including 2-deoxyglucose, lonidamine, and 3-bromopyruvate[2], which could be used in clinical trials with vismodegib. A caveat to combination therapy is drug-drug interactions, which would require additional preclinical testing to parse out. These readily available compounds with established toxicity and safety profiles would significantly expedite the bench-to-clinic timeline of this dual targeting strategy. More specific HK2 inhibitors, however, are not on the market as their development has been technically difficult. This year, Lin et al just published their synthesis of a selective HK2 inhibitor[3]. While this new compound has vast potential, it currently lacks the preclinical data required for testing in clinical trials.

5.3 REFERENCES

1 Witney TH, James ML, Shen B, Chang E, Pohling C, Arksey N *et al.* PET imaging of tumor glycolysis downstream of hexokinase through noninvasive measurement of pyruvate kinase M2. *Sci Transl Med* 2015; **7**: 310ra169-310ra169.

2 Tennant D a, Durán R V, Gottlieb E. Targeting metabolic transformation for cancer therapy. *Nat Rev Cancer* 2010; **10**: 267–277.

3 Lin H, Zeng J, Xie R, Schulz MJ, Tedesco R, Qu J *et al.* Discovery of a Novel 2,6-Disubstituted Glucosamine Series of Potent and Selective Hexokinase 2 Inhibitors. *ACS Med Chem Lett* 2016; **7**: 217–222.